BERICHTE
aus dem Fachbereich Geowissenschaften
der Universität Bremen

No. 157

Xu, W.

MASS PHYSICAL SEDIMENT PROPERTIES AND TRENDS IN A WADDEN SEA TIDAL BASIN

Berichte, Fachbereich Geowissenschaften, Universität Bremen, No. 157,
127 pages, Bremen 2000

ISSN 0931-0800

The "Berichte aus dem Fachbereich Geowissenschaften" are produced at irregular intervals by the Department of Geosciences, Bremen University.

They serve for the publication of experimental works, Ph.D.-theses and scientific contributions made by members of the department.

Reports can be ordered from:

Gisela Boelen

Sonderforschungsbereich 261

Universität Bremen

Postfach 330 440

D 28334 BREMEN

Phone: (49) 421 218-4124

Fax: (49) 421 218-3116

e-mail: boelen@uni-bremen.de

Citation:

Xu, W.

Mass physical sediment properties and trends in a Wadden Sea tidal basin.

Berichte, Fachbereich Geowissenschaften, Universität Bremen, No. 157, 127 pages, Bremen, 2000.

ISSN 0931-0800

Mass Physical Sediment Properties and Trends in a Wadden Sea Tidal Basin

Dissertation
zur Erlangung des
Doktorgrades der Naturwissenschaften
im Fachbereich 5
der Universität Bremen

vorgelegt von

Weidong Xu

Bremen 2000

Tag des Kolloquiums:

20.06.2000

Gutachter:

Prof. Dr. B. W. Flemming

Priv. Doz. Dr. R. Stein

Prüfer:

Prof. Dr. G. Wefer

Prof. Dr. H. D. Schulz

Gedruckt mit Unterstützung des Deutschen Akademischen Austauschendienstes

Acknowledgements

I am very grateful to Professor Dr. B.W. Flemming for giving me the opportunity to carry out this research project at the Senckenberg Institute, Division of Marine Science, and accepting the role as my academic supervisor. Professor Dr. G. Wefer promoted this study throughout and I wish to express my gratitude to him.

Furthermore, I wish to thank the whole staff of the institute for their cooperation, assistance, and especially also social support. Special thanks go to the crew of the research vessel "FK SENCKENBERG" for their cooperation and patience under any weather conditions. I also wish to acknowledge my student fellows who assisted me in the field. I will never forget the many beautiful, but sometimes also difficult days in the tidal flats. Astrid Raschke is thanked for her support in the laboratory, and Dr. Monique Delafontaine for scientific advice and discussion.

Finally, I would like to express my sincere gratitude to the Deutscher Akademischer Austauschdienst (DAAD) for its financial support.

Weidong Xu

Wilhelmshaven, March 2000

Abstract

Mass physical properties of sediments are increasingly receiving attention in sedimentology, geochemistry and environmental science beside their traditional fields of soil science and engineering geology. Sediment composition, bulk density, porosity, water content, shear strength and the relationships between these parameters were systematically investigated in a tidal basin of the German Wadden Sea. In most cases high correlations between these parameters are observed. Furthermore, distinct trends within the tidal basin reveal obvious relationships between the mass physical properties of the sediments and the depositional processes.

In general, the surficial sandy and muddy sediments are physically very different. Thus, a significant mass physical change occurs around a mud content of 50%. In the sandy part (< 50% mud), there is a progressive decrease in the mass of sand as the mass of mud increases in a given volume of sediment. In the muddy part (> 50% mud), by contrast, the mass of mud in a given volume of sediment does not continue to increase but either remains constant or else decreases with the continuing decrease in the mass of sand. In the latter case, the void ratio increases dramatically, the sediment becoming extremely porous and hence soft. The shear strengths of the muddy sediments are very low, usually below 20 kPa which matches their high void ratio. In the sandy sediments the shear strengths vary between 10 kPa and about 100 kPa, being mostly > 30 kPa. The shear strength tends to decrease with increasing mud content, although the scatter is considerable.

There is a distinct seasonal pattern in the mass physical properties of the sediment, the changes differing in mud and sand. Shear strengths are usually lower in summer and higher in winter, both in the sand and the mud. On the sand flats the bulk densities are higher in winter than in summer as there is more mud in the sediment in the summer seasons. On the mud flats, the seasonal changes of the mass physical properties are not as obvious as on the sand flats. It seems that the mud content here is somewhat higher in winter than in summer. The most obvious seasonal changes of the mass physical properties occur in the biogenically influenced muddy sediment. Such sediments have the highest water and mud contents in the summer season, and the lowest in the winter season which demonstrates the strong influence

of the mussel *Mytilus edulis* on the depositional process of fine-grained sediments in the Wadden Sea.

Grain size analyses of the fine-grained fraction of the sediment has revealed a pronounced deficit of particles around 7Φ (8μm), the mud being composed of a better sorted coarse population (<7Φ) and a less well sorted fine population (>7Φ). With the exception of biogenic sediment production, the content of the fine grain size population in the mud fraction is strongly controlled by the energy regime in the tidal basin. The sediments in the study area are usually mixtures of sand and mud, the mud being transported in suspension and deposited from suspension. High-resolution grain-size distributions of the sediments therefore reveal both sediment mixing as well as depositional processes. A detailed comparison of textural parameters demonstrates that grain-size parameters determined by the statistical moment method describe a sediment better in all size ranges than does the percentile statistical method. The mean-sorting, mean-skewness, and mean-kurtosis relationships in combination with the spatial distribution patterns of the grain-size parameters highlight local differences in depositional processes. Moment measures are thus clearly superior to the simplified percentile methods designed by Inman (1952) and Folk and Ward (1957).

Numerous cross-correlations have revealed that the absolute water content is a universal master variable by which many of the mass physical properties of the surficial sediments can be predicted. Thus, the wet bulk density (WBD), the dry bulk density (DBD) and the mud content (M) of common terrigenous sediments can be accurately predicted by means of the absolute water content (W) using the following equations:

$$WBD = (0.37949017 + 0.0065738815 \cdot W)^{-1} \qquad (r = 0.9711,\ N = 321)$$

$$DBD = -0.37768025 + 2.8854035 \cdot e^{\left(\frac{-W}{49.613606}\right)} \qquad (r = 0.9939,\ N = 321)$$

$$M = -39.203351 + 2.1951787 \cdot W - 0.0049787926 \cdot W^2 \qquad (r = 0.9688,\ N = 321)$$

Since these relationships are of universal applicability they can be used for the quick determination of bulk sediment properties which, amongst others, form the basis for any mass balance of sediment components, including heavy metals, trace elements, or particulate organic matter.

Zusammenfassung

Neben ihrer traditionellen Anwendung in der Bodenkunde und Ingenieurgeologie gewinnen physikalische Sedimenteigenschaften heute auch zunehmend an Bedeutung in der Sedimentologie, Geochemie und Umweltforschung. In der vorliegenden Arbeit wurden die Sedimentzusammensetzung, sowie die Raumdichte, die Porosität, der Wassergehalt und die Scherfestigkeit der Oberflächensedimente eines Gezeiteneinzugsgebietes des Wattenmeeres systematisch untersucht. In den meisten Fällen ergaben sich hohe Korrelationen zwischen diesen Eigenschaften. Die Verteilungsmuster dieser Parameter im untersuchten Einzugsgebiet zeigen deutliche Beziehungen zwischen den physikalischen Sedimenteigenschaften und den Sedimentationsprozessen.

Generell haben sandige und schlickige Sedimente sehr unterschiedliche physikalische Eigenschaften. Eine besonders markante physikalische Veränderung ist bei einem Schlickgehalt von ca. 50% zu erkennen. In sandigen Sedimenten (< 50% Schlick) nimmt die Masse des Schlickes in einem Referenzvolumen bei abnehmendem Sandgehalt stetig zu. In schlickigen Sedimenten dagegen (> 50% Schlick) bleibt der Massenanteil des Schlickes im Referenzvolumen, trotz weiter abnehmendem Sandanteil, entweder konstant oder nimmt sogar ab. In letzterem Fall nimmt das Porenvolumen dramatisch zu und das Sediment wird extrem plastisch. Solche schlickigen Sedimente haben sehr niedrige Scherfestigkeiten, die normalerweise unter 20 kPa liegen. In sandigen Sedimenten streuen die Scherfestigkeiten stärker (10 kPa und 100 kPa), liegen aber generell über 30 kPa. Die Scherfestigkeit nimmt bei zunehmenden Schlickgehalt somit generell ab.

Es wurden saisonale Veränderung in den physikalischen Eigenschaften der Wattsedimente festgestellt, wobei deutliche Unterschiede zwischen sandigen und schlickigen Sedimenten zu beobachten sind. In allen Sedimenten sind die Scherfestigkeiten im Sommer niedriger als im Winter. Die Raumdichte im Sandwatt ist in der kalten Jahreszeit höher als in der warmen Jahreszeit, weil im Sommer der Schlickgehalt des Sediments ansteigt. Dagegen sind saisonale Veränderungen in den physikalischen Eigenschaften des Schlickwattes weniger ausgeprägt als im Sandwatt. Allerdings sind die saisonalen Veränderungen im biogenen Schlick ebenfalls sehr deutlich. Solche Sedimente haben im Sommer die höchsten Schlickgehalte und Wassergehalte. Damit dokumentiert sich ein deutlicher Einfluß der Muschel *Mytilus edulis* auf den Sedimentationsprozess.

Korngrößenanalysen der Schlicke haben ein allgemeines Defizit an Partikeln um 7Φ (8μm) aufgezeigt. Die Schlicke bestehen aus einem besser sortierten groben Anteil (<7Φ) und einem schlechter sortierten feinen Anteil (>7Φ). Mit Ausnahme der biogenen Sedimente, wird die Korngrößenzusammensetzung der Schlicke offensichtlich durch hydrodynamische Prozesse gesteuert. Da die Sedimente im Untersuchungsgebiet normalerweise aus Sand-/Schlickgemischen bestehen, enthalten die Korngrößenverteilungen Informationen über den Mischungs- und Sedimentationsprozeß. Durch detaillierte Vergleiche zwischen momentstatistischen und perzentilstatistischen Sedimentparametern konnte gezeigt werden, daß die Momentstatistik die Sedimente besser beschreibt als die Perzentilstatistik. Die Beziehungen zwischen Mittelwert und Sortierung, Mittelwert und Schiefe sowie Mittelwert und Kurtosis auf der Basis der Momentstatistik heben räumliche Unterschiede in den Korngrößenparametern deutlicher hervor als auf der Basis der Perzentilstatistik von Inman (1952) und Folk und Ward (1957). Die momentstatistischen Korngrößenparameter sind als Indikatoren für örtliche Ablagerungsprozesse den perzentilstatistischen Parametern somit deutlich überlegen.

Vielfältige Kreuzkorrelationen haben ergeben, daß der absolute Wassergehalt ein universeller Parameter ist, anhand dessen sich viele physikalische Eigenschaften oberflächennaher Sedimente prognostizieren lassen. So können beispielsweise die nasse Raumdichte (WBD) und die trockene Raumdichte (DBD) und der Schlickgehalt (M) terrigener Sedimente mit Hilfe des absoluten Wassergehaltes (W) durch die folgenden Formeln berechnet werden:

$$WBD = (0.37949017 + 0.0065738815 \cdot W)^{-1} \qquad (r = 0.9711,\ N = 321)$$

$$DBD = -0.37768025 + 2.8854035 \cdot e^{\left(\frac{-W}{49.613606}\right)} \qquad (r = 0.9939,\ N = 321)$$

$$M = -39.203351 + 2.1951787 \cdot W - 0.0049787926 \cdot W^2 \qquad (r = 0.9688,\ N = 321)$$

Der universelle Charakter dieser Formeln erlaubt eine schnelle Bestimmung von physikalischen Sedimenteigenschaften, die u.a. zur Bestimmung von Massenbilanzen unterschiedlichster Sedimentkomponenten, einschließlich Schwermetallen, Spurenelementen und partikulären organischen Substanzen erforderlich sind.

Table of Contents

List of Figures

List of Tables

1 Introduction

1.1 Research problem

The Wadden Sea depositional system is an important transition zone between the Southern North Sea and the land. It is a nursery ground for juvenile fish, and an economic resource for man. The area investigated in this study has a mesotidal range (2.7 m) and is influenced by strongly variable meteorological conditions characterized by frequent storm surges. In the course of the Holocene it went through dramatic morphological transformations resulting from constant erosion and redeposition in the course of the postglacial sea-level rise. In more recent times it was strongly influenced by human activities such as dredging, land reclamation and the construction of dikes. Because of its position at the land/sea boundary, the Wadden Sea is a very sensitive environment which responds rapidly to global changes in climate and human activities. It is thus an ideal natural laboratory for the study of sedimentological and morphological process/response mechanisms.

Most of the studies in this area before 1990 formed part of regional overview investigations (e.g., Sindowski, 1966; Barckhausen et al., 1973; Figge et al., 1980; Figge, 1981; Ragutzki, 1982; Grotjahn, 1990). In the 1990's many multidisciplinary studies combining sedimentology, geochemistry, biology and hydrodynamics were carried out (e.g., Antia, 1993; Antia et al., 1994; Davis and Flemming, 1995; Delafontaine et al., 1996; Flemming, 1991; Flemming et al., 1992; Flemming and Davis, 1994; Flemming and Delafontaine, 1994; Flemming and Nyandwi, 1994; Flemming and Ziegler, 1995; Hertweck, 1995; Hertweck and Liebezeit, 1996; Michaelis et al., 1995; Nyandwi and Flemming, 1995; Zens et al., 1997). These studies improved our knowledge of the interactions between the sediments, the biology and the hydrodynamic conditions in the back-barrier tidal basins, amongst others leading to the establishment of the shore-normal energy gradient model (cf., Flemming and Nyandwi, 1994; Nyandwi and Flemming, 1995; Flemming and Bartholomä, 1997). Nevertheless, there is still a general lack of knowledge concerning the behaviour of the fine-grained sediments in the system.

Fine-grained sediments are a common component in local tidal waters and hence play an important role in the depositional processes of the tidal basins. Because fine-grained

sediments are transported and deposited by a different process than coarse-grained sandy sediments, the mixing process can strongly influence the mass physical and geotechnical properties of the sediments. Petrologically, the muds may occur as matrix in some cases, and as the main sediment component in other cases. Since fine-grained particles are important carriers of rare elements and contaminants, their occurrence and variation in the sediment are of substantial environmental significance. To date, the mass physical properties of coastal sediments have received far less attention than those of deep-water sediments (e.g., Bennet et al., 1971; Lambert and Bennett, 1972; Keller, 1974; Hamilton, 1974; Silva and Brandes, 1998). Mass physical properties describe the physical characteristics of sediments. They have in the past been more commonly studied for geotechnical purposes rather than for the solution of sedimentological problems. In many cases the unit of measure is "concentrations", i.e. mass per unit volume, rather than "contents", i.e. mass per unit mass. As shown by Flemming and Delafonaine (2000) there is considerable confusion in the literature concerning the correct use of these dimensions (and terms), the misapplications having led to wrong interpretations in some cases.

In this study the whole sediment is taken into consideration, not only the coarse-grained sand fraction or the fine-grained mud fraction, as is commonly the case. Through a systematic comparison of bulk sedimentological and high-resolution textural properties of surficial intertidal sediments the study aims at highlighting important relationships between the mass physical properties of the sediments and the depositional processes within a Wadden Sea tidal basin. The results are expected to be of regional significance, applying in principle to the Wadden Sea depositional system as a whole.

1.2 Study area

The Wadden Sea of the Southern North Sea coast begins at Den Helder in the Netherlands and ends at Skallingen in Denmark, being about 500 km long and covering an area of about 9300 km² (Lozán et al., 1994). The East Frisian Wadden Sea is situated between the Dollart and the Jadebusen along the northwest coast of Germany, and forms the middle part of the Wadden Sea system. On the North Sea side the East Frisian Wadden Sea is lined by seven major barrier islands and some minor sandbanks (Fig. 1-1) which protect an extensive system of backbarrier tidal flats (Backhaus, 1943).

The study area - Otzum tidal basin - is the catchment of the Otzum inlet and is situated behind the islands of Spiekeroog and Langeoog. It is located geographically between 7° 35´E and 7° 49´E and 53° 41´N to 53° 48´N, covering an area of about 75 km².

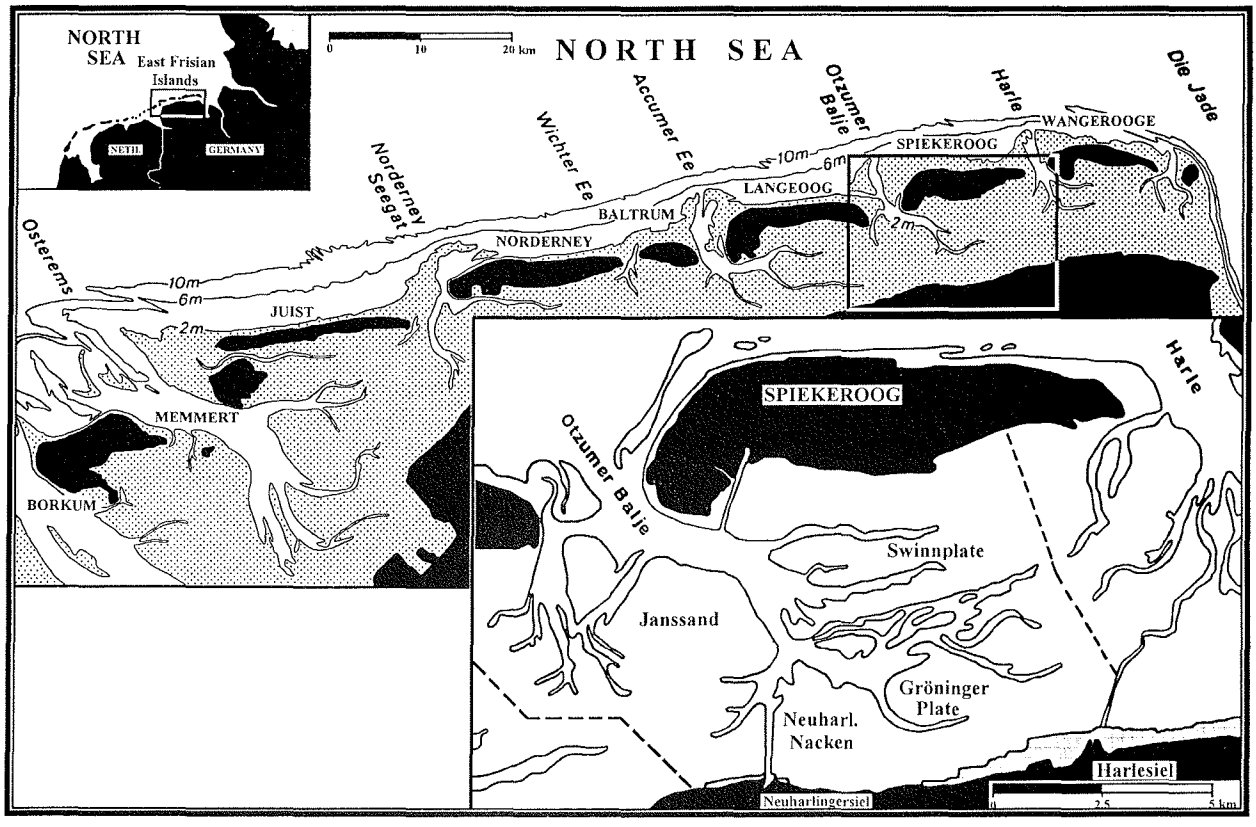

Figure 1-1 The East Frisian Wadden Sea system and the study area

1.2.1 Regional setting

1.2.1.1 The Pleistocene

The Quaternary history of the study area is dominated by the effects of the glacial and interglacial climatic cyclicity. The geological succession of the German coastal zone forms part of the depositional system of the larger North Sea basin, being characterized by a sequence of transgressional and retrogressional cycles under the influence of tectonic movements and isostatic adjustments during periods of deglaciation.

The Pleistocene has been documented by a set of three glacial periods, namely the Elsterian, Saalian and Weichselian, as well as two interglacial periods, the Holsteinian and Eemian (Sindowski, 1970; Behre et al., 1979). The sediments of the glacial periods usually comprise glacio-fluvial sands with dark clay layers, whereas the sediments of the interglacial periods are composed of marine sands intermingled with mollusc shell hash. The Holsteinian transgression did not affect the whole East Frisian coastal sector, reaching far inland only in the Jade-Weser region. During the Saalian glacial period, the whole North Sea basin, including the northwestern German low lands were covered by ice. The subsequent transgressive Eemian marine sediments are widely distributed in the North Sea basin. In the coastal region the Eemian marine sediments are less widely distributed than the Holsteinian ones, the Eemian coastline having a similar outline as the present coast.

During the Weichselian glacial period the East Frisian coast and the Southern North Sea were not covered with ice. Instead, the glaciers only reached the Dogger Bank area during the last glacial maximum, damming up a meltwater lake in the Southern North Sea. In the course of ice recession the basin emptied towards the north and rivers such as the Elbe, Weser and Ems extended into the North Sea basin.

1.2.1.2 The Holocene sea-level rise and coastal evolution

The Holocene of the Southern North Sea basin and the East Frisian coastal region is dominated by a number of transgressive events. Sea level initially rose very rapidly, reaching

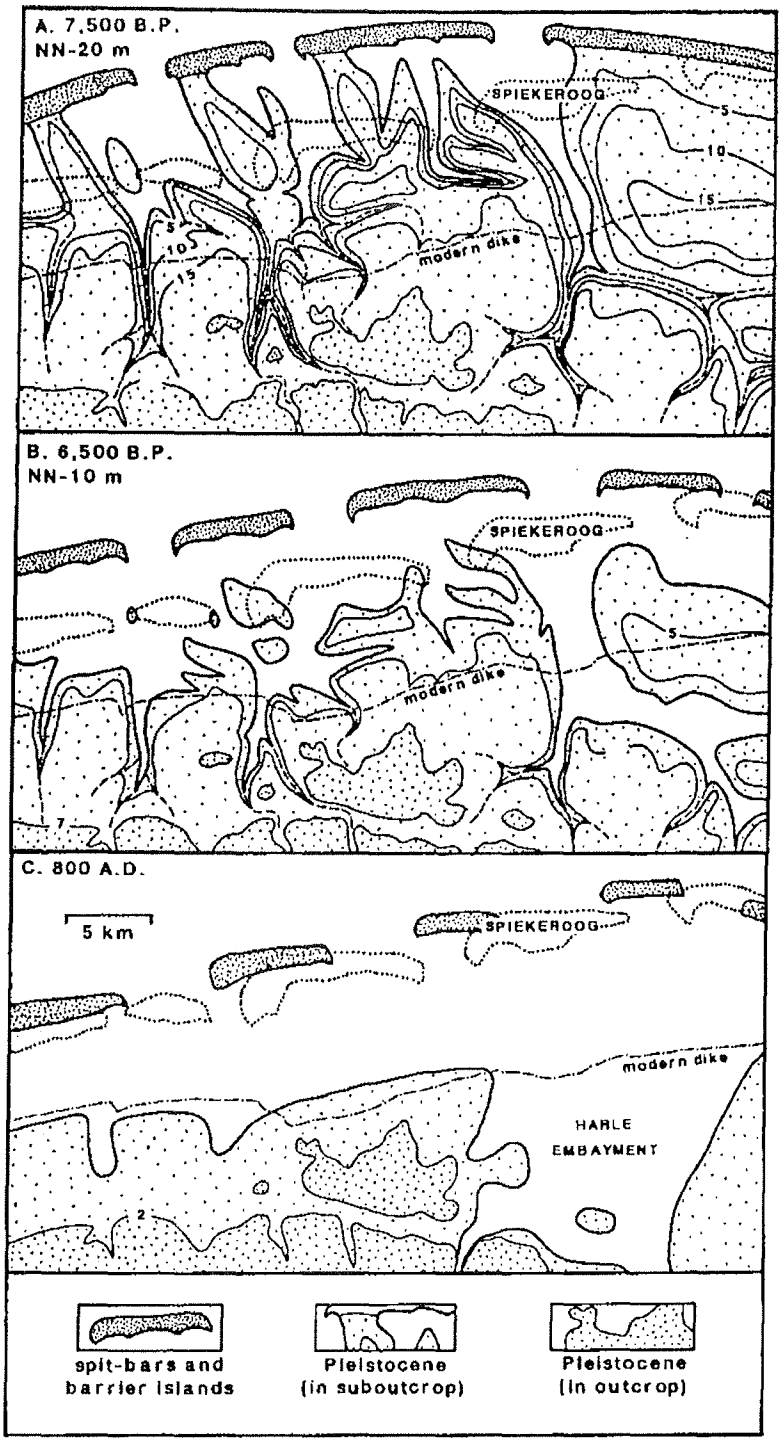

Figure 1-2 Paleogeographic reconstruction of the East Frisian coastal evolution during the Holocene (after Flemming, 1991)

the northern margin of the Dogger Bank around 9000 a BP (Jelgersma, 1979). The coastline reached the Southern North Sea margin at about NN – 24m around 7900 a BP (NN: German topographic chart datum), as revealed in a core recovered north of Wangerooge (Hanisch, 1980). Around 7500 a BP the sea-level stood at about NN -20m, i.e. just north of the modern East Frisian Islands which coincides with the seaward margin of an elevated Pleistocene sand body. At this time the sea water penetrated into the lower reaches of the local rivers to form estuaries. Wave action began to rework the coastal sediments to produce a series of spit-bars. This situation marks the beginning of the East Frisian coastal evolution (Flemming, 1991).

According to Flemming (1991), the sea level rose continuously to an elevation of about NN -10m at approximately 6500 a BP. At the same time the tidal range progressively increased from about 1.3 m to 2.2 m. With the rising sea level and a growing tidal range, the estuaries expanded and flooded increasingly larger areas of land until neighbouring estuaries eventually coalesced behind the beach barriers. In this manner the coastal barrier-spits were transformed into detached barrier islands. The expanding backbarrier tidal waters and further increasing tidal range resulted in the widening of the inlets at the expense of the barrier islands. This process continued until about 1000 AD, when human interventions began to influence the natural process (Fig. 1-2).

1.2.1.3 Coastal evolution in historical times

As early as 1300 AD the whole East Frisian coast was diked (Ehlers, 1988). In the course of diking the catchment area of the Harle bay, for example, was reduced from > 180 km^2 in 1362 to only 60 km^2 in 1960; this corresponds to a reduction of the original catchment (Fig. 1-3) and also the tidal prism to 33%. The filling up of the western part of the Harle inlet was accompanied by an eastward growth of Spiekeroog island. In correspondence, the tidal drainage divides between neighbouring tidal basins also migrated eastwards. As a result, the effective catchment of the Otzum inlet increased and the eastern arm of the Otzum inlet behind Spiekeroog expanded with time (Homeier and Luck, 1969; Homeier, 1979). The modern Otzum tidal basin has thus experienced substantial morphological modifications in the course of the last 1000 years (Fig. 1-4).

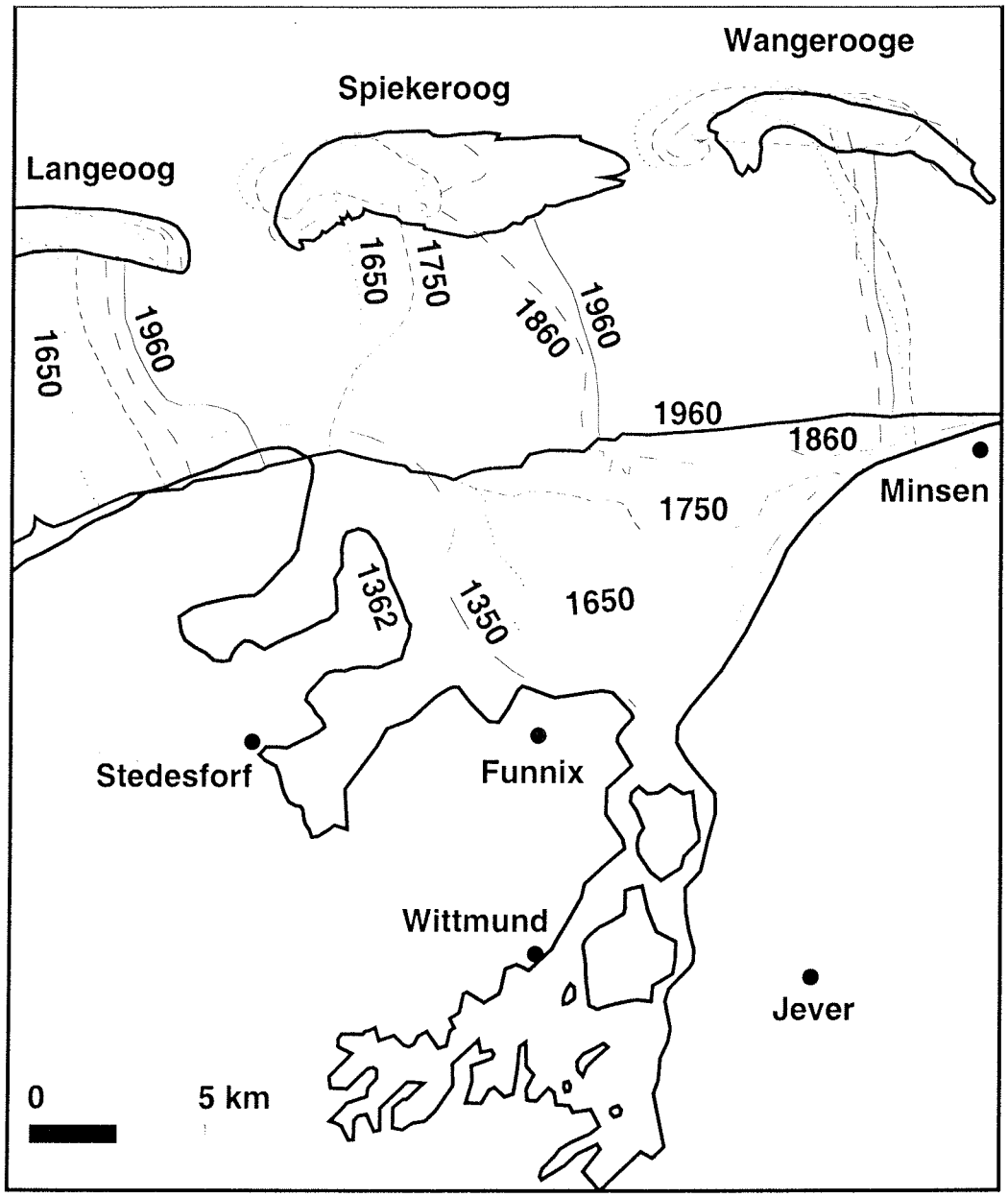

Figure 1-3 Changes in the size of the Harle tidal catchment as a result of land reclamation in the Harle Bay (after Flemming, 1991)

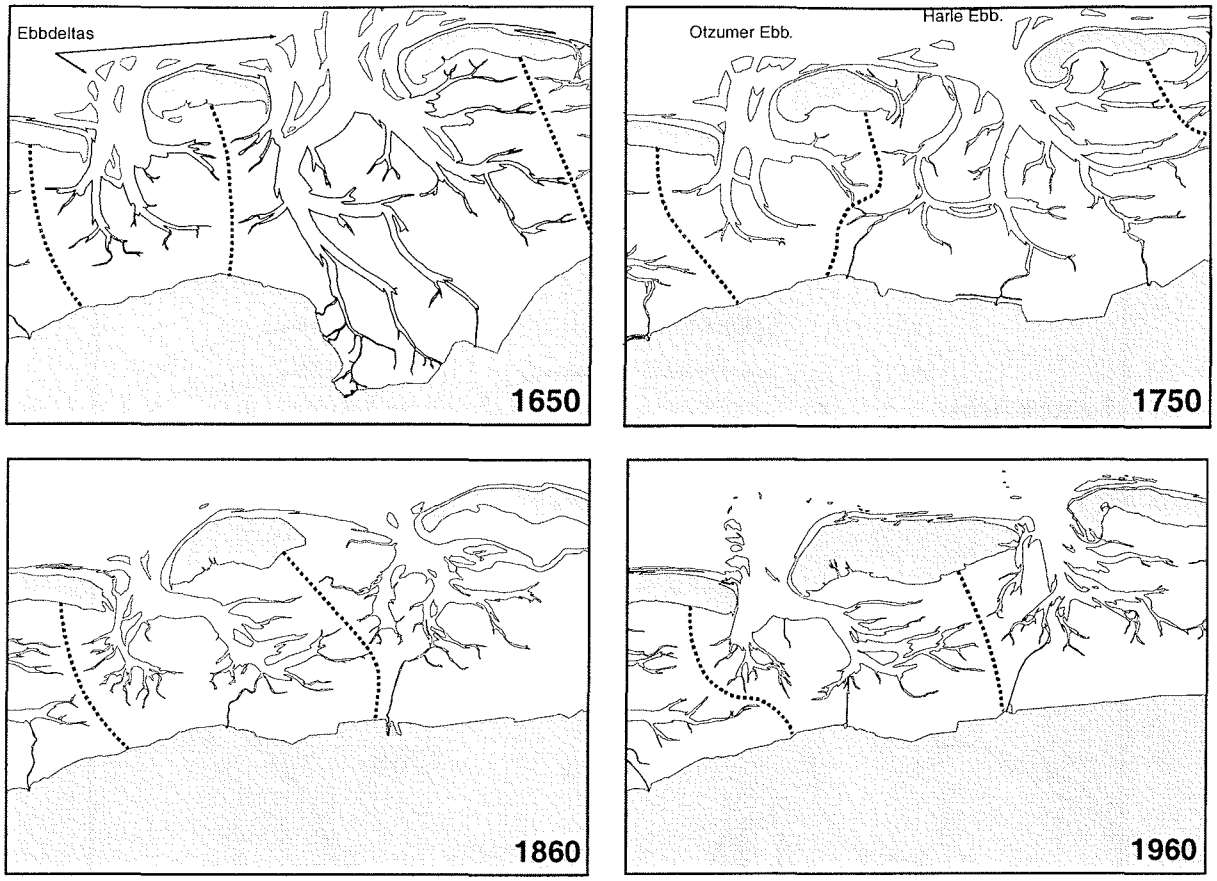

Figure 1-4 Morphological evolution of the North Sea barrier islands in historical times in Spiekeroog area (after Homeier and Luck, 1969)

1.2.2 Hydrology

1.2.2.1 Tides

The movement of tidal water in the North Sea is driven by a system of three amphidromic points, one is situated in the north near the Norwegian coast, another in the central North Sea northwest of the German Bight and the third in the south within the English Channel (e.g., Huntley, 1980). In the Southern North Sea the tidal circulation is controlled by the central amphidromic point, around which the M_2 tide revolves in anti-clockwise fashion

(Fig. 1-5). Relative to the barrier island chain this results in an increase in tidal range both towards the coast and from west towards the east along the coast.

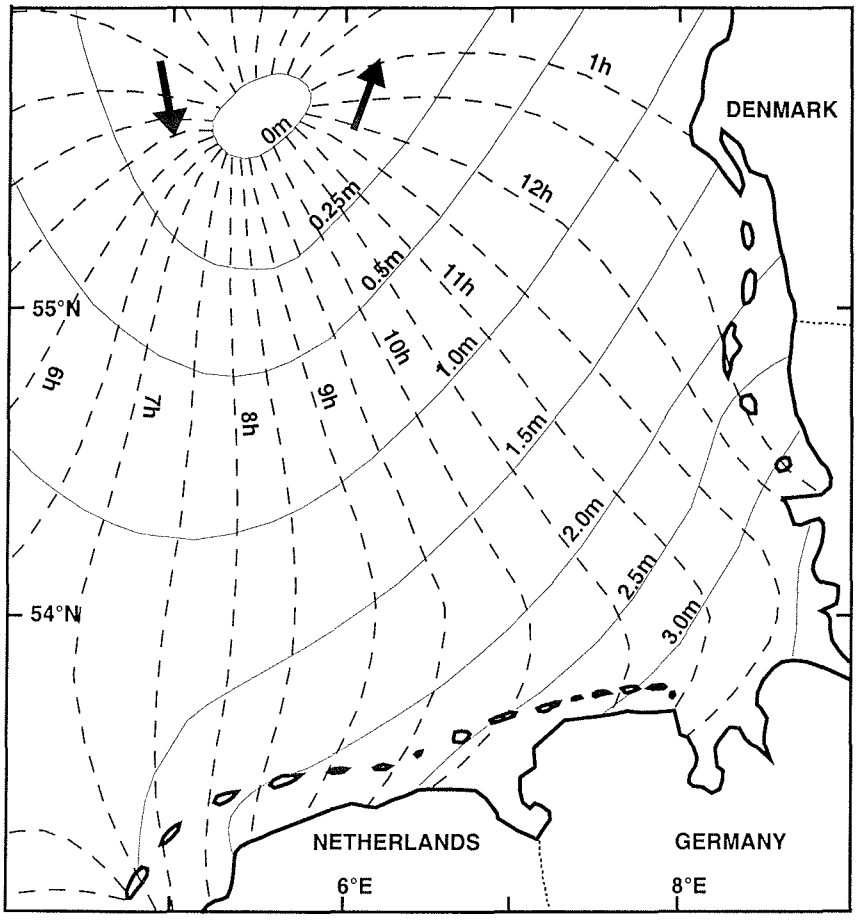

Figure 1-5 Tidal circulation in the North Sea (after Huntley, 1980)

The mean tidal high water level and the mean tidal low water level in the Otzum tidal basin occur at elevation of NN +1.26 m and NN -1.46 m respectively. This corresponds to a mean tidal range of 2.72 m (Siefert and Lassen, 1985; Ferk, 1995). In the main tidal channels the maximum current velocities can exceed 1.0 m/s. There is a pronounced time-velocity asymmetry, characterized by shorter and faster ebb tide currents. The strongest current velocities occur in the inlet mouth and decrease towards the tidal drainage divides which are controlled by the topography of the tidal basin, in particular the channel system (Hübner and Backhaus, 1997).

1.2.2.2 Winds and waves

The wind regime in the study area is represented by the meteorological data collected on Nordeney. In the period from September to March the prevailing winds blow from the southwest quadrant, reaching an average strongest wind velocity of 36 km/hr. During the remainder of the year the prevailing winds blow from the northwest quadrant, but are less strong (Luck, 1976). Analysis of the data of 1965 - 1986 (Antia, 1993) shows that 85% of the winds >10 Beaufort occur in the winter months, 30% of which are confined to November. Of these strong winds, 47% are contributed by the northwest, 30% by the west, 19% by the southwest, and 4% by the north quadrant. Since the 1950s the frequency of storms along the North Sea coast has markedly increased (Führböter, 1979; Stephan, 1982). In the back-barrier basins the influence of wind on the hydraulic conditions is twofold. The first and most important process is flow enhancement caused by wind-induced coastal water setup as a result of the prevailing westerly to northwesterly storms. This was demonstrated by a study in the Norderney inlet (Koch and Niemeyer, 1978). A comparison of the measurements made under fair weather conditions with those of stormy weather revealed an increase in the ebb tidal current velocities and a corresponding reduction of the flood current velocities.

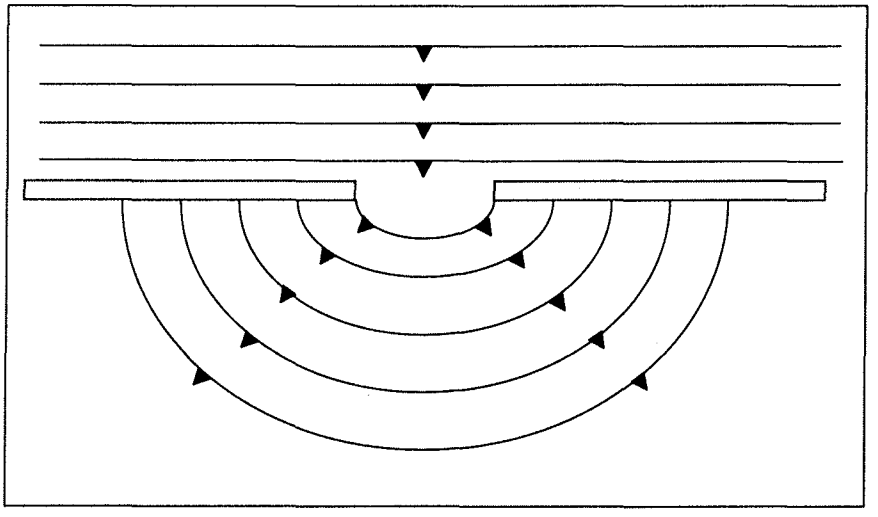

Figure 1-6 Diffraction of waves through an inlet (after Allen, 1977)

Wave action is another process associated with strong wind. As demonstrated by observations in the neighbouring Langeoog back-barrier basin (Delft Hydraulics, 1995), significant waves always approached from the open North Sea. However, due to the sheltering effect of the islands, only 8% of the wave energy actually penetrated the inlet (Niemeyer, 1986). This penetrating wave energy is strongly dispersed in the back-barrier tidal basin due to both wave refraction and wave diffraction (Fig. 1-6). In addition, the influence of incoming waves also depends on the water level. As a result, most of the wave energy is dissipated on the inlet shoals. Within the tidal basin, wave action is strongly reduced, although the energy flux associated with waves tends to enhance the shoreward energy gradient resulting from the asymmetry of the tidal wave (Groen, 1967).

1.3 Materials and methods

1.3.1 Field work

For the purpose of this study a regular sampling and observation grid was designed, the geographic intervals being 0.5′ Longitude and 0.3′ Latitude. This corresponds to a grid of 500 m × 550 m with about 200 sampling positions and covers the whole intertidal flat of the Otzum tidal basin. In the vicinity of tidal channels, the sampling positions were adjusted to the topography in order to achieve a balanced sample distribution over the whole study area (Fig. 1-7). The field work was carried out during low water, and the positions were determined by a NAV 5000D handy GPS from MAGELLAN™. The shear strength of the surface sediment was measured *in situ* using a GILSON HM-504 hand torvane. Shear strength measurements were repeated at least 5 times in each case to avoid extraneous values, average shear strengths being calculated from these measurements after eliminating extreme values. At the same positions an undisturbed sediment sample was taken using a cylindrical plastic vial which was about 2 cm deep and had a constant volume of 52 cm^3. The vial with the sample was immediately sealed to avoid the loss of pore water. In addition, the geomorphological and biological features at every sampling site and along the sampling route were documented for later reference. This work was carried out in the warm period between late spring and autumn of 1996 and 1997.

Suspended material was collected seasonally from the water column at station W in the channel between Spiekeroog and Janssand (W position in Fig. 1-7) in 1996 and 1997

using a pump centrifuge. The pump nozzle was placed at a depth of 5 m and samples were collected at 2-hour intervals over a 12-hour tidal cycle. At the same time, the hydrographic conditions were monitored by a CTD probe.

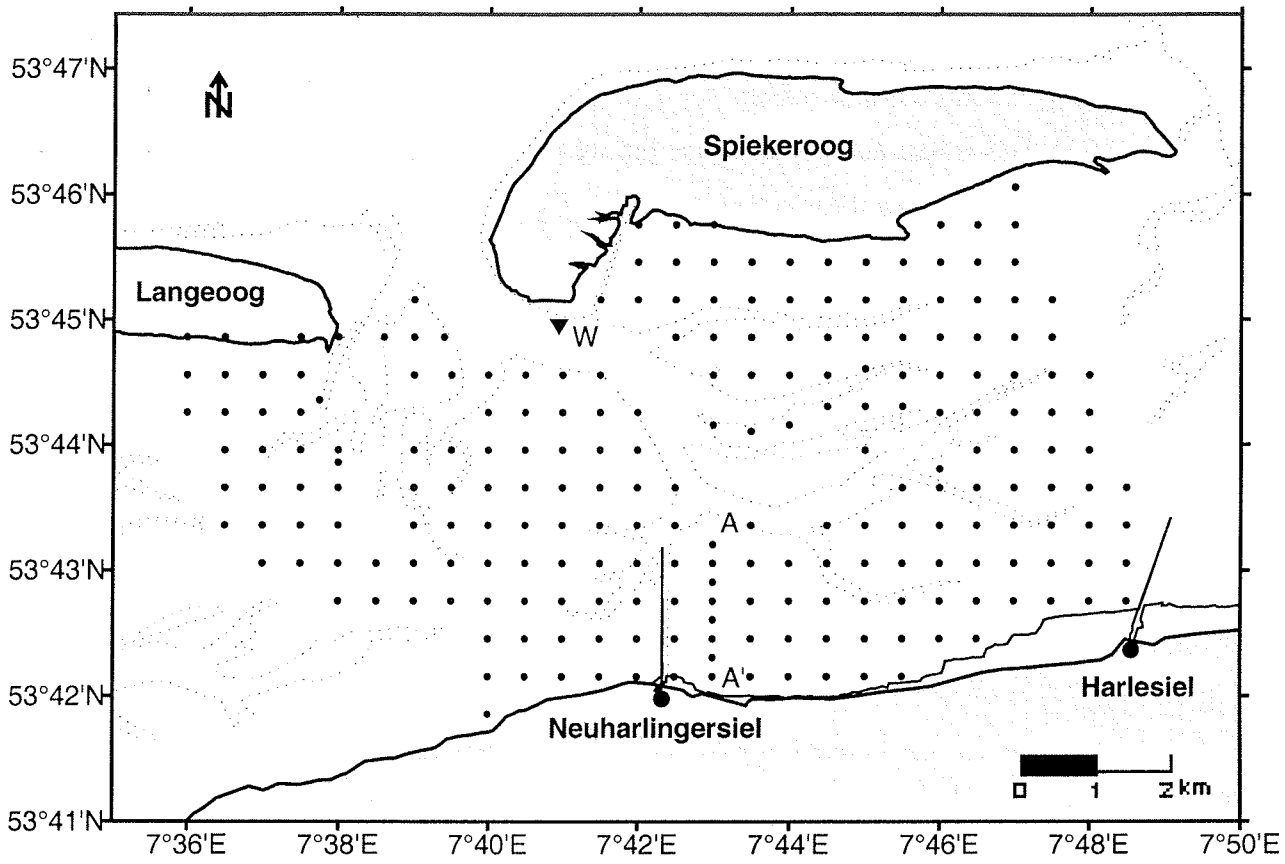

Figure 1-7 Sampling positions in the study area

In order to assess potential seasonal changes of the mass physical sediment properties a control transect was set up on the Neuharlingersieler Nacken tidal flat near the dike (A – A' in Fig. 1-7). Sampling and environmental observations were repeated monthly at eight points along the transect, spaced about 250 m apart, in the period from April 1997 to March 1998.

1.3.2 Laboratory work

In order to avoid the loss of pore water, the samples were processed as quickly as possible in the laboratory following standard procedures (e.g. Müller, 1967; Carver, 1971). At first, the sealed vials containing the sediment were weighed. All of the sediment was then removed from the vial and dried for at least 24 hours at a temperature of 70°C. Thereafter, the dry weight of the sediment, including the salt, and the weight of the vial were determined respectively. The sediment was then dialyzed under flowing water for at least 12 hours. After desalination the sample was washed through a 0.063mm (4 Φ) sieve and separated into sand and mud fractions. The sand fraction was dried at 110 °C for 24 hours and then weighed. The dried sand fraction was split down by a sample divider to obtain suitable sub-samples for granulometric analysis. After days and sometimes weeks of sedimentation, the mud fraction was collected and dried at 70°C for at least 24 hours before being weighed and stored for later analysis.

1.3.2.1 Grain size analysis

1.3.2.1.1 Grain size classification

In this study, the standard grain size classification of Friedman and Sanders (1978) (Table 1-1) is applied, i.e. grain sizes greater than 63μm (4Φ) are referred to as sand, the fraction from 63μm (4Φ) to 2μm (9Φ) as silt, and the material smaller then 2μm (9Φ) as clay. In addition, the term "mud" is used to refer to the total material smaller than 63μm (4Φ).

1.3.2.1.2 The sand fraction

The grain size distributions of the sand fractions were determined by measuring the particle settling velocities using an automated settling tube system - MacroGranometer™ (cf. Brezina, 1979, 1980), and then converting the settling velocities into equivalent settling diameters. The grain size measurements by settling tube are based on the principle of hydraulic equivalence of the particles (Flemming and Thum, 1978; Flemming and Ziegler, 1995). According to this principle, particles which have the same settling velocity are

considered to be hydraulically equivalent and are thus expressed in terms of the same settling diameter in spite of different geometric sizes, shapes and densities. Since most sediments are deposited in the course of hydraulic transport (e.g. Inman, 1949; Bagnold, 1968; Middleton, 1976; Passega, 1957, 1964, 1977; Sly et al., 1983), equivalent settling diameters are thought to better represent the hydraulic size sorting process.

Table 1-1 Standard size classes of sediment (after Friedman and Sanders, 1978)

Limiting Particle Diameter			Size Class		
mm	Φ	Micron			
2048	-11		V. Large	Boulders	Gravel
1024	-10		Large		
512	-9		Medium		
256	-8		Small		
128	-7		Large	Cobbles	
64	-6		Small		
32	-5		V. Coarse	Pebbles	
16	-4		Coarse		
8	-3		Medium		
4	-2		Fine		
2	-1		V. Fine		
1	0		V. Coarse	Sand	
½	+1	500	Coarse		
¼	+2	250	Medium		
1/8	+3	125	Fine		
1/16	+4	62	V. Fine		
1/32	+5	31	V. Coarse	Silt	Mud
1/64	+6	16	Coarse		
1/128	+7	8	Medium		
1/256	+8	4	Fine		
1/512	+9	2	V. Fine		
				Clay	

The resolution of the settling tube system is 0.02 psi, where psi represents the negative binary logarithm of the settling velocity (v) of the particles measured in cm/s:

$$psi = -\log_2 v$$

The settling process is controlled by the GRM™ software (Brezina, 1986) which saves the data of the cumulative mass of the settling particles per unit time increment. The raw data can then be further processed by the SedVar™ software which is part of the MacroGranometer system. Before each measurement the mean water temperature in the settling tube is automatically recorded to determine the viscosity value of the fluid which is required for the computation of equivalent settling diameters. The processing software uses the more versatile

equation of Brezina (1979) rather than that of Gibbs et al. (1971) and allows the choice of any particle shape factor and grain density for the computation.

In the present case the smooth glass sphere standard was used which corresponds to a grain density of 2.65 g/cm³ and a hydraulic shape factor of SF' = 1.18, the local gravity acceleration being 9.79633 m/s². The computed grain size distributions are then saved in the form of frequency and cumulative percentage values at 1/10Φ, 1/4Φ, 1/2Φ and 1Φ intervals.

1.3.2.1.3 The mud fraction

Grain size distributions of the mud fractions were measured by a SediGraph 5100 particle analyser (Micromeritics™). The SediGraph determines the size distribution of particles dispersed in a liquid assuming Stokes' Law of settling. It measures the attenuation of a finely collimated X-ray beam as a function of time and height in a settling suspension. The ratio of X-ray transmission of the cell when filled with pure sedimentation liquid is measured and transformed into concentration values indicated linearly as cumulative mass percentages on the Y-axis of an X-Y-chart. In order to minimize the time required for analysis, the sample cell is continuously lowered relative to the X-ray beam so that the effective sedimentation depth decreases with time. The cell movement is synchronized with the X-axis of the recorder to indicate the equivalent spherical diameter corresponding to the time and depth. Before each analysis the particle density, liquid density and viscosity, and the starting diameter of the analysis are entered into the computer controlling the SediGraph.

The mud samples were treated overnight with 1% hydrogen peroxide to remove the organic matter. The samples were then well dispersed with a 0.1% sodium pyrophosphate liquid in an ultrasonic bath for at least 15 minutes. Before analysis, every sample was again dispersed ultrasonically for 2 minutes in a Tech5100 probe supplied by Micromeritics™. All the mud samples in this study were analysed in the size range of 100 μm to 0.5 μm at 37 °C. The mean grain density was assumed to correspond to that of quartz, i.e. 2.65 g/cm³. To avoid hindered settling and thus an overweighing of the fine fractions, the concentration of the sediment suspension was controlled at about 0.025 - 0.05 g/ml, as recommended by Stein (1985) and Singer et al. (1988). Every sample was usually measured twice to confirm the reliability of the analysis. The result of the analysis was then converted into frequency and cumulative data at 1/4Φ intervals using the operating program.

1.3.2.2 The density of materials: pycnometer method

Since mass physical parameters were to be studied and many mass physical parameters of the sediments refer to the volumes of the grain particles, the pore space and the foreign materials in the sediments, not only weight measures but also volume measures are needed. There are several methods to determine the volume of particulate solids, some requiring expensive instrumentation. In the present case a simple procedure was chosen by which the volume of solid material can be inferred if the density of the material is known. The pycnometer method is a common procedure for density measurements (e.g., Keil, 1954; Black et al., 1965; Liu and Evett, 1984). The following steps are required:

1) The pycnometer is cleaned, dried and then weighed. The weight of the pycnometer (Wp) is recorded.
2) The pycnometer is filled with distilled water which has a temperature of Ti, and the weight of the pycnometer plus water { $Wpw(Ti)$ } is accurately measured and recorded.
3) Some oven-dried solid material is weighed (Ws). It is placed into the empty pycnometer. Distilled water is then added to cover the solid material. The pycnometer with water and solid material is then gently heated in a water bath until all gas bubbles have been eliminated.
4) The heated pycnometer is cooled down and filled completely with distilled water. The new water temperature Tx is recorded and the filled pycnometer ($Wpws$) is weighed.
5) The value of $Wpw(Tx)$ can then be computed for any other water temperature Tx as follows:

$$Wpw(Tx) = \frac{\rho_w(Tx)}{\rho_w(Ti)}(Wpw(Ti) - Wp) + Wp \qquad \textbf{1-1}$$

6) Finally, the density of the solid material Gs is determined by the relationship:

$$Gs = \frac{K \cdot Ws}{Ws + Wpw(Tx) - Wpws} \qquad \textbf{1-2}$$

where K is a conversion factor used to transform the measured fluid density at temperature T_x into the equivalent density of water at 20 °C (the value of K can be determined from Table 1-2); ρ_w is the water density; Ws is the weight of the oven-dried sample; $Wpw(Tx)$ is the weight of the pycnometer filled with water at temperature Tx; Tx is the temperature of the contents of the pycnometer when $Wpws$ is determined; $Wpws$ is the weight of the pycnometer with solid material and filled up with water of temperature Tx.

Depending on the mass of the material to be measured, two pycnometers of different sizes were used in this study. One had a volume of 50 ml and was used if the available solid material amounted to 10 - 15 g. The other had a volume of 25 ml and was used if the available mass of the material was 5 - 10 g.

Table 1-2 Correction factors to compensate for different water temperatures in particle density measurements using pycnometer (after Liu and Evett, 1984)

Temperature °C	Relative density of Water g/cm³	Correction Factor *K*
18	0.9986244	1.0004
19	0.9984347	1.0002
20	0.9982343	1.0000
21	0.9980233	0.9998
22	0.9978019	0.9996
23	0.9975702	0.9993
24	0.9973286	0.9991
25	0.9970770	0.9989
26	0.9968156	0.9986
27	0.9965451	0.9983
28	0.9962652	0.9980
29	0.9959761	0.9977
30	0.9956780	0.9974

1.3.2.3 Organic matter content

In the present study it was necessary to determine the organic matter content of the sediment because its influence on mass physical properties was to be assessed. An easy method to measure organic matter content is by loss of ignition. A temperature of 550°C is generally considered sufficient to combust the organic matter. Higher temperatures may cause loss of weight owing to the disassociation of carbonate (Fairchild et al., 1988).

The oven-dried samples were kept in a desiccator for 12 hours. They were then weighed and placed in a muffle furnace at a temperature of 500°C for 6 hours. The combusted samples were returned to the desiccator to cool down to room temperature before being

weighed once more. The loss of weight after combustion is considered to reflect the mass of the organic matter which is expressed as a percentage of the total weight of the sample.

1.3.2.4 $CaCO_3$ content

The $CaCO_3$ content of the mud in the study area was measured by means of a "Karbonat-Bombe" introduced by Müller and Gastner (1971). The "Karbonat-Bombe" device is a closed cylinder with a pressure gauge, in which a specified mass (usually 1 g) of dried, powdered sediment is allowed to react with hydrochloric acid. The carbon dioxide gas generated by this procedure is proportional to the calcium carbonate content of the sediment and is measured by a manometer gauge. Since the measured gas pressure is dependent on the atmospheric temperature and pressure, a standard mass of pure calcium carbonate must be analysed to calibrate the measurements of a sample set on a particular day. In order to eliminate the acid vapour pressure generated by the concentrated hydrochloric acid and hence to avoid overweighing the $CaCO_3$ content, a less concentrated hydrochloric acid solution of 6 M was used as suggested by Dunn (1980).

The standard mass of pure $CaCO_3$ required for the carbonate bomb used in this study is 0.79 g. For every measurement series, six standard pure $CaCO_3$ samples were analysed (99% purity in our case). Three of the standards were analysed at the beginning and another three at the end of a measurement series to calibrate the instrument for fluctuations in the atmospheric pressure. In each case an average value for the pure $CaCO_3$ was calculated from the six measurements (m1 – m6). Based on this procedure, the correction factor is defined as

$$\frac{99}{\frac{m1+m2+m3+m4+m5+m6}{6}}$$

and was used to correct every measurement in a particular measurement series.

1.3.3 Data processing and visualization

Standard commercial software packages were used for data processing and visualization. Thus, SigmaPlot™ and TableCurve™ of Jandel Scientific were applied for

most of the data visualisation and curve fitting. For the generation of isoline maps and geographic maps, Surfer™ of Golden Software was employed. PeakFit™ of Jandel Scientific was used to determine the divides between grain populations in grain-size frequency distributions. In addition, two Fortran77 programs were specifically written to calculate the grain size parameters on the basis of percentile and moment methods, respectively. The programs were operated under freeware GNU Fortran77 Compiler for Linux operating system on PCs.

2 Mass physical sediment properties

2.1 The total sediment

2.1.1 Sediment type

Based on the classification of Shepard (1954), of the 217 samples collected on the regular grid, 85.46% classified as sand, 8.81% as silty sand, 4.85% as sandy silty clay, and 0.88% as clayey silt and sandy silt. In terms of the hydrodynamic subdivision introduced by Pejrup (1988) the large majority of samples fall into the hydrodynamic group III (Fig. 2-1).

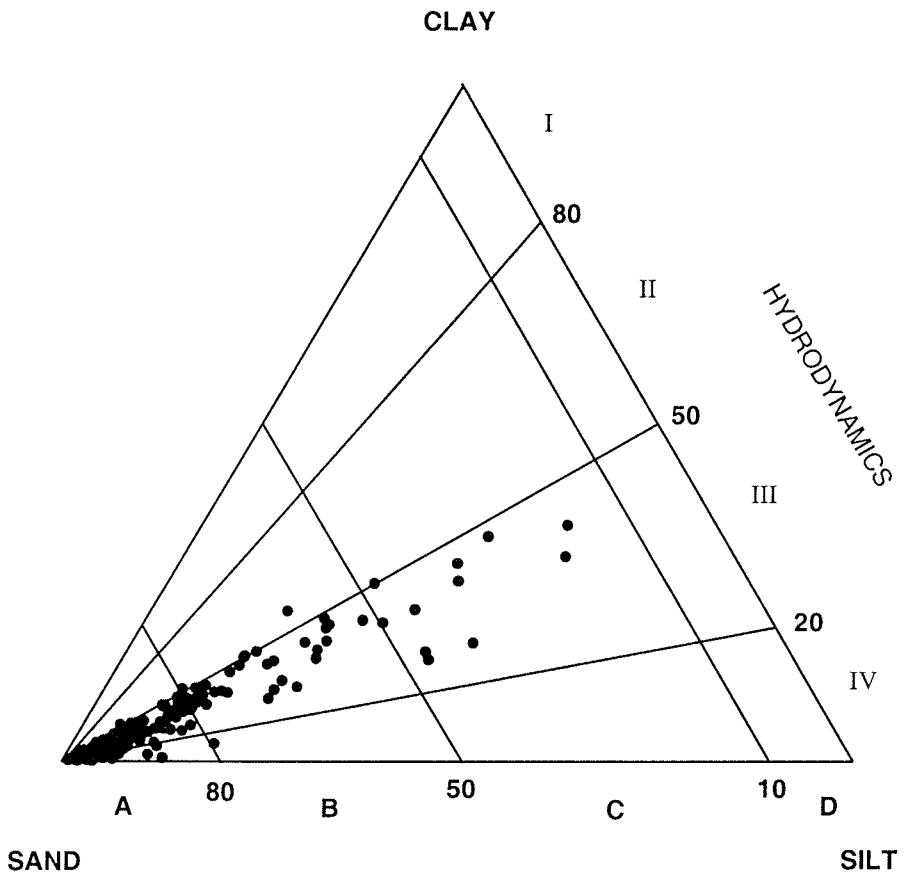

Figure 2-1 Classification of the sediments after Pejrup (1988)

2.1.2 Compositional character of mud

The grain size composition of the muds were found to be different in every sample. Most of the samples display a single obvious peak on the coarse side of the distribution and a flat tail on the fine side (Fig. 2-2). Only a few samples have tails on the fine side only and no coarse peaks. This means that the mud in the study area is predominantly composed of two sub-populations.

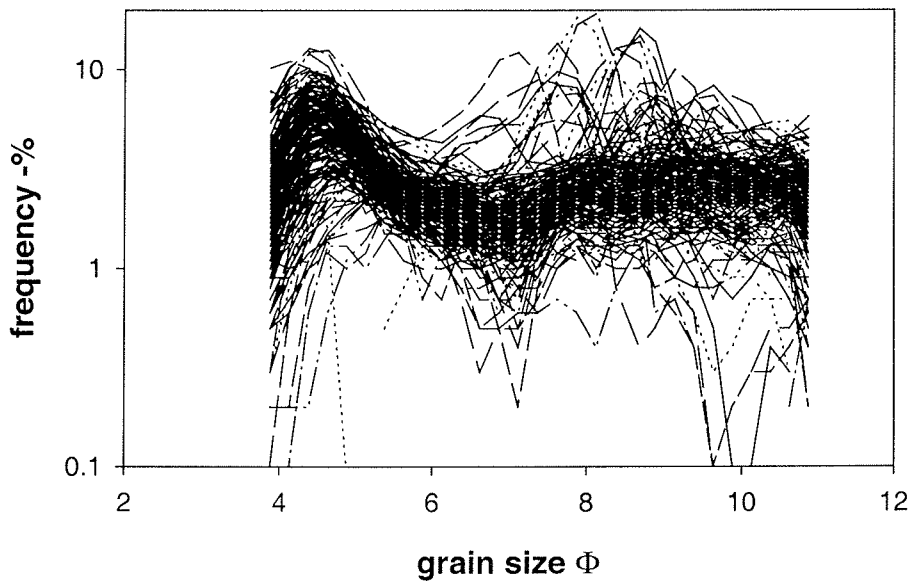

Figure 2-2 Grain size distributions of the muds in sediment

In order to visualize an average trend in the size distributions, the frequency distributions of 291 mud samples were pooled and then averaged in discrete steps (Fig 2-3). From this average distribution curve it is clearly evident that the mud is composed of two differently sorted sub-populations. The better-sorted sub-population has a narrow peak centred around 4.50Φ, its fine tail ending at about 6.00 - 6.50Φ. In fact, on many distribution curves only half of this peak appears, suggesting that the coarse silt population probably

represents the fine tail of the sand population. The main components of the fine sub-population, by contrast, begin at about 8.00Φ and end at or beyond 11.00Φ, many samples being truncated at 11.00Φ because of the size limits chosen for the SediGraph analyses. Within this fine range every size category occurs with almost the same probability. In another words, this part of the particle size distribution does not appear to be sorted.

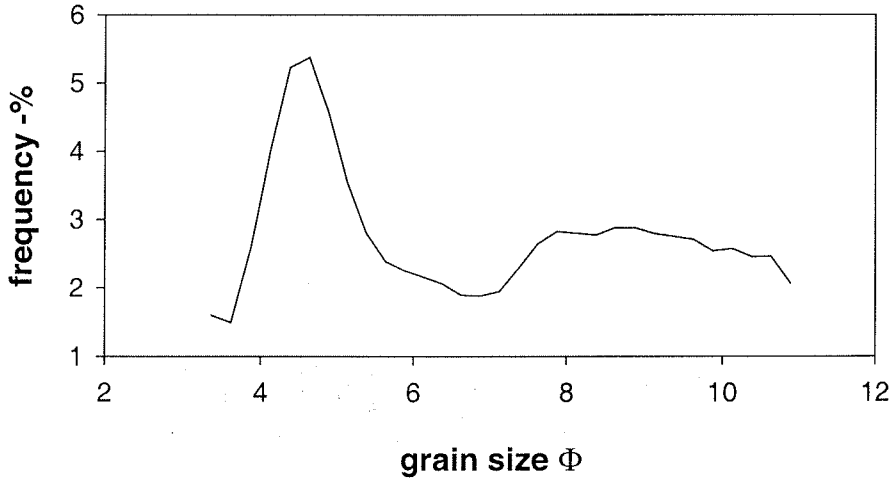

Figure 2-3 Average grain size distribution of the mud fraction

In order to verify the significance of the average grain-size distribution curve, all the size distributions of the 291 mud samples were analysed using the program PeakFit™ of Jandel Scientific. The grain size frequencies of every 1/4Φ size interval were first inverted to change the "valleys" of the curve which represent the lowest frequencies, into "peaks". The transformed data was read into the program, and "peaks" were then fitted using the options of "no-baseline" and "with residual". From this analysis the centres (in Φ) and the amplitudes of all the valleys on the original size distribution curves were determined. Fig 2-4 presents the frequency distribution of the deepest valley in all 291 samples. Clearly, the deepest valley occurs most frequently at a size around 7Φ, or more exactly from 6.7Φ to 7.3Φ. This analysis thus verifies that the 6.7 - 7.3Φ size fraction has the lowest frequency in all mud samples. It

defines the division between the coarse and the fine sub-populations in the mud and thus confirms the trend illustrated by the average distribution curve. In Danish Wadden Sea sediments a grain size of 7Φ has been regarded as a limiting size under which the accumulation process becomes less efficient (Bartholdy and Pheiffer Madsen, 1985). Similar results have also been reported from contourites in the Atlantic (Driscoll et al., 1985; McCave, 1985; McCave et al., 1995; Wang and McCave, 1990).

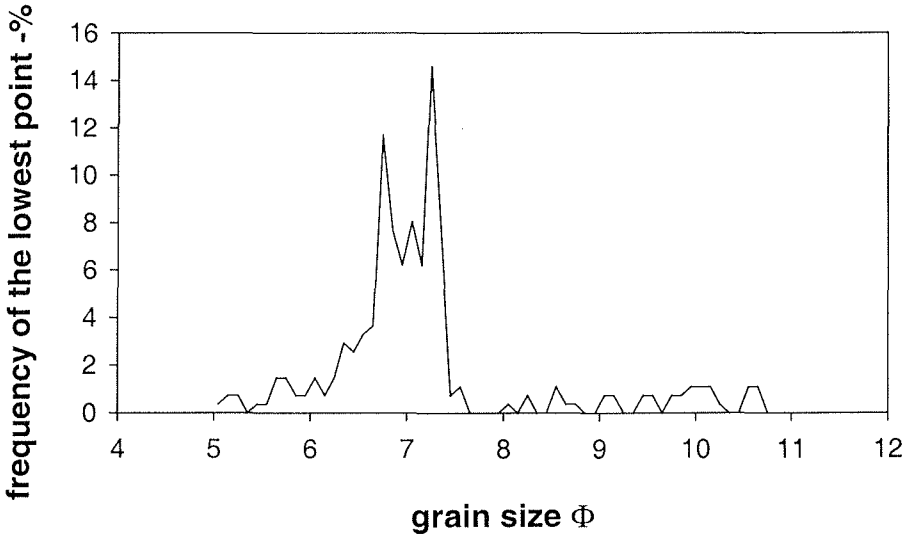

Figure 2-4 The frequency distribution of the lowest point in all mud samples

2.2 Correction procedure for shells and shell fragments

Since many of the mass physical properties describe the structural features of the sediments, they usually not only deal with the weights of the materials but also with the volumes of the particles, voids, interstitial water, and so on. In order to convert masses into volume and *vice versa*, the density of the solid materials must be determined.

Considering the high biological activity in the tidal flat sediments and the sampling method commonly used, it is inevitable that some shells, shell fragments and even living molluscs are included in the sediment samples. Since these commonly represent foreign objects that are not part of the physically transported material, their weight and volume should be removed from the sample if mass physical properties of the transported sediment are to be determined. Instead of direct measurements on every shell and shell fragment, it is more efficient to determine an average density. The volumes are then calculated by means of their weight and the average density of the shell material.

Big shells and shell fragments were separated with a 2 mm mesh sieve and weighed. According to Hertweck (1978, 1995) and Wehrmann and Hertweck (1998), *Cerastoderma edule, Mytilus edulis, Scrobicularia plana, Mya arenaria* and *Littorina littorea* are common molluscs in the East Frisian tidal flats. Shells of these molluscs were therefore also collected in the field. In the laboratory, the shells were broken down and mixed, and their density measured by pycnometer (see 1.3.2.2). The average density of these shells is 2.79 g/cm^3 which is the average of 7 measurements with a maximum of 2.80 g/cm^3, a minimum of 2.77 g/cm^3, and a standard deviation of 0.01 g/cm^3 (Table 2-1). This average shell density of 2.79 g/cm^3 was then used to calculate shell volumes on the basis of their weights. All the mass physical parameters discussed in this study were corrected in this way.

Table 2-1 Measurement of the density of common shell material

Number of Samples	Max. Density g/cm^3	Min. Density g/cm^3	St. Deviation g/cm^3	Average Density g/cm^3
7	2.80	2.77	0.01	2.79

2.3 The grain density of the sediments

In this study, all the samples were collected using vials with a constant volume of 52 cm^3. After the correction for shell volumes and weights, the wet and dry bulk densities were directly calculated using the corrected wet weights. Because the sediments in the study area range from pure sands to sandy silty clays, it was not considered advisable to use a single average grain density to cover such a wide span of different sediment types. In order to obtain

a more accurate picture of sediment-specific grain densities, some 60 subsamples were taken from the sand fraction (>4Φ) and 16 from the mud fraction (<4Φ). Of these, the grain density of the sand and the mud were measured separately using the pycnometer method (see 1.3.2.2). Among the 60 sand samples, the maximum and the minimum grain densities were 2.74 g/cm³ and 2.50 g/cm³, respectively; this corresponds to an average density of 2.66 g/cm³ with a standard deviation of 0.03 g/cm³. In the 16 mud samples, the maximum grain density was 2.68 g/cm³ and the minimum one 2.45 g/cm³; this corresponds to an average of 2.56 g/cm³ with a standard deviation of 0.06 g/cm³ (Table 2-2). Depending on the sediment composition of every sample, i.e. the proportions of mud and sand, the average grain density of every sample was calculated using the above mean values. The results show that the grain density of the sediment in the study area varies between 2.58 g/cm³ and 2.66 g/cm³, depending on the proportions of sand and mud in the samples, the average being 2.64 g/cm³.

Table 2-2 Statistics of the grain density measurements

Material	Sand	Mud	All
Number of Samples	60	16	321
Max. Density (g/cm³)	2.74	2.68	2.66
Min. Density (g/cm³)	2.50	2.45	2.58
St. Deviation (g/cm³)	0.03	0.06	0.02
Average Density (g/cm³)	2.66	2.56	2.64

2.4 Porosity and void ratio

Porosity (n) is an important mass physical parameter of the sediment. It is defined as the percentage of the volume of the voids in a given volume of a sediment sample. Another parameter, the void ratio (e), is also used. It represents the volume of voids divided by the volume of the solid material. For non-gaseous, water-saturated sediment the porosity and void ratio can be transformed from one into the other using the following equations:

$$n = \frac{e}{1+e} \qquad \textbf{2-1}$$

and:

$$e = \frac{n}{1-n} \qquad \textbf{2-2}$$

The volume of the voids is equal to the volume of pore water in non-gaseous, water-saturated sediment. The water content can thus be applied to directly calculate the porosity if the total volume of the water-saturated sediment sample is known. Alternatively, if the total volume of the water-saturated sediment sample is not known, then the porosity can be approximated by using the water content and the average grain density in the following equation (Lambert and Bennett, 1972):

$$n = \frac{Vw + Vss}{\frac{Wd}{Dg} + Ww} \times 100 \qquad \textbf{2-3}$$

where Vw is the volume of the water (being approximately equal to the weight of the water Ww in g); Wd is the weight of dry solids including salts; Dg is the average grain density; Vss is the volume of the salt.

2.4.1 Salt correction

Along the Wadden Sea coast the salinity of the water is not 35‰, but varies between 26‰ and 33‰. To correct for seawater with different salinities the density of the sea surface water is calculated using the International Equation of State of Seawater recommended by UNESCO (1981). By definition, the density of sea water at one standard atmosphere ($\rho = 0$) is to be computed from the practical salinity (S) and the temperature (t °C) with the following One Atmosphere International Equation of State of Seawater of 1980:

$$\begin{aligned}\rho(s,t,0) = \; & \rho_w + (8.24493\times10^{-1} - 4.0899\times10^{-3}t + 7.6438\times10^{-5}t^2 \\ & - 8.2467\times10^{-7}t^3 + 5.3875\times10^{-9}t^4)S + (-5.72466\times10^{-3} \\ & + 1.0227\times10^{-4}t - 1.6546\times10^{-6}t^2)S^{3/2} + 4.8314\times10^{-4}S^2\end{aligned} \qquad \textbf{2-4}$$

where ρ_w, the density of the Standard Mean Ocean Water (SMOW) taken as pure water reference, is given by:

$$\begin{aligned}\rho_w = \; & 999.842594 + 6.793952\times10^{-2}t - 9.095290\times10^{-3}t^2 \\ & + 1.001685\times10^{-4}t^3 - 1.120083\times10^{-6}t^4 \\ & + 6.536332\times10^{-9}t^5\end{aligned} \qquad \textbf{2-5}$$

The One Atmosphere International Equation of State of Seawater of 1980 is valid for practical salinities from 0 to 42‰ and temperatures from -2 to 40°C. For seawater with salinity S and a water content of X g the volume of the salt (Vss) is calculated as follows:

$$Vss = \frac{X + \frac{S \cdot X}{1000 - S}}{\rho(s,t,0)} - Vw = (\frac{1 + \frac{S}{1000 - S}}{\rho(s,t,0)} - 1)Vw \qquad \textbf{2-6}$$

If:

$$k = \frac{1 + \frac{S}{1000 - S}}{\rho(s,t,0)} - 1 \qquad \textbf{2-7}$$

then:

$$Vss = k \cdot Vw \qquad \textbf{2-8}$$

Table 2-3 Salts correction factors at 23°C

Salinity ‰	k	Salinity ‰	k	Salinity ‰	k
1	0.0027	15	0.0063	29	0.0103
2	0.0030	16	0.0066	30	0.0106
3	0.0032	17	0.0069	31	0.0109
4	0.0035	18	0.0072	32	0.0112
5	0.0037	19	0.0074	33	0.0115
6	0.0040	20	0.0077	34	0.0117
7	0.0042	21	0.0080	35	0.0120
8	0.0045	22	0.0083	36	0.0123
9	0.0047	23	0.0085	37	0.0126
10	0.0050	24	0.0088	38	0.0129
11	0.0053	25	0.0091	39	0.0133
12	0.0055	26	0.0094	40	0.0136
13	0.0060	27	0.0097	41	0.0139
14	0.0061	28	0.0100	42	0.0142

Using equations 2-4, 2-5 and 2-7, a list of k for seawater with different salinities at room temperature (23°C) was computed (Table 2-3). In the Otzum tidal basin, the average sea water salinity is 30‰. This corresponds to a Vss of about 1.06% of the volume of the water.

For seawater with 35‰ the *Vss* is 1.2%. This value is identical to the one of Lambert and Bennett (1972).

2.4.2 Porosities determined directly and indirectly

As a measure of reliability, porosities of all the samples in the study area were determined using equation 2-3. These results were compared with the porosities determined

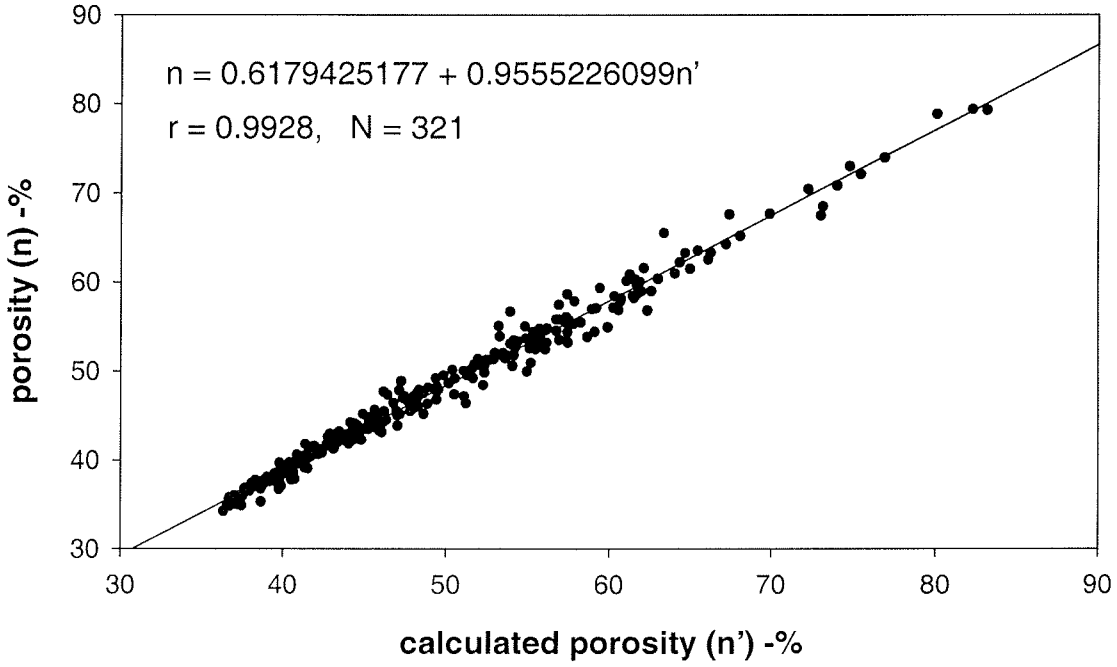

Figure 2-5 The correlation between calculated and measured porosities

directly by the vial method after shell correction and salt correction, i.e. the volume of water in every sample was taken as the volume of the void. The relationship between the directly and indirectly determined porosities is as follow (Fig. 2-5):

$$n = 0.6179425177 + 0.9555226099 \cdot n' \quad (r = 0.9928,\ N = 321) \qquad \textbf{2-9}$$

Here, n is the directly determined porosity after shell and salt corrections in %; n' is the porosity computed using equation 2-3. Although the correlation is excellent (r = 0.9928) the regression line is offset by a small amount. The offset may be due to the values of Wd in the equation, i.e. the weight of solids including salt. Nevertheless, the method of Lambert and Bennett (1972) to determine the porosity through average grain density and water content can evidently also be applied with good confidence in this case.

2.4.3 Porosity, void ratio and the structural characteristic of the sediment

An interesting characteristic of the sediment in the study area is that the porosity increases linearly with increasing mud content. By contrast, the void ratio also increases with mud content, but there is an inflection point at a mud content of about 50%, i.e. for mud contents > 50% the volume of the voids increases more rapidly than that for mud contents < 50% (Fig. 2-6). This means that around 50% mud content there is a structural break between the sandy and the muddy sediments. The mass of mud in a given volume, namely the mud concentration, is evidently a very important index for the structural character of the sediment.

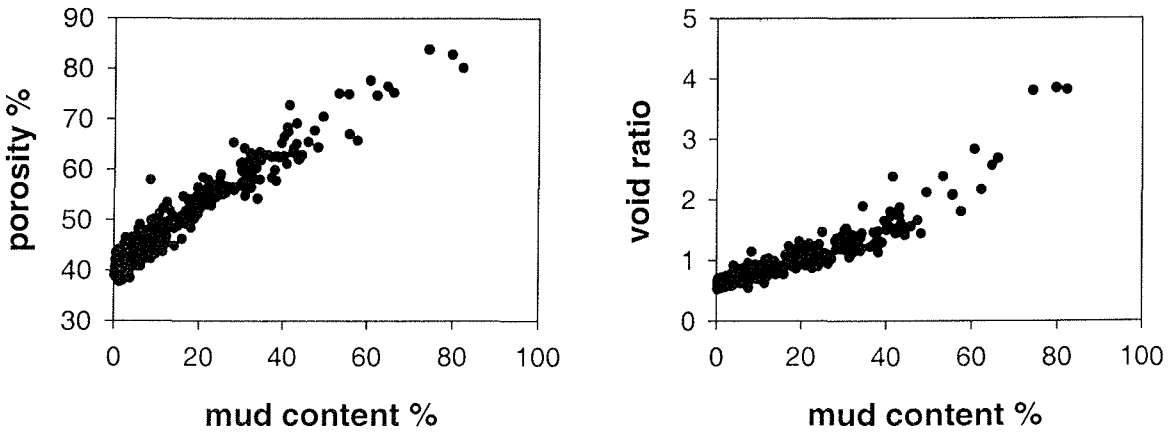

Figure 2-6 Relationships between porosity, void ratio and mud content

Fig. 2-7 illustrates some measures commonly applied to describe the character of the marine sediments. In this case the two different concepts as critically analysed by Flemming and Delafontaine (2000) are highlighted. Concentration here refers to the mass of material in a unit volume, whereas content denominates a mass in a unit mass.

Since marine sediments are usually composed of sand, mud and water, the relationships between sand content, mud content and water content can be easily deduced. Their spatial relationships, however, are not easily determined because these are dependent on sediment structure. Sediments with the same sand and mud content can have quite different structures. For example, a group of sediments with the same sand and mud components but different porosities or water contents, will have different structural attributes. This is illustrated in Fig. 2-7. If the mud content increases, then the sand content must obviously decrease. Similarly, if the mud concentration increases, the sand concentration also decreases, but when the sand concentration reaches about 0.5 g/cm^3, the mud concentration begins to fluctuate, i.e. it seems to remain constant on average. The mud concentrations of the surface sediments in the study area at first increase in curvi-linear fashion as the mud content increases. However, as the mud content reaches about 50%, its concentration begins to depart from the general trend. The values begin to fluctuate and seem to approach a maximum at a mud content of about 60% before beginning to drop again. If the relationships between water concentration, sand concentration and mud concentration, i.e. between the mass of water, the mass of sand, and the mass of mud in a given volume, are compared, it can be seen that under natural condition the increase of the mass of mud in a given volume is proportional to the decrease of the mass of the sand in the same volume, while the increase of the mass of water in the same volume is proportional to the increase of the mass of the mud. However, when the mud content exceeds about 50%, any further reduction of the mass of the sand in a given volume is no longer compensated by a proportional increase in the mass of the mud. Instead, the mass of the water in the same volume increases rapidly. This is reflected by the inflection point in the mud content/void ratio relationship (cf. Fig. 2-6). As a result, the sediments become extremely soft. This is also evident in Fig. 2-13 which shows that these sediments have the lowest shear strength.

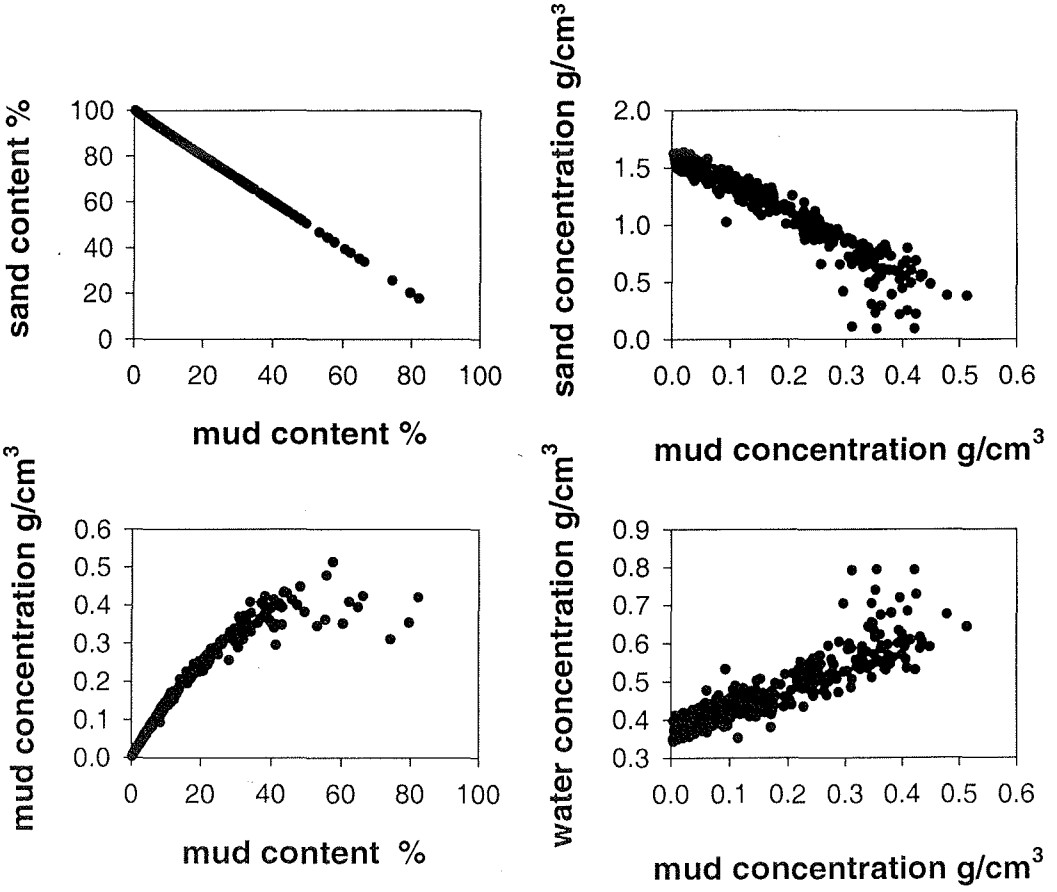

Figure 2-7 Comparison between weight measures (contents) and volume measures (concentrations)

From these observations it can be concluded that under natural, surficial depositional conditions water-saturated sediments are petrographically characterized by three textual components, namely particles (sand particles), matrix (mud fractions) and the pore water or pore space. A particle-dominated sediment is very different from a matrix-supported sediment. If the sediment is sandy and particle dominated, i.e. if the mud content is < 50%, the relationship between the particles and the matrix is inversely proportional, i.e. an increase of the mass of the matrix is associated with a decrease in the mass of the particles. On the

other hand, if the sediment is matrix dominated, i.e. if the mud content is > 50%, then the mass of the water plays an important role. In such cases, a decreasing mass of sediment particles is rapidly compensated by an increase in the mass of water but not by a corresponding increasing in the mass of matrix materials. The latter remains either unchanged or even decreases slightly. If the water contents of such sediments are known, then the mud content can be calculated by the following equation (Fig. 2-8):

$$M = -39.203351 + 2.1951787 \cdot W - 0.0049787926 \cdot W^2 \quad (r = 0.9688,\ N = 321) \qquad \textbf{2-10}$$

M - mud content (%); W - water content (%).

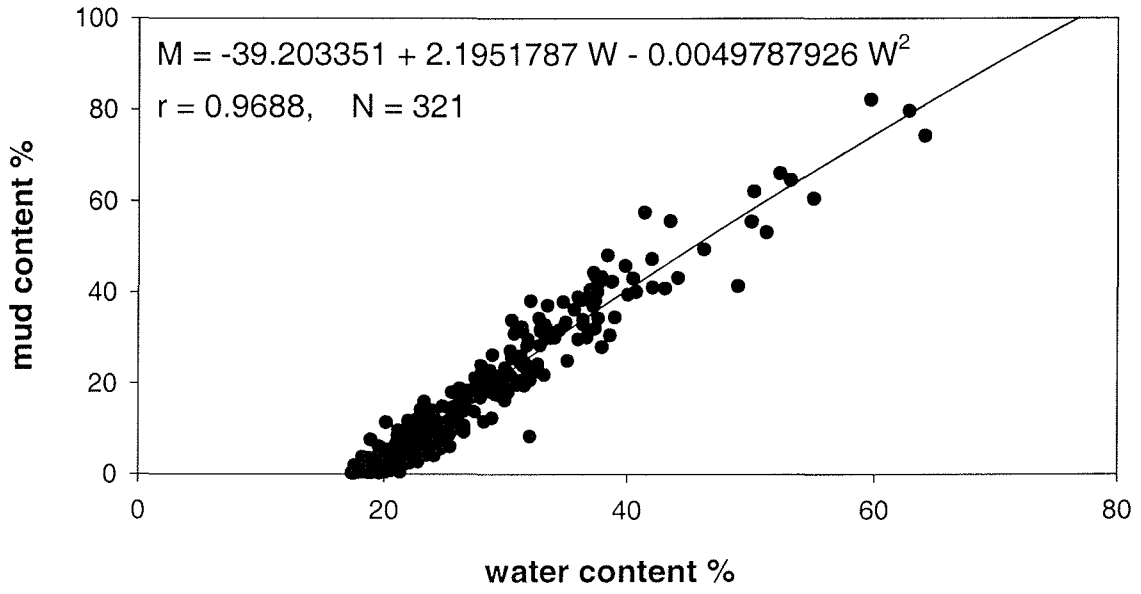

Figure 2-8 Relationship between water content and mud content

2.5 Bulk density

Bulk density is the weight of an object or material divided by its volume, including the volume of its pore spaces (Bates and Jackson, 1980). It is called "unit weight" in geotechnology. By definition, it does not take care of the degree of water saturation. However, marine sediments are usually water-saturated and hence wet bulk density has to be distinguished from dry bulk density.

Bulk density is a variable quantity for a given type of sediment. It varies with structural condition of the sediment, especially with grain packing. For this reason, it is often used as a measure of sediment structure. A common technique for measuring unit weight is by inserting a container of known volume into a sediment, extracting the container filled with non-compacted sediment and then determining sediment weight. This gives the mass of sediment in a unit volume. In the present study, all the samples were collected directly on the tidal flats during low tide using the technique described above. Since biological activity is common and often intense on tidal flats, it is inevitable that some shells, big shell fragments or even living molluscs may be incorporated into the sediment sample. Such material is often extraneous and its weight and volume should thus be removed from the sediment mass if the unit weight is to be determined.

In the present study the term "wet bulk density" is used to refer to the unit mass of the original water-saturated sample without shells or shell fragments. The term "dry bulk density" is used to refer to the unit mass of the original sample without salt and shells or shell fragments after drying.

2.5.1 Wet bulk density

In the present context, wet bulk density is the wet mass of material in a unit volume of sediment. Wet bulk density is a mass physical sediment property which is used in geotechnical engineering to calculate, amongst others, the overburden of sediment over subaqueous structures such as pipelines. In geology it would, amongst others, be applied to estimate compaction factors for underlying strata.

In non-gaseous, water-saturated sediment, wet bulk density or wet unit weight is correlated with water content and average grain density. Bennett et al. (1971) provide a rapid, universal method of determining wet unit weight if the water content and the average grain density are known:

$$\gamma = \frac{Wt}{\frac{Wd}{Dg} + Ww} = \frac{Wt \cdot Dg}{Wd + Ww \cdot Dg} \qquad \textbf{2-11}$$

where γ is the wet unit weight or wet bulk density (g/cm³), Wt is the total weight (g), Wd is the weight of the dry solids including salt (g), Ww is the weight of the water (g), and Dg is the average grain density (g/cm³).

If sediments are composed of the same material, then the variability of wet bulk density should be a good indicator of sediment structure, in particular the degree of compaction. Indeed, Jepsen et al. (1997) and Roberts et al. (1998) demonstrated this when studying the effects of bulk density on the rate of sediment erosion. Keeping the shear stress constant, they found that the erosion rate decreased with increasing bulk density (i.e. with increasing sediment compaction). This dependence was very pronounced in fine sediments but disappeared completely in coarse sediments.

2.5.1.1 Comparison of the wet bulk densities

As shown above, wet bulk densities can be approximated on the basis of equation 2-11 if the water contents and the average grain densities are known. Comparing such calculated wet bulk densities with directly measured ones reveals a surprisingly good correlation (Fig. 2-9).

It will be noted that the regression line in Fig. 2-9 is slightly offset, such that the measured wet bulk densities are 0.025-0.03 g/cm³ lower than the calculated ones. The small offset in the correlation between the two data sets may have two explanations. Firstly, it should be noted that equation 2-11 is an approximation method which provides first order estimates only. Its accuracy is dependent on the accuracy of the assumed grain density, and any systematic error will automatically produce an offset of the type observed in Fig. 2-9.

Secondly, all the measured wet bulk densities were derived after correction for shell content, no such corrections having been applied in the case of the calculated wet bulk densities. As in the previous case, the resulting differences between the two data sets will obviously produce a small offset in the position of the regression line. Nevertheless, the rather small offset, coupled with an overall good correlation, demonstrates that the method of Bennett et al. (1971) produces very good approximations, and that its use can be safely recommended in circumstances where direct measurements are not possible. The relationship is expressed by the equation:

$$WBD = -0.027619184 + 0.9938426319 \cdot WBDc \qquad r = 0.9716,\ N = 321 \qquad 2\text{-}12$$

where WBD is the wet bulk density (g/cm³), and $WBDc$ is the calculated wet bulk density (g/cm³).

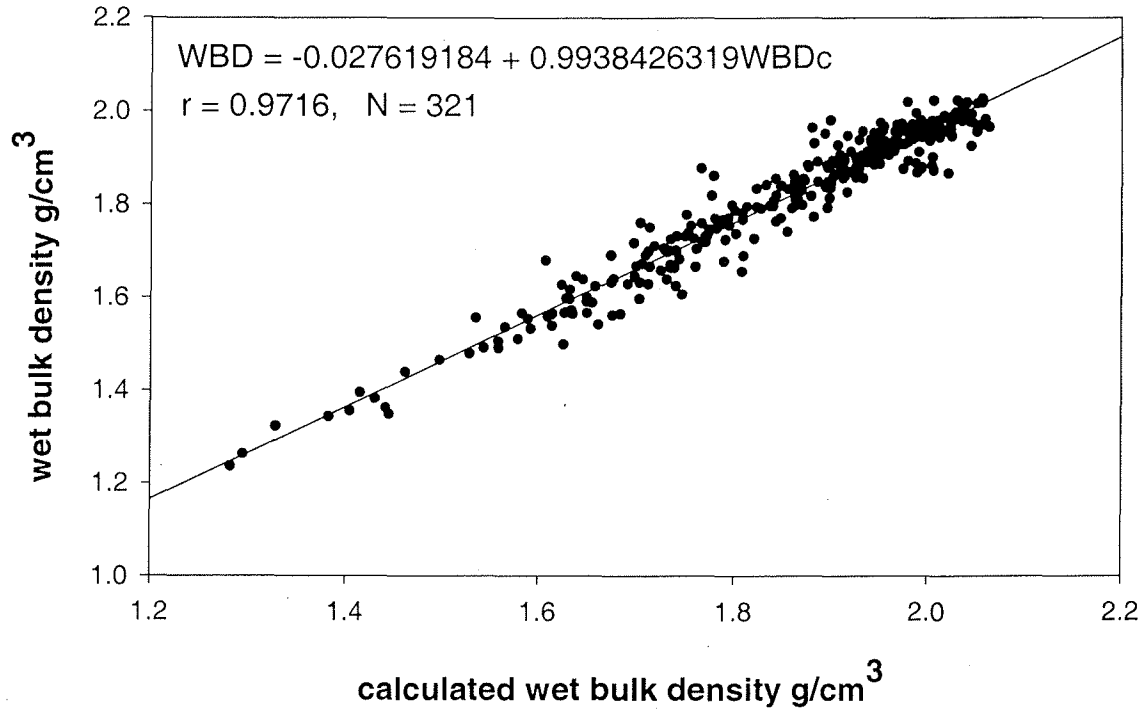

Figure 2-9 The relationship between measured wet bulk density and calculated wet bulk density using equation 2-11

2.5.1.2 A rapid method for obtaining wet bulk density

As pointed out above, wet bulk density varies as a function of grain density and water content. Grain density, in turn, is not constant but depends on the sand/mud ratio in a sediment sample. In the study area, grain density was shown to vary between 2,66 g/cm³ for pure sand and 2.56 g/cm³ for pure mud. Knowing the sand/mud ratios, it was thus possible to calculate the mean grain density and hence the wet bulk density for every sample. Since water contents were also measured, it was possible to define the relationship between the two parameters (Fig. 2-10).

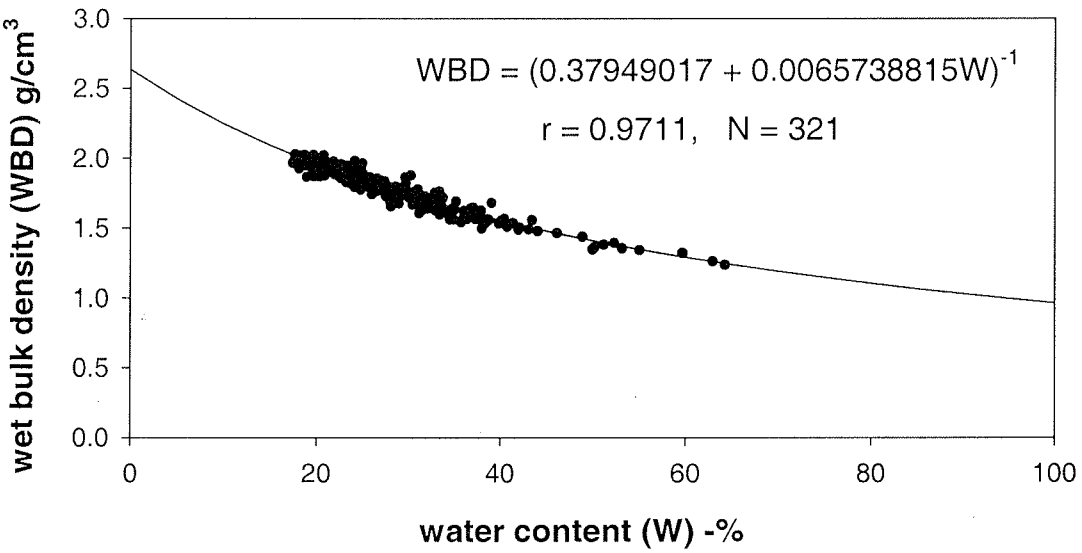

Figure 2-10 Water content versus wet bulk density

Fig. 2-10 illustrates the extremely good correlation between wet bulk density and water content. Ideally, the correlation coefficient should be 1, the slight scatter in the data reflecting inadvertent but overall small errors introduced in the course of sediment sampling, sample transport and laboratory processing. The relationship can be accurately described by the equation:

$$WBD = (0.37949017 + 0.0065738815 \cdot W)^{-1} \quad (r = 0.9711,\ N = 321) \qquad \textbf{2-13}$$

where WBD is the wet bulk density (g/cm³), and W is the water content in weight-% (i.e. the weight of water divided by the weight of the sediment sample including water and salt, multiplied by 100) (Fig. 2-10). Provided a sediment is predominantly composed of average terrigenous mineral matter, as is the case in the Otzum tidal basin and the whole Wadden Sea, for that matter, equation 2-13 can be applied universally for the prediction of wet bulk density purely on the basis of water content. This is of particular value since water contents are determined more easily, more rapidly, and with less technical effort than, for example, sand/mud ratios.

2.5.2 Dry bulk density

2.5.2.1 Structural affinities of dry bulk density

Dry bulk density is a measure quantifying the dry mass of material in a unit volume. As shown in Fig. 2-11, the dry bulk density of any given sediment is directly proportional to the wet bulk density, both decreasing with increasing mud content, the former more rapidly than the latter.

The sediments of the study area, which comprise almost pure quartz sands, have an average wet bulk density of about 2.00 g/cm³, and an average dry bulk density of about 1.60 g/cm³. The difference between the two bulk density measures for pure sand thus amounts to about 0.4 g/cm³. If a sediment has a mud content of 50%, its wet bulk density and dry bulk density are about 1.50 g/cm³ and 0.80 g/cm³, respectively. The wet bulk density is 0.70 g/cm³ higher than the dry bulk density in this case. If the mud content is 80%, then the wet bulk density is about 1.30 g/cm³ and the dry bulk density about 0.40 g/cm³, the difference now amounting to about 0.9 g/cm³.

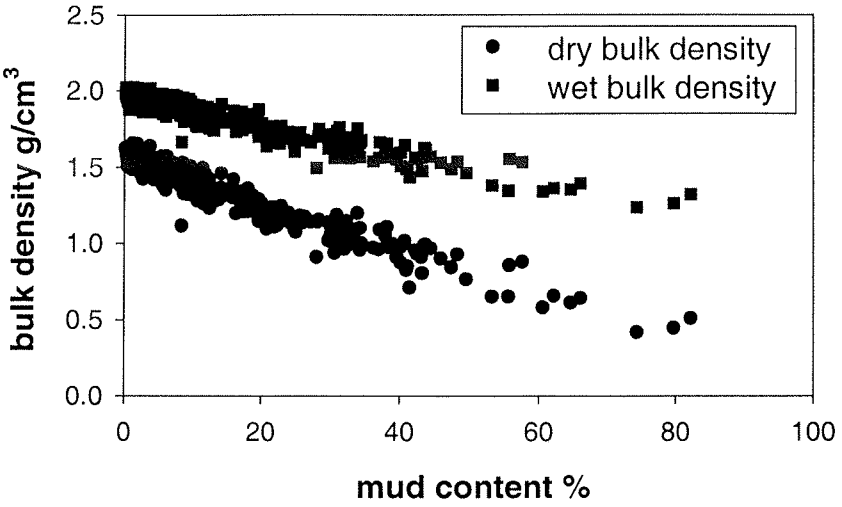

Figure 2-11 Variation of wet and dry bulk densities as a function of mud content

As pointed out earlier, both porosity and void ratio increase with increasing mud content, the latter more rapidly once the mud content reaches 50%. In comparison to sand, muds have a much larger pore volume and hence a larger void ratio and water content. In similar sediments, especially if they are muddy, any scatter in the dry bulk density data always indicates differences in compaction (i.e. fluctuating water contents). As evident from Fig. 2-11, such scatter is commonly observed in most field data. As a consequence, if data on mass physical sediment properties are required, preference should always be given to site-specific measurements over estimates based on some mean reference value.

2.5.2.2 A rapid method for calculating dry bulk density

In cases where the exact masses of sediment or sedimentary components in a given area or volume are required, e.g., when mass balancing sediment turnover, or when monitoring the fluxes of organic matter and other particulate substances, accurate measurements of dry bulk density are necessary. For example, if two sediment samples with

the same grain-size composition both contain 10% by weight of a contaminant but, on account of different sediment compactions, one has a dry bulk density of 1.00 g/cm³ and the other of 0.5 g/cm³, the concentration of the contaminant is 0.10 g/cm³ in the first case, and 0.05 g/cm³ in the second case. As demonstrated by Flemming and Delafontaine (2000), such bulk-density controlled differences in contents and concentrations can have far-reaching ecological implications. Since mass physical sediment properties are receiving increasingly more attention world-wide for a number of reasons (cf. Introduction), it would clearly be of considerable benefit if dry bulk density could be determined by a similarly simple and rapid method as wet bulk density. Since dry bulk density is directly proportional to wet bulk density (cf. Fig. 2-11), the former must obviously be similarly well correlated with water content as the latter. This is illustrated in Fig. 2-12.

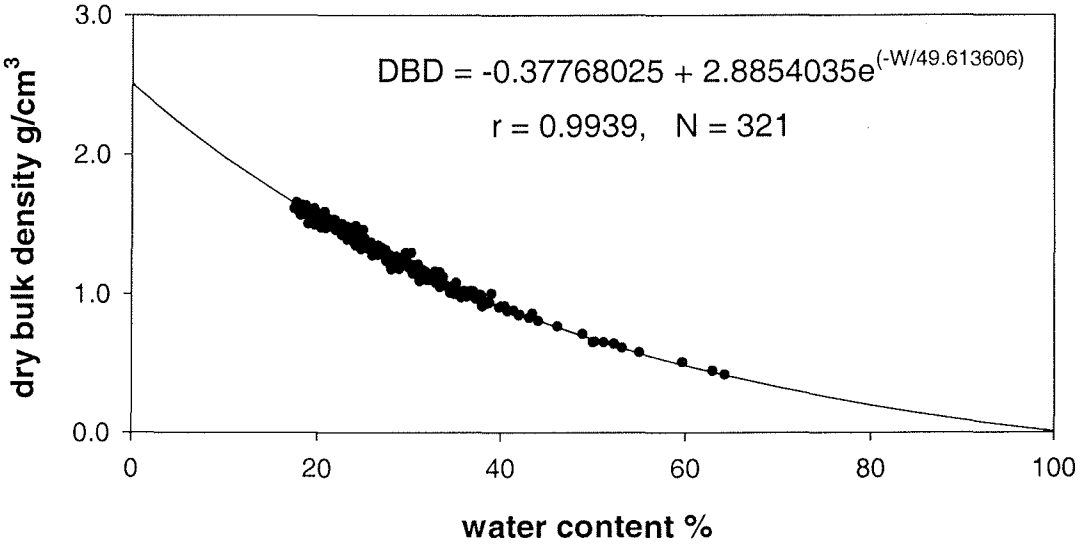

Figure 2-12 Water content versus dry bulk density

Interestingly, with r = 0.9939 the correlation coefficient of the regression in Fig. 2-12 is slightly higher than that in Fig. 2-10 (r = 0.9711), i.e. the scatter of the data is lower. This is easily explained by the fact that the measurement of dry bulk density is less intricate than in

the case of wet bulk density. The difference, however, is marginal and of little consequence. The relationship between dry bulk density and water content of the sediments in the study area can be most accurately described by an exponential equation. Thus,

$$DBD = -0.37768025 + 2.8854035 \cdot e^{\left(\frac{-W}{49.613606}\right)} \qquad (r = 0.9939,\ N = 321) \qquad \textbf{2-14}$$

where DBD is the dry bulk density (g/cm³), and W is the water content (weight-%). Again, for average terrigenous mineral matter, this relationship has universal character. It can hence be applied world-wide to sediments of similar composition as those of the Wadden Sea. Thus, to accurately determine dry bulk density, i.e. the most important parameter required for mass balance calculations, it suffices to accurately measure the water content of the sediment.

2.6 Shear strength

The shear strength of a sediment quantifies the resistance of the granular material to deformation when exposed to a tangentially applied force. This resistance includes the internal friction and adhesion of the material. Keil (1954) defined shear strength as the force needed to overcome the resistance of internal friction and adhesion of rock (or a sediment in this case). The shear strength can be expressed as:

$$\tau_s = \sigma \cdot \mu + k_e + k_s \qquad \textbf{2-15}$$

where τ_s is the shear strength, $(\sigma \cdot \mu)$ is the internal friction, and k_e and k_s are measures of the cohesive and adhesive forces between the particles. Internal friction refers to the friction involved in the movement of one particle relative to another which includes both sliding and removal or displacement of particles from interlocking action between adjacent particles. Adhesion is an electro-chemical inter-particle force (bond) which depends on factors such as particle size and shape, minerals types, or the composition of the pore water.

In cohesion-less sediments, the inter-particle forces (adhesion forces) do not play a significant role in the stress-strain behaviour. The dominant resistance comes from solid

friction developed at inter-particle contacts, and interlocking effects due to packing arrangement. In cohesive sediments, by contrast, inter-particle adhesion plays a dominant role in the stress-strain behaviour. Because of the many complex states which a sedimentary system can adopt, the shear strength of a given sediment is not an invariant property. Such states range from a viscous fluid character without strength at the time of deposition, to a solidified rock with high strength under pressure. As a result, shear strength can in some cases be an important indicator of the mass physical properties of a sediment.

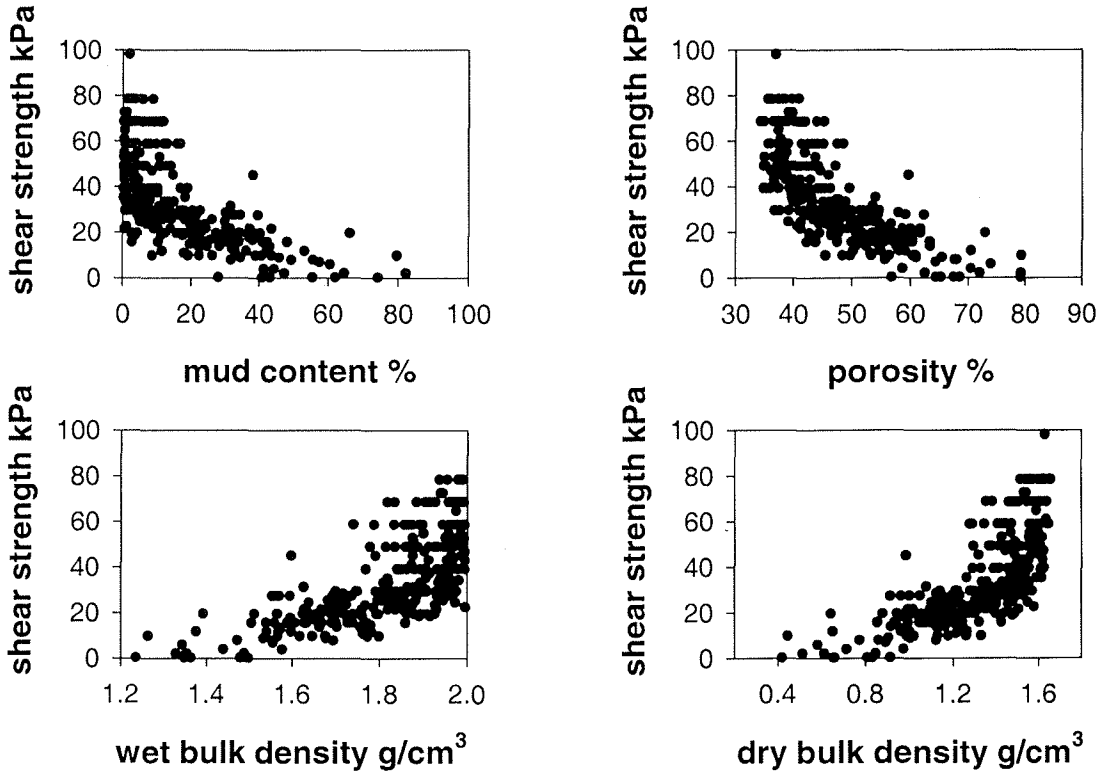

Figure 2-13 Shear strength versus selected mass physical properties

A systematic study of the shear strengths of the sediments in the study area demonstrates that there are marked differences between sand-dominated and mud-dominated sediments. In general, the shear strength decreases with increasing mud content and increasing porosity, muddy sediments having lower shear strengths than sandy sediments, and the latter showing much greater variability. This is illustrated in Fig. 2-13.

The scatter diagrams of Fig. 2-13 demonstrate that sediments having the same or similar mass physical properties, e.g., mud content, porosity, or wet and dry bulk density, can have quite different shear strengths, whereas sediments having different mass physical properties can have similar shear strengths. The scatter diagram illustrating shear strength vs. mud content, for example, reveals that the shear strengths of sediments containing <20% mud show quite a large scatter, the values commonly varying between 10 kPa and 100 kPa. Sediments containing >20% mud, by contrast, show much less fluctuation, the measurements varying between 0 kPa and 30 kPa. How can this phenomenon be explained?

Sands containing <20% mud have a grain-supported framework, i.e. sand grains are in direct contact with each other. As a result, shear strength is mainly controlled by internal friction, the influence of adhesion being negligible. In more muddy sediments, as water content and porosity increase, the grain-supported framework is progressively replaced by a more matrix-supported framework. In correspondence, the role of adhesion increases at the expense of internal friction in defining the shear strength. Since grain-supported sediments can adopt a wide range of packing densities, internal friction shows considerable variation, thus explaining the large range of shear strengths documented in Fig. 2-13.

2.7 Seasonal variability of mass physical sediment properties

2.7.1 Spatial variability (Figs. 2-14 and 2-15)

The Wadden Sea is located at latitudes which experience considerable seasonal changes in air and water temperatures. As a result, the biological activity of intertidal organisms is high in summer and low in winter. It is therefore not unreasonable to expect corresponding changes in at least some of the mass physical properties of the sediments in the study area. In order to monitor potential seasonal changes, a 2 km long test transect was set up on the Neuharlingersieler Nacken (cf. Fig. 1-7). Along this transect eight bulk density and shear strength measurements were repeated at monthly intervals for a period of one year from April 1997 to March 1998. Starting about 150 m from the dike the monitoring stations were spaced about 250 m apart. The four landward stations had mud contents >25%, station 4 being situated close to an intertidal mussel bank. The three seaward stations were dominated

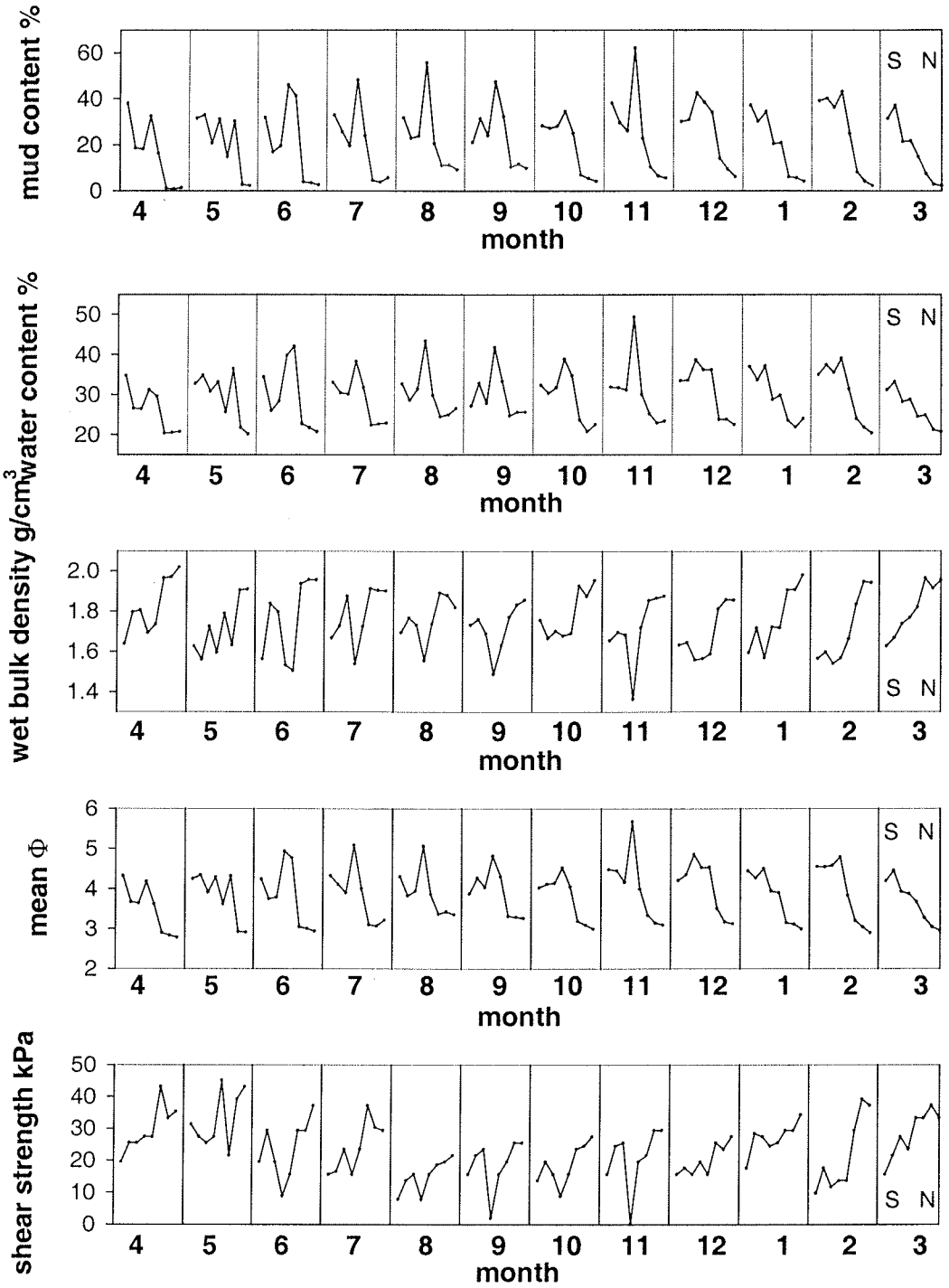

Figure 2-14 Spatial variability of selected mass physical properties along the test transect between April 1997 and March 1998

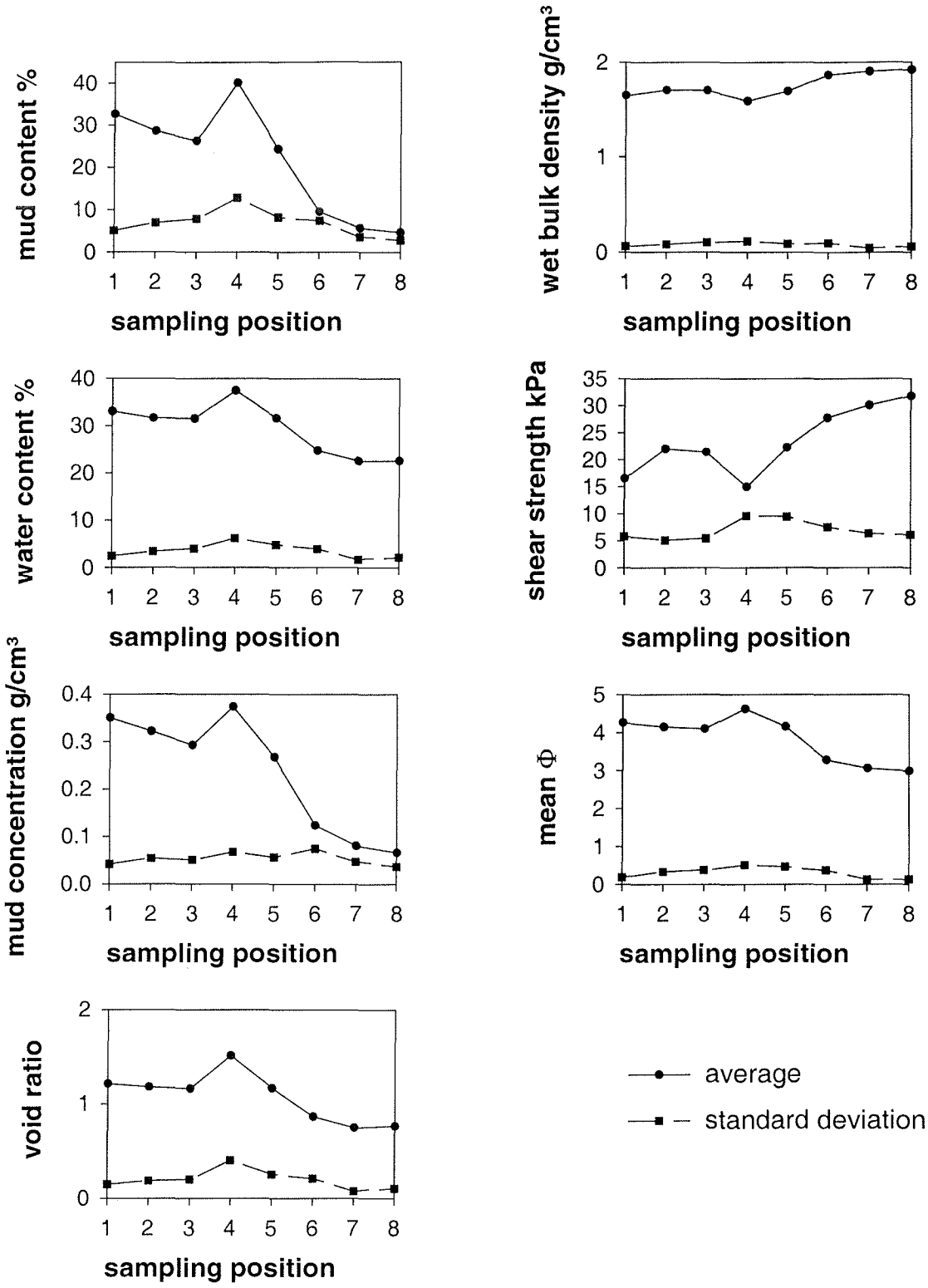

Figure 2-15 Yearly means and standard deviations of measured and calculated mass physical properties along the test transect

by sand (<10% mud), while the intermediate station had a mud content of almost exactly 25%.

The spatial variability of mud contents, water contents, wet bulk densities, mean grain size and shear strength at each station along the test transect in the course of the year is illustrated in Fig. 2-14. In each monthly plot the most landward station (number 1) is located on the left and the most seaward station (number 8) on the right. From this time series the yearly averages and standard deviations for mud contents, mud concentrations, water contents, void ratios, and mean grain sizes were calculated for each sample station (Fig. 2-15). The results clearly show that mud contents, mud concentrations, water contents, and void ratios on average decrease from south (landward) to north (seaward) along the transect. The average measures of wet bulk density, shear strength, and grain size, by contrast, show an opposite trend.

The spatial pattern is in each case dominated by two major trends separated by a pronounced offset between station 5 and 6. In assessing these trends it should be noted that the inflection point at station 4 does not constitute a real, but merely an apparent misfit in the trend defined by stations 1-5. Normalized to mud content, station 4 would occupy a position to the left of station 1 where it would fit perfectly well into the trend defined by this sample group. Similarly, the offset observed in the trend of samples 6-8 is caused by the large change in mud content between station 5 and 6.

The data therefore clearly show that the difference in the mass physical behaviour of the sample suite is controlled by the mud content. Thus, the mean annual mud content at stations 1-5 is 25% and higher, whereas at stations 6-8 it is <10%. In the former case the mud concentrations lie at or above 0.25 g/cm^3, in the latter case they lie <0.1 g/cm^3. The mean annual grain size at stations 1-5 is over 4Φ (i.e. <0.063mm), whereas at stations 6-8 it is around 3Φ (0.125mm). The average water content of stations 6-8 is <30% which corresponds to an average void ratio of <1. By contrast, the water content of stations 1-5 is >30% which corresponds to an average void ratio of >1. As a result, the mean annual wet bulk density and shear strength of stations 6-8 are higher than those of stations 1-5. By comparison, the mass physical properties at station 4 appear to be very different from the other stations at first sight. Interestingly, they also show the largest standard deviations, indicating that the proximity to

the mussel bank induces a larger variability in the mass physical sediment properties in the course of the year (Fig. 2-15).

In summary, it can be concluded that the spatial variability in mass physical properties along the transect are mainly controlled by the site-specific mud contents. As a result, the overall mean annual trends follow the general pattern observed in the larger tidal basin, only the biogenic muds showing a larger variability over the year. The trends also demonstrate that there is a general shoreward directed gradient from which only the biogenic muds depart. The rate of change along this gradient, however, is not uniform but accelerates (or decelerates) for individual properties the closer one gets to the dike.

2.7.2 Temporal variability (Fig. 2-16)

The temporal variability of mass physical sediment properties along the transect are highlighted by the trends observed at stations 2, 4, and 7 (Fig. 2-16). Station 2 is representative of the muddier, landward sample suite, station 7 of the sandier, seaward sample suite, and station 4 represents the influence of the locally produced biogenic muds.

Along the sandy section of the transect (stations 6-8), represented by station 7 in Fig. 2-16, the trend lines described by the mud content, water content, mud concentration, and void ratio have a convex shape, the values peaking at the end of the summer season (September), before dropping again to reach their lowest values at the end of the winter season (May). Corresponding to the trend of the mud content, the bulk densities and shear strengths are highest where mud content is lowest, i.e. at the end of the winter season. The mean grain size at station 7 shows a similar trend, being coarsest in May (ca. 2.8 phi) and finest in September (ca. 3.4 phi).

In contrast to the sandy stations, the seasonal trends of the mass physical properties at the muddy, landward end of the transect (represented by station 2 in Fig. 2-16), are not as straightforward. If anything, the trend lines defined by the mud contents, water contents, mud concentrations, and void ratios have a more concave shape, the values peaking in February

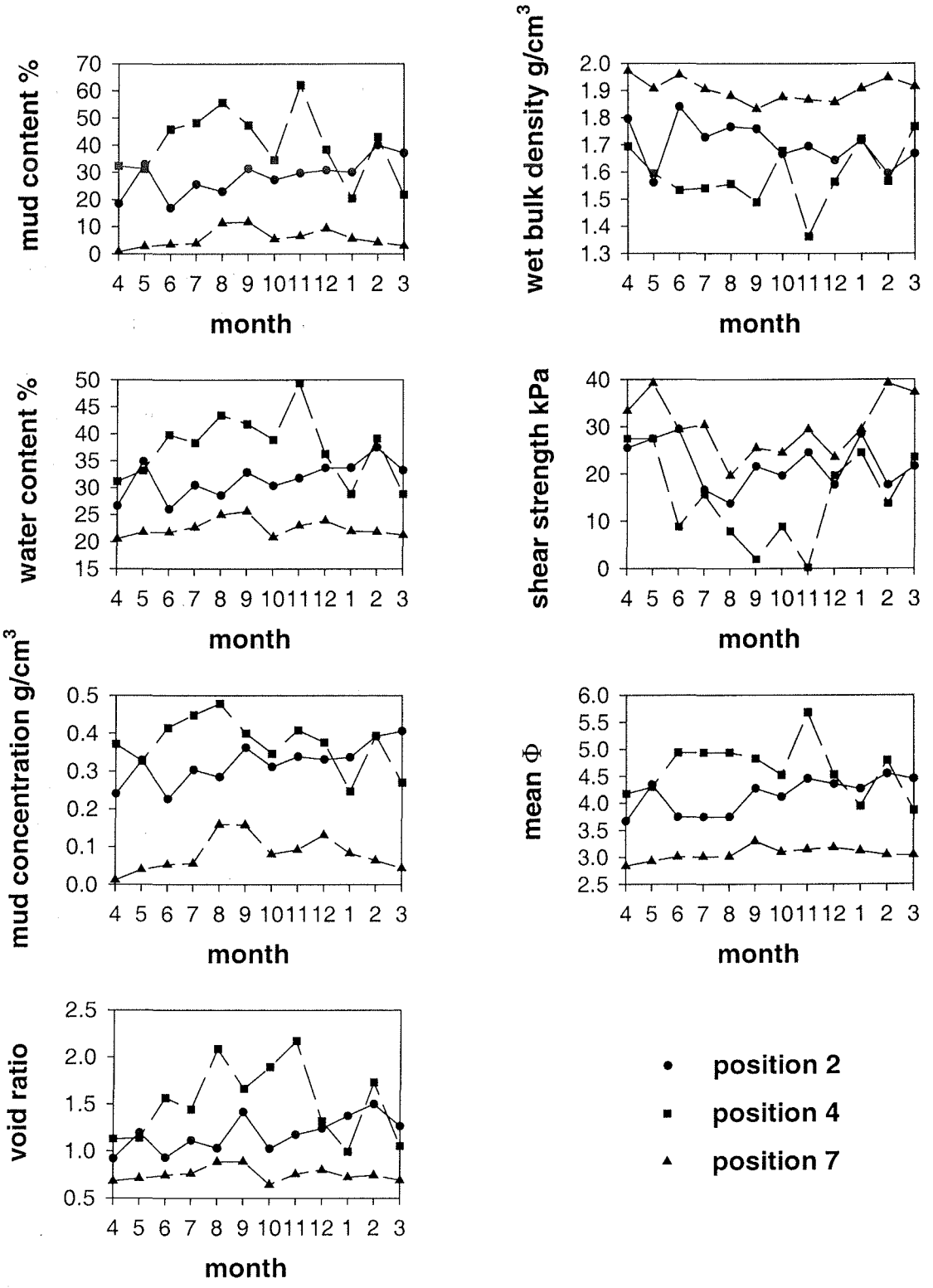

Figure 2-16 Seasonal variability of some mass physical sediment properties at station 2, 4 and 7 along the test transect

and reaching lowest readings in June. The wet bulk densities and the shear strengths peak in June and reach lowest values in May and August, respectively. The mean grain size is coarsest in April (ca. 3.6 phi), and finest in February (ca. 4.6 phi). In comparison to the sandy stations, the muddier stations thus show an essentially reversed trend, the peaks and valleys being offset by a month or two. In addition, the muddy stations are characterized by a greater month to month variability.

The seasonal trends of the mass physical properties at station 4, which is characterized by maximum biogenic mud contents in November (ca. 60%) and lowest in January (ca. 20%), are not, as would intuitively be expected, similar to those of the muddy nearshore stations. Instead, they follow the general trends observed at the sandy stations. However, the rate of change, the month to month variability, and also the range covered by individual parameters are largest at station 4. In this respect it corresponds more to the trends at the muddier stations.

The temporal data on mass physical properties along the test transect clearly demonstrate that there is a measurable seasonal signal in the trend of each parameter. Mud, for example, tends to be more widely distributed in summer and autumn, this dispersal being revealed by a slight increase in the mud contents on the sandy tidal flats and a reduction in mud contents on the muddy tidal flats. In winter and spring, by contrast, the fine-grained sediments deposited on the sandy tidal flats in the course of summer and autumn are resuspended and removed, the proportion of mud in the sediment now increasing on the muddy tidal flats near the mainland dike. Since there is a vigorous exchange of resuspended muds with newly imported suspended material, the observed trend can not be interpreted to simply represent a seasonal redistribution of the fine-grained sediment available in the tidal basin. However, since a basin-wide budget for fine-grained sediment, i.e. an import-export mass balance, is still lacking at this time, many problems concerning the dynamic behaviour of the suspended sediment fraction in the Wadden Sea remain to be resolved.

The extraordinary temporal variability in the mass physical sediment properties at station 4 highlights the fact that biogenic effects, in this case induced by the mussel *Mytilus edulis*, can locally have a strong influence on the character of the sediment. Mussel beds have long been recognized as important mud traps in the Wadden Sea (e.g. Linke, 1954; Flemming and Delafontaine, 1994; Oost, 1995; Meadows et al., 1998). According to Flemming and

Delafontaine (1994), mean accretion rates in intertidal mussel beds are higher in the summer season, whereas in the winter season net deposition decreases to zero or shows erosional trends. Through its filtering activity, *Mytilus edulis* concentrates and deposits mud in the form of faeces and pseudo-faeces. The proximity of station 4 to a mussel bed thus explains the trends in the mass physical sediment properties at this station. In accordance with the filtering activity, the highest mud contents, mud concentrations, water contents and void ratios are reached in the summer season. Such sediments are extremely soft, and due to their low shear strengths, they are particularly prone to resuspension by winter storms.

2.7.3 $CaCO_3$ and organic matter contents in the muds along the test transect

2.7.3.1 Spatial variability (Fig. 2-17)

The mean annual $CaCO_3$-contents of the mud fractions along the transect lie between 10% and 12%. With the exception of stations 4 and 5 which have slightly more elevated values, the $CaCO_3$-contents of the mud fractions show a decreasing tendency in the seaward direction. In general, the mean $CaCO_3$-contents of the muds are thus higher in sediments with higher mud contents (muddy tidal flats) than in sediments with lower mud contents (sandy tidal flats). At stations 4 and 5, i.e. adjacent to the mussel bed, the carbonate contents are slightly higher. In the case of station 4 this is consistent with the fact that here the mud content reaches its highest value along the transect. Only station 5 thus departs from the general trend, the reason for this being unknown.

The mean annual organic matter content in the muds along the transect varies from 5% to 7%, the trend being reversed to that of the carbonate content. The lowest organic matter content occurs at station 1 near the dike, the highest at station 7. In contrast to the mean annual $CaCO_3$-content, the mean annual organic matter contents in the mud fractions are thus higher in sediments with low mud contents (sandy tidal flats), and lower in sediments with higher mud contents (muddy tidal flats). In this case station 8 departs from the general pattern, the reason being again unknown. Interestingly, with respect to mud and organic matter content station 4 shows the highest annual variability as revealed by the relatively large standard deviations. With respect to carbonate content, on the other hand, it has the lowest variability of all stations.

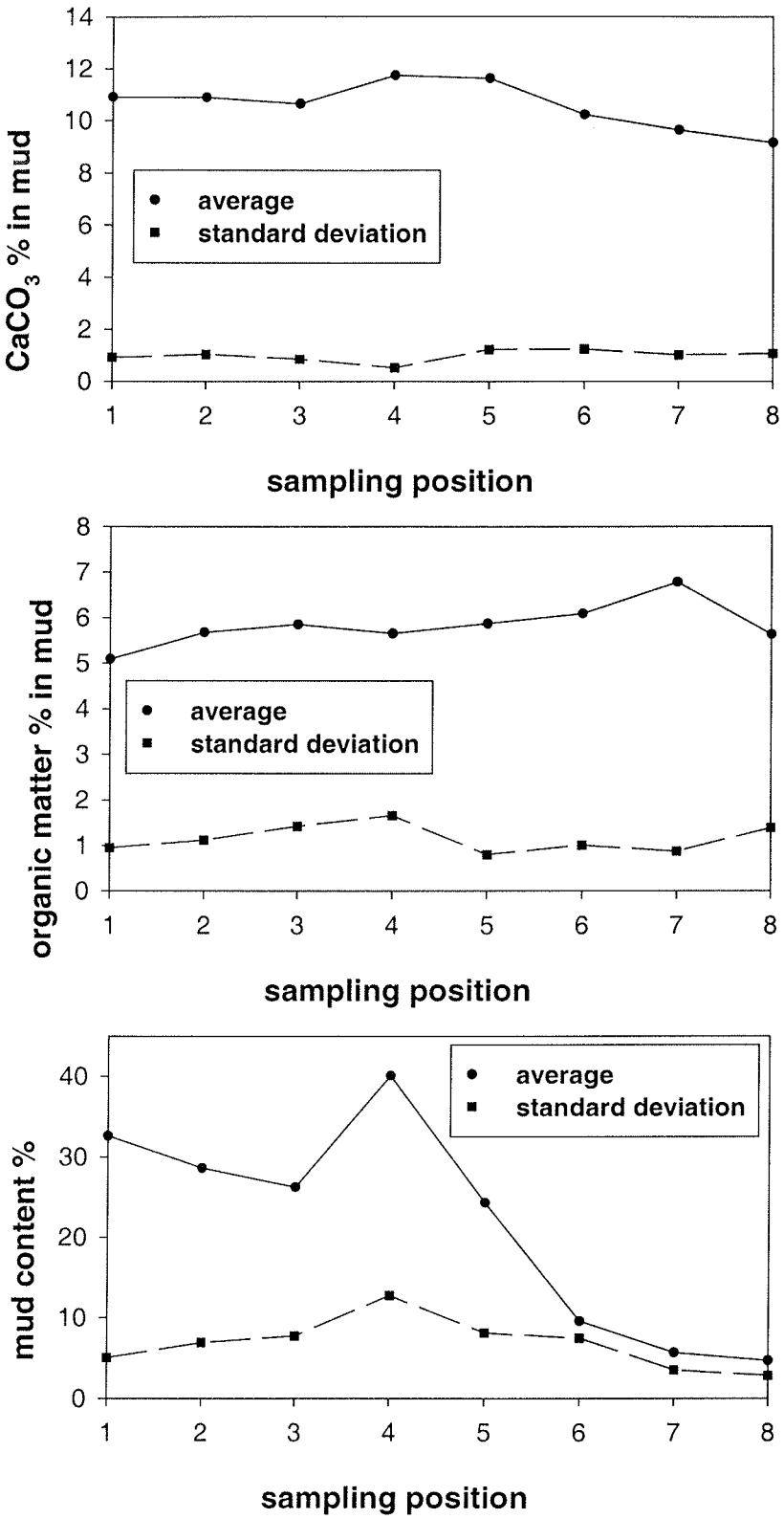

Figure 2-17 Annual means and standard deviations of $CaCO_3$ and organic matter contents in the mud fractions along the test transect

2.7.3.2 Temporal variability (Fig. 2-18)

The seasonal variability in $CaCO_3$-content and organic matter content in the mud fractions along the test transect are illustrated in Fig. 2-18. As in the case of the mass physical sediment properties (section 2.7.2), stations 2, 4, and 7 were selected as representative examples illustrating the general trends observed in the muddy sample suite, the biogenic muds, and the sandy sample suite, respectively.

In the muddy sediments adjacent to the dike, represented by station 2, the $CaCO_3$-contents reach their highest values (>11%) in the months of December-May (winter and spring), and their lowest values (<10.5%) in the months of June-November (summer and autumn). On the sandy tidal flats (station 7) the trend is reversed, the $CaCO_3$-contents being in general lower than on the muddy tidal flats. The values are now higher in the period from September-January (>10%), and lower from February-August (<9.5%). At station 4, by contrast, the $CaCO_3$-contents are relatively high (i.e. similar to the highest values at station 2), and on average show a progressively increasing trend from May-March, the values beginning to fluctuate more strongly on a month to month basis from September onwards.

In comparison to the $CaCO_3$-contents, the organic matter contents of the muds along the transect have no obvious seasonal signature, the values fluctuating strongly on a month to month basis throughout the year. This holds for both the sandy and the muddy tidal flats, but not for station 4. Near the mussel bed the organic matter in the mud fraction is lowest in March and April, increasing gradually with some degree of month to month variability to reach its highest value in February.

In summary, there is a clear indication that the $CaCO_3$-contents in the mud fractions are proportional to the mud content of the sediment, hence showing the same seasonal signature. The more mud there is in the sediment, the higher is the $CaCO_3$-content of the mud. The same can not be said for the organic matter content which, with the exception for the biogenic muds, shows no seasonal pattern whatsoever.

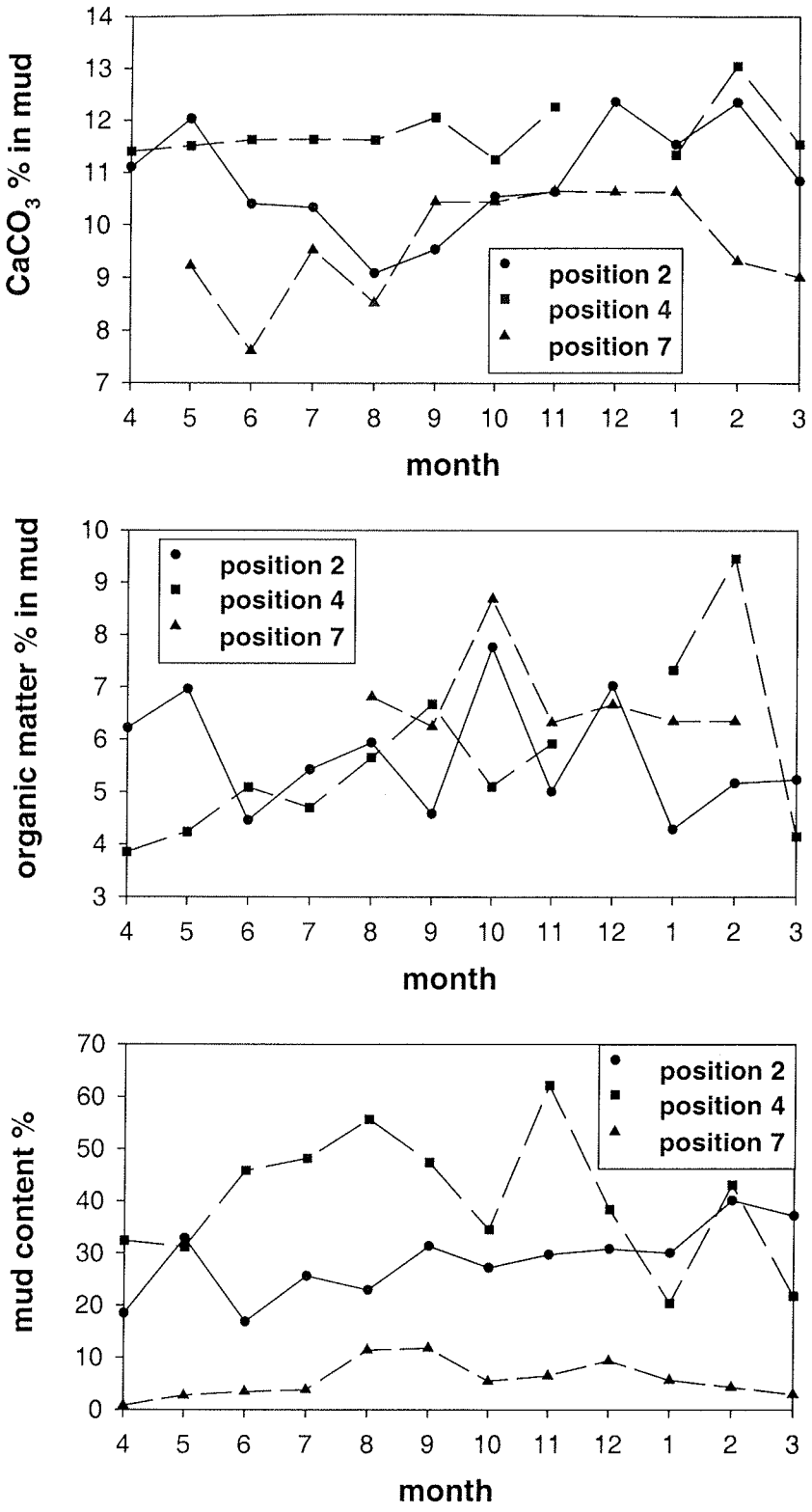

Figure 2-18 Seasonal variability of $CaCO_3$ and organic matter contents in the mud fractions along the test transect

3 Spatial distribution patterns of sediment fractions and mass physical sediment properties

3.1 The sediment

3.1.1 Distribution of the sand fraction (Fig. 3-1)

The surface sediments of the Otzum tidal basin are dominated by sand. Over most of the area the sediment consists of >85% sand (Fig. 3-1). Only in narrow zones along the western and eastern watersheds, and along the landward boundary adjacent to the dike does the sand fraction drop under 85%. Lower values are also observed north-west of the Neuharlingersiel channel breakwater, an area traditionally occupied by mussel banks. Nowhere within the sampling grid did the sand contents of the sediment drop below 30% at the time of the study.

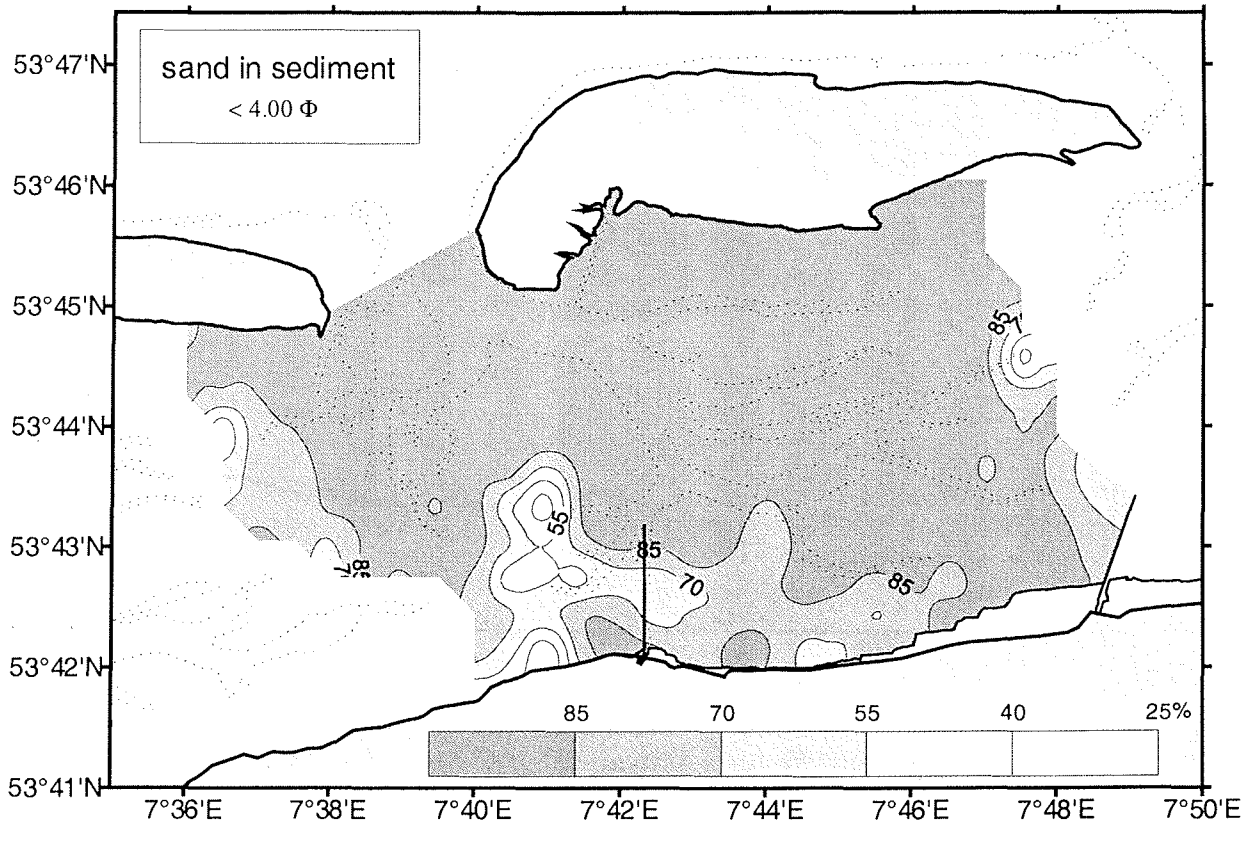

Figure 3-1 Distribution of the sand fraction in the intertidal sediments of the Otzum tidal basin

3.1.1.1 Distribution of medium sand (1.00 – 2.00Φ)

Looking at the main grain-size components of the sand fraction, it is found that the coarsest particle group of the intertidal sediments is composed of medium sand (1.00 - 2.00Φ, or 0.5 - 0.25mm). This size fraction is mainly concentrated in the rear of the barrier islands of Langeoog and Spiekeroog (Fig. 3-2), where the contents reach >16% and >20%, respectively. A minor arm extends to the Janssand in the central part of the tidal basin south of the inlet, the contents here barely reaching 8%. As shown by Flemming and Ziegler (1995), the islands and island beaches are composed of this grain size, and its extension into the back-barrier island flats thus documents overwash activity as well as aeolian input from the islands.

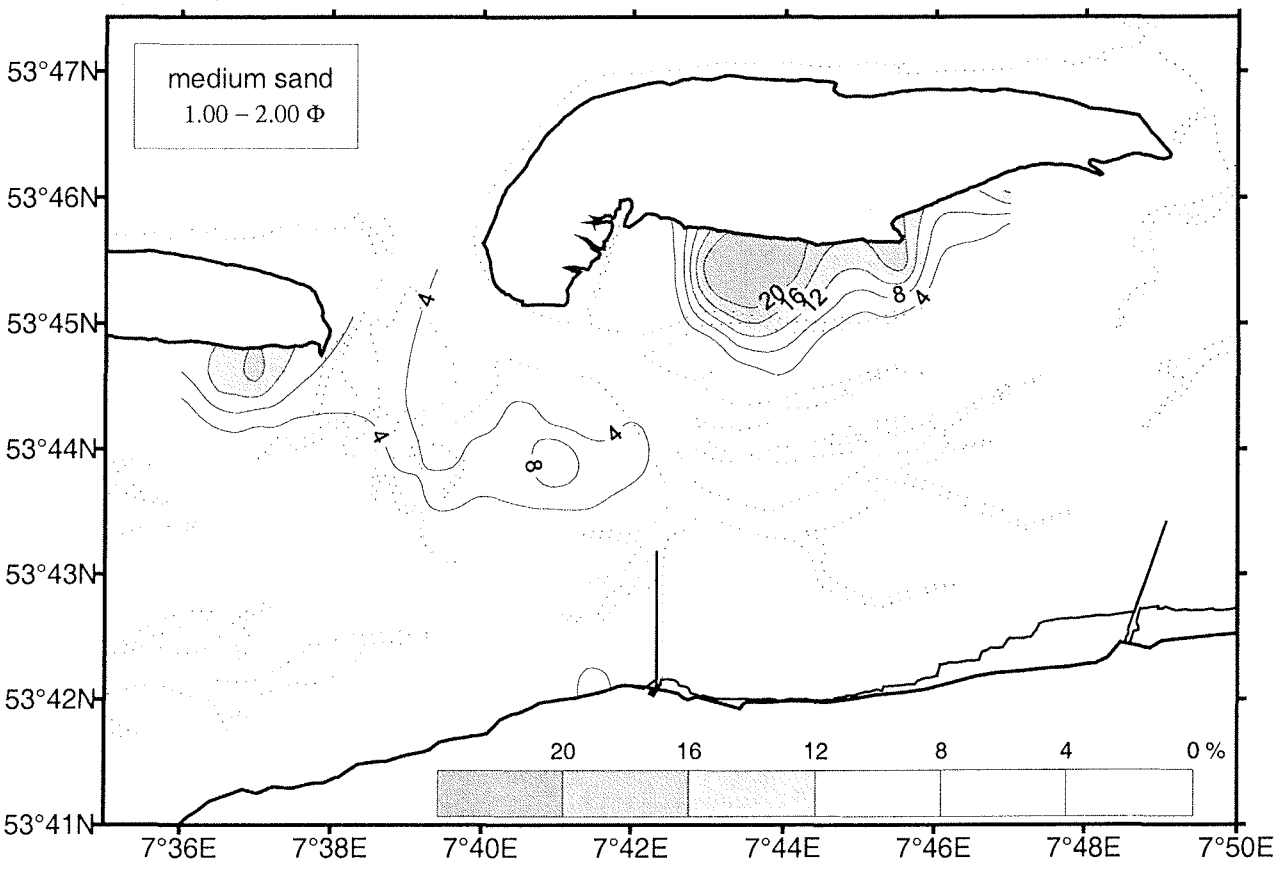

Figure 3-2 Distribution of medium sand in the Otzum tidal basin

The concentration of medium sand in the rear of the barrier islands is well illustrated by the Frequency-% versus Latitude diagram of Fig. 3-3. The diagram clearly shows the steep gradient with which the medium sand fraction suddenly appears on the scene. It evidently represents the landward tail of a more prominent medium sand facies centred around a more northerly position.

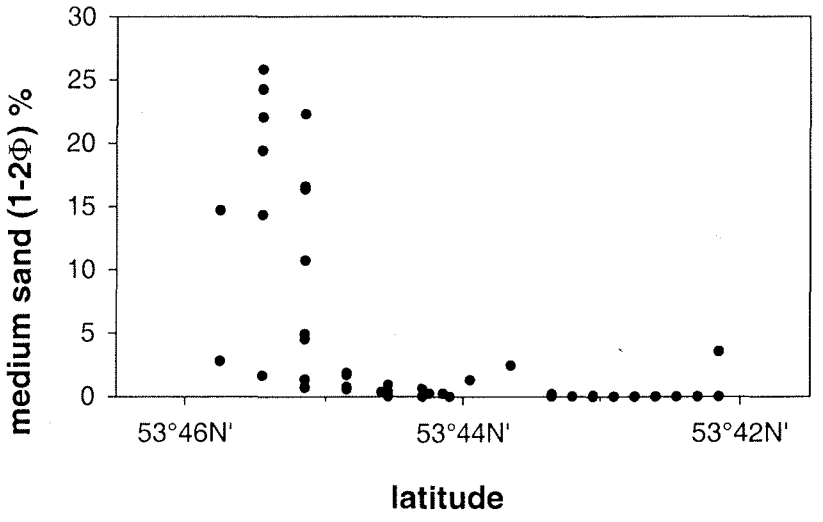

Figure 3-3 Frequency of medium sand in weight-% as a function of Latitude in the Otzum tidal basin (7°42.5'E – 7°45.5'E)

3.1.1.2 Distribution of fine sand (2.00 – 3.00Φ)

At least 66% of the Otzum tidal basin area is dominated by the fine sand fraction (2.00 - 3.00Φ, or 0.25 – 0.125mm). Over large parts it contributes >80% to the sediment, notably in and around the tidal inlet, and on the Janssand (Fig. 3-4). Smaller patches also occur to the east of the Janssand. The dispersal of fine sand appears to be controlled by the channel system, the inlet being the main entrance point. Towards the dike flats the fine sand fraction rapidly drops to <20%. Behind the two islands the fine sand fraction contributes over 60% to the sediment. This emphasises the point that the medium sand in this region forms the

landward tail of a more prominent medium sand depocentre situated further north on the islands and island beaches. The fine sand fraction thus evidently overlaps with the medium sand fraction to the north.

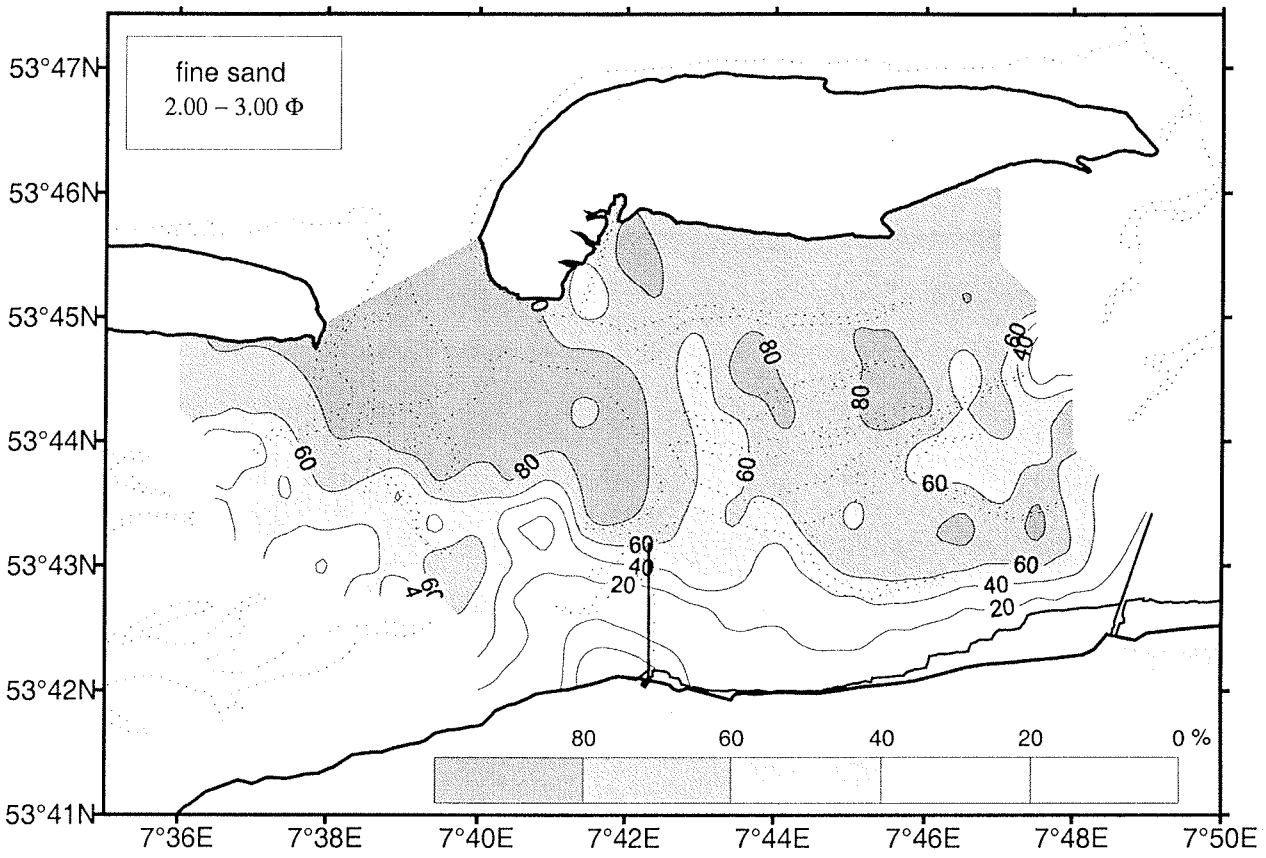

Figure 3-4 Distribution of fine sand in the Otzum tidal basin

The nature of the distribution of the fine sand fraction is highlighted on the Frequency-% versus Latitude diagram of Fig. 3-5. Viewed from the south, the fine sand fraction appears on the scene at a latitude of about 53°42'N. It rapidly grows in proportion to peak between Latitudes 53°44'N and 53°45'N. Its northern tail section is then truncated at the northern limit of the sample grid. It is quite clear, however, that it would continue across the islands at least as far north as the island beaches, thereby documenting the overlap with the medium sand fraction which occupies this area.

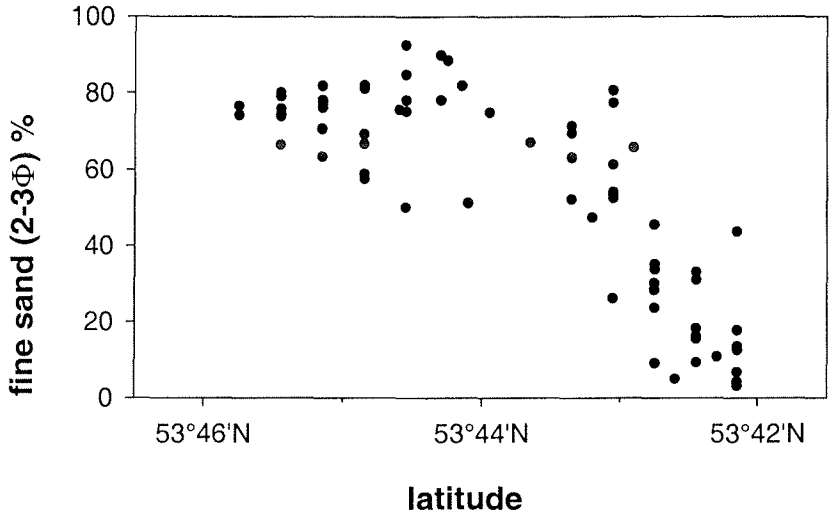

Figure 3-5 Frequency of fine sand in weight-% as a function of Latitude in the Otzum tidal basin (7°42.5'E – 7°45.5'E)

3.1.1.3 Distribution of very fine sand (3.00 – 4.00Φ)

Very find sand (3.00 - 4.00Φ, or 0.125 – 0.063mm) occurs over most of the Otzum tidal basin but reaches higher contents (>80%) only along the mainland shore adjacent to the dike (Fig. 3-6). From there it decreases progressively in a northward direction, reaching contents of <15% on the island flats, around the mouth of the Otzum inlet, and on most of the Janssand. In fact, the areas where the sediment contains <15% of very fine sand correspond almost perfectly with those where the medium sand fraction reaches values >12%. The two fractions thus appear to be mutually evasive, i.e. the energy conditions which are just able to move medium sand are too high to allow very fine sand to be deposited. A similar pattern is observed in the south near the dike, now involving the fine sand fraction. Here the very fine sand fraction exceeds 45% only in places where the fine sand fraction attains contents of >40%.

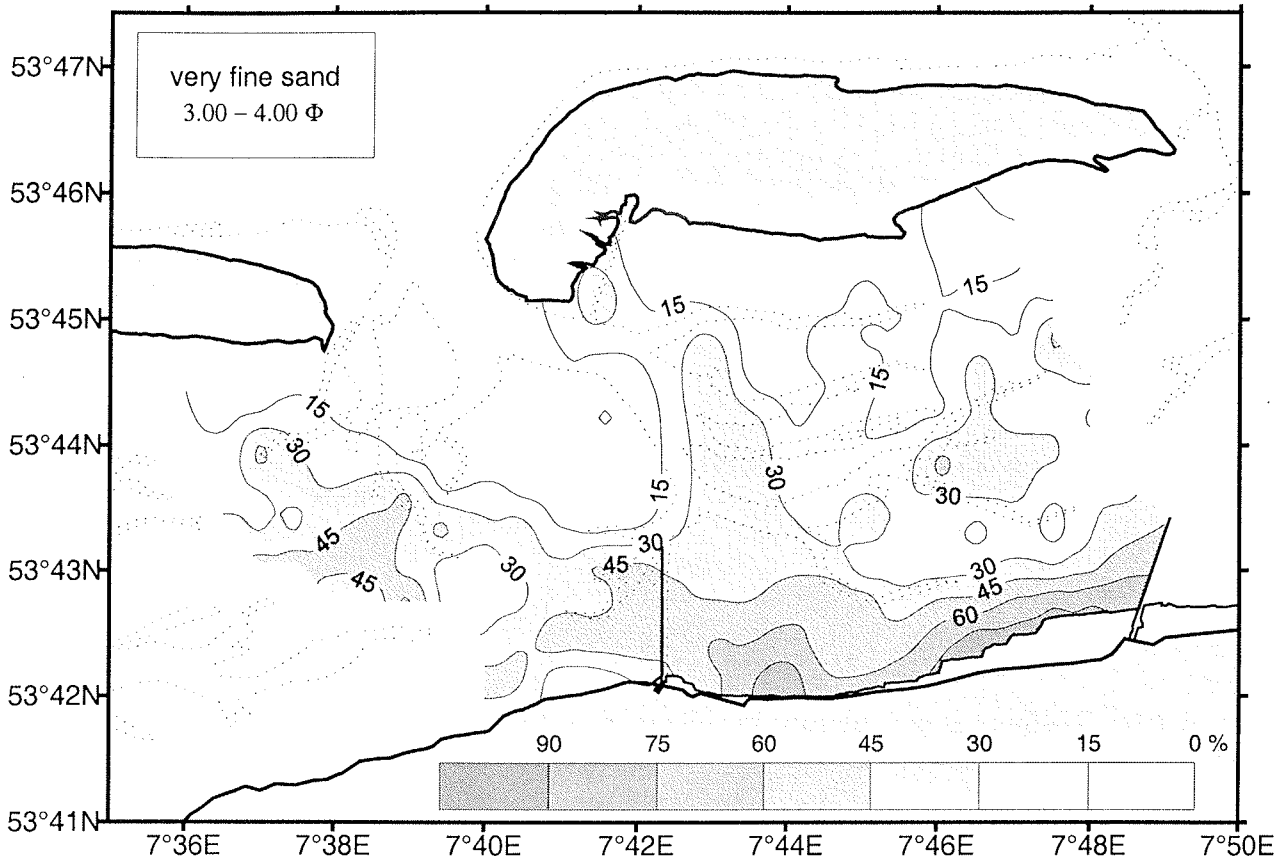

Figure 3-6 Distribution of very fine sand in the Otzum tidal basin

Looking at the Frequency-% versus Latitude diagram (Fig. 3-7) reveals that we are evidently dealing here with the northern half of a frequency distribution which appears to have been truncated by the dike. The distribution reaches its northern limit at or just north of 53°46'N, while peaking at or just south of 53°42'N. According to this interpretation the other half of the very fine sand belt should be situated in the reclaimed marshlands to the south of the dike. Indeed, this is precisely what Flemming and Nyandwi (1994) have postulated, i.e. that land reclamation has excluded most of the sediments finer than about 0.1 mm from the system.

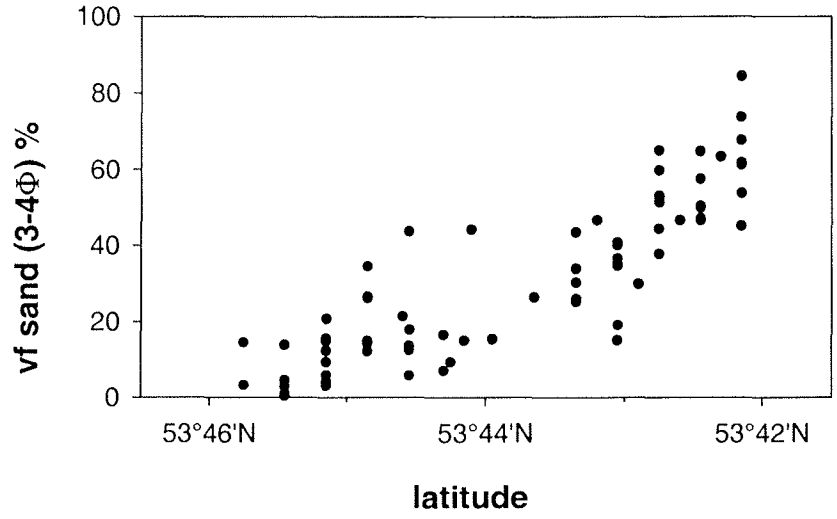

Figure 3-7 Frequency of fine sand in weight-% as a function of Latitude in the Otzum tidal basin (7°42.5'E – 7°45.5'E)

3.1.2 The distribution of mud in the Otzum tidal basin

Mud is the finest sediment fraction that can be deposited in particulate form. It is usually transported in and deposited from suspension. Pure mud flats are not found in the Otzum tidal basin at all, muddy sediments containing various amounts of mud forming an irregular semi-circular belt incorporating the watersheds and the area adjacent to the dike (Fig. 3–8). Contents rarely exceed 30%, higher mud values being restricted to a few local spots along the watersheds and north-west of the breakwater lining the approach channel to the Neuharlingersiel harbour. Here the mud contents can exceed 50%. Most of these localities coincide with existing or former mussel beds (e.g., Hertweck, 1995), the muds evidently being of biogenic origin. Very small amounts of mud (generally <2%) can be found in almost all intertidal sediments. This mud appears to be trapped in the interstitial water in the course of sediment reworking.

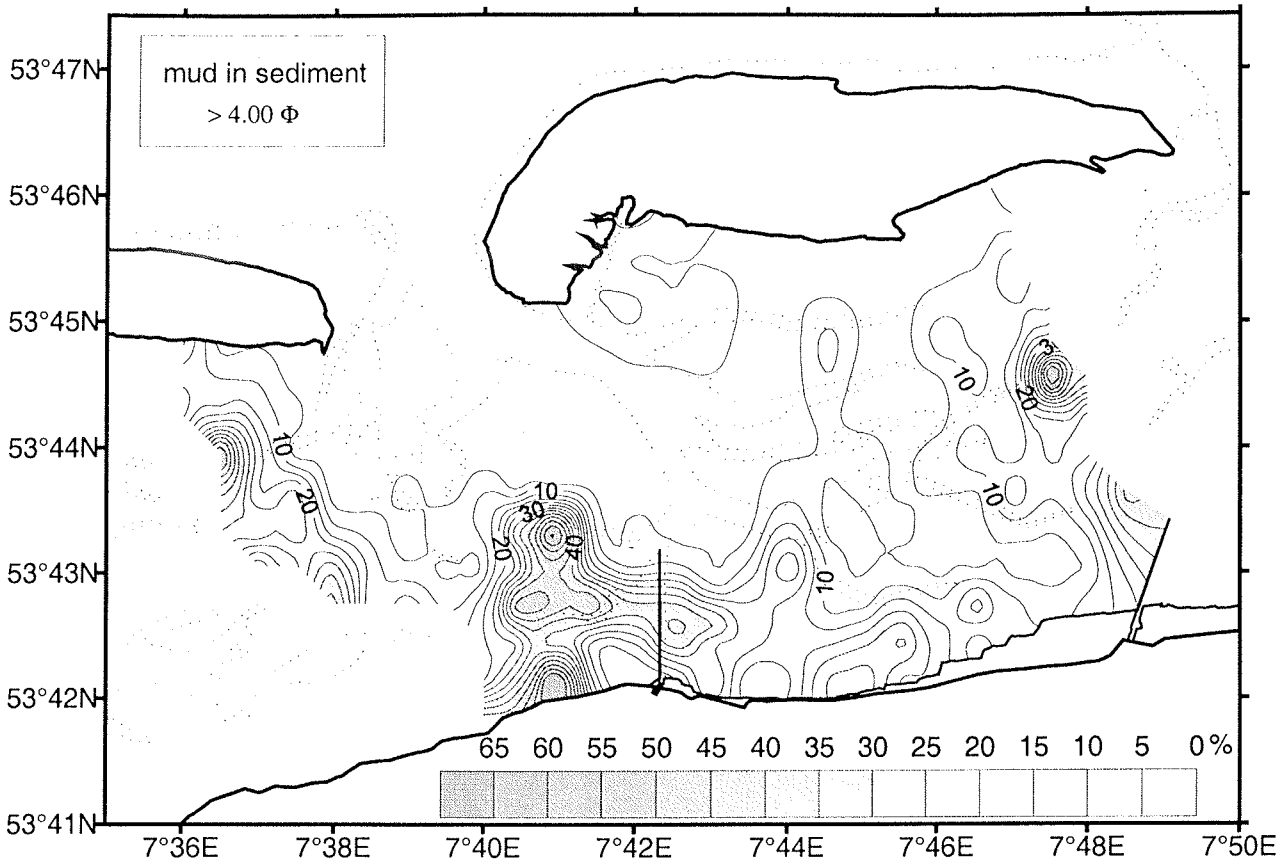

Figure 3-8 Distribution of mud in the Otzum tidal basin

A test implication of the sediment exclusion hypothesis proposed by Flemming and Nyandwi (1994), and which was supported by the distribution data of various sand fractions presented above, would be a dearth of mud in the modern tidal basin. If the biogenic deposits are excluded, then the Otzum tidal basin is indeed characterized by a deficiency of mud, i.e. there are no open mud flats and muddy sediments are restricted to maximum mud contents of 30%. The mud distribution pattern (without the biogenic muds) again suggests that we are dealing with the northernmost tail end of a more prominent mud depocentre formerly situated to the south of the dike. This observation therefore supports the exclusion hypothesis.

In the following sections the distribution patterns of individual mud size fractions are presented. It should be noted, however, that the contents are presented as weight percentages of the mud fraction and not of the total sediment. The sole aim of the exercise is to investigate

whether the hydraulic size sorting process is subtle enough to separate coarser mud fractions (e.g., very coarse, coarse, and medium silt) from finer mud fractions (e.g. fine and very fine silt, and clay).

3.1.2.1 Distribution of very coarse silt (4.00 – 5.00Φ)

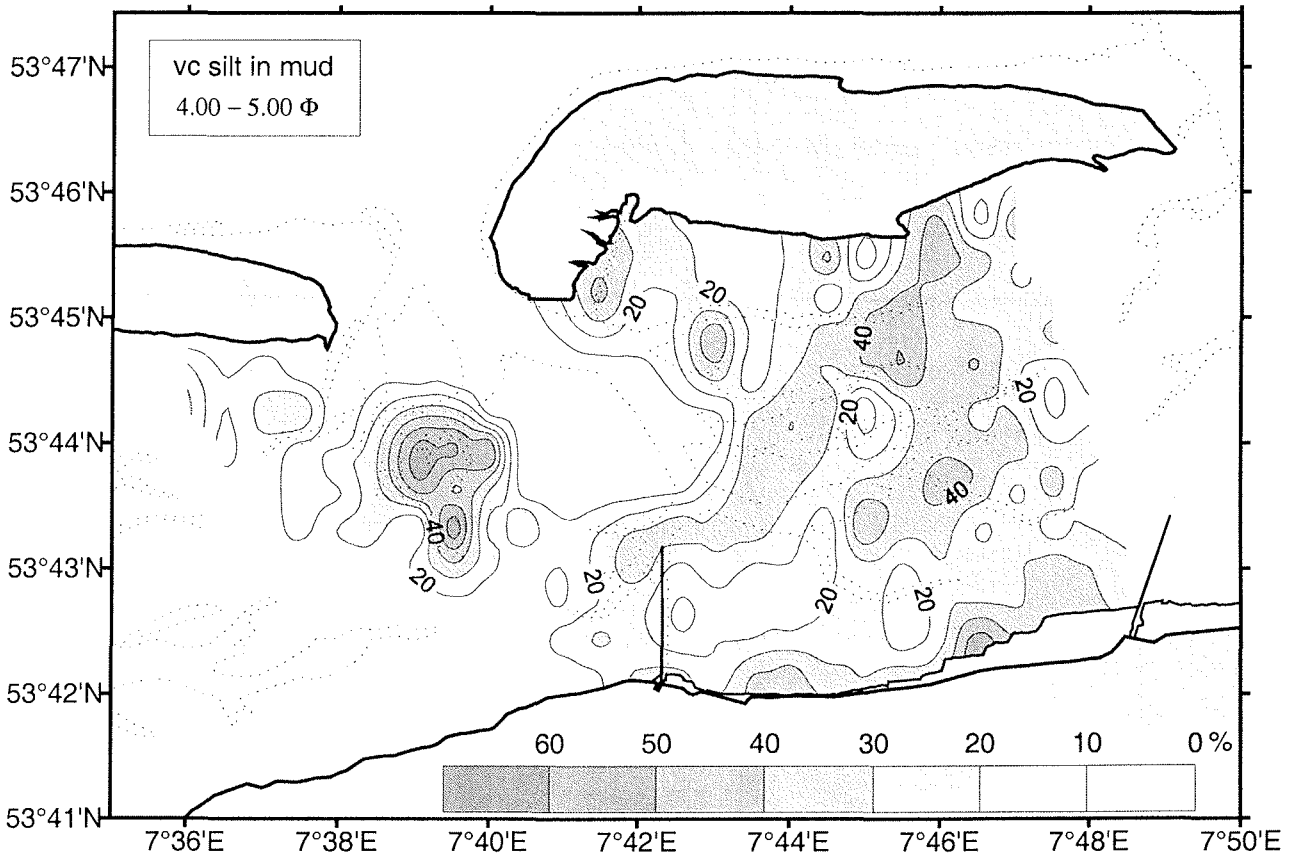

Figure 3-9 Distribution of very coarse silt in the mud fraction

The average content of very coarse silt in the mud fraction is 26.12%, the minimum content being 2.13% and the maximum 73.55%. As illustrated in Fig. 3-9, most muds contain over 10% of very coarse silt. However, with the exception of the very low contents in and adjacent to the inlet, there is no clear trend in the distribution pattern. Large areas of the remaining tidal basin, notably also a narrow fringe adjacent to the dike, have very coarse silt contents of more than 30%. Along the watersheds, on the other hand, which were preferable

mud depocentres, the very coarse silt contributes less than 30% to the mud fraction. The highest very coarse silt contents are found on two intertidal sand flats south of the inlet. Here it locally exceeds 50%. This area is characterized by very low mud contents. The distribution of very coarse silt in the mud fraction thus demonstrates that it is not simply linked to the mud content but that it follows a distinctly independent pattern. It might be construed that the very coarse silts form the tail end of the very fine sand fraction. However, with the exception of the narrow fringe along the dike, there is no obvious link between the distribution patterns of these two fractions.

3.1.2.2 Distribution of coarse silt (5.00 – 6.00Φ)

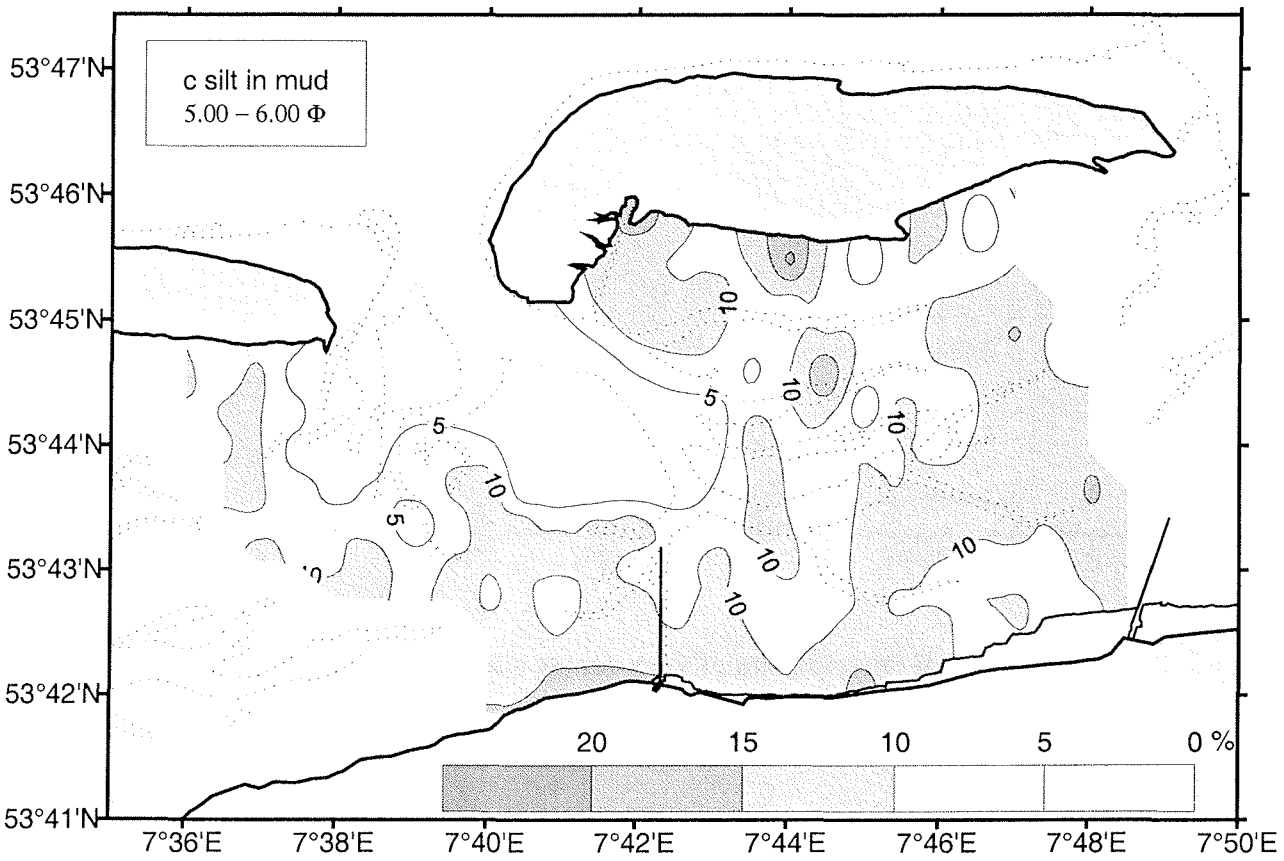

Figure 3-10 Distribution of coarse silt in the mud fraction

As in the case of very coarse silt, the coarse silts in the mud fraction are dispersed across the entire tidal basin, reaching lowest values in and adjacent to the inlet (Fig. 3-10). The contents vary between 3.58% and 21.84% with an average content of 10.67%. The distribution pattern of coarse silt is distinctly different from that of the very coarse silt, and also different from that of the mud. The only recognizable trend is a tendency for higher coarse silt contents along the edges of the tidal basin where it locally exceeds 20%. Notably, these local highs are distinctly offset from the highs at which very coarse silts are concentrated. There are thus first signs that individual mud fractions are individually sorted in the course of hydraulic transport.

3.1.2.3 Distribution of medium silt (6.00 – 7.00Φ)

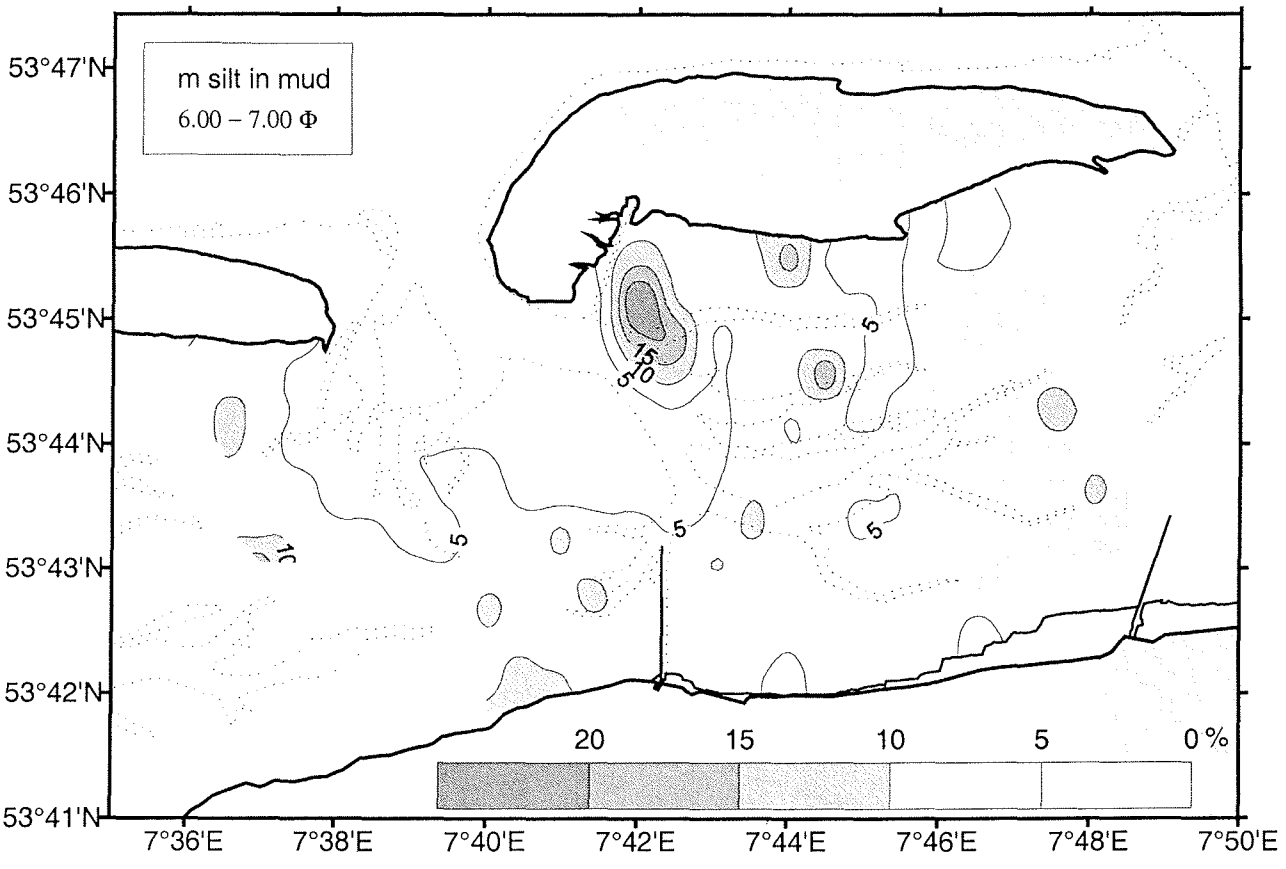

Figure 3-11 Distribution of medium silt in the mud fraction

Medium silt also follows the same broad pattern as observed for the coarser silt fractions (Fig. 3-11). However, with a value of only 7.77% it has the lowest mean content of all the mud fractions, the minimum content being 2.78%, the maximum 30.29%. In most places the content of medium silt in the mud fraction lies between 5% and 10%. Even the watersheds don't show elevated values. In departure from the coarser silt fractions, the locations of local medium silt highs reveal a partial affinity to the distribution pattern of coarse silt. Thus, the three depocentres south of Spiekeroog island partly coincide with similar highs defined by the coarse silt fraction. On the other hand, contrary to the coarse silt fraction, the medium silt fraction does not show elevated values along the mainland dike.

3.1.2.4 Distribution of fine silt (7.00 – 8.00Φ)

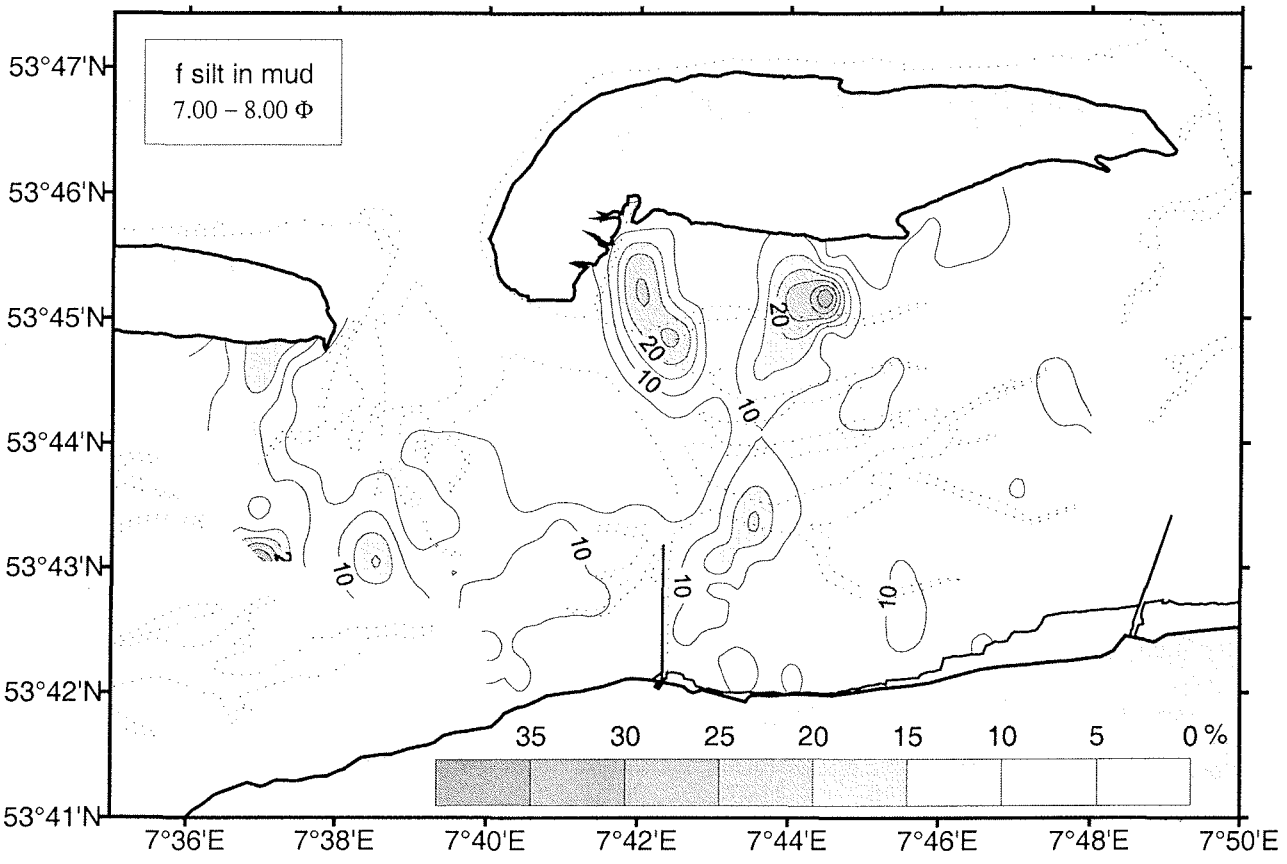

Figure 3-12 Distribution of fine silt in the mud fraction

The fine silt fraction contributes between 2.41% and 43.63% to the mud fraction, the average being 9.46% (Fig. 3-12). Similar to the medium silt, the fine silt contents also lie between 5% and 10% in most parts of the Otzum tidal basin. Along the watersheds fine silts occur in local patches having slightly elevated values. These coincide with locations of highest mud contents. Two major depocentres occur on the island flats south of Spiekeroog where contents of >20% are found. It is interesting to observe that the depocentre situated to the west coincides with a similar depocentre formed by medium silts. The depocentre to the east, however, is situated exactly between two medium silt depocentres. It would thus appear that part of the fine silt is linked to the medium (and coarse) silt fractions, whereas another part is independent of these.

3.1.2.5 Distribution of very fine silt (8.00 – 9.00Φ)

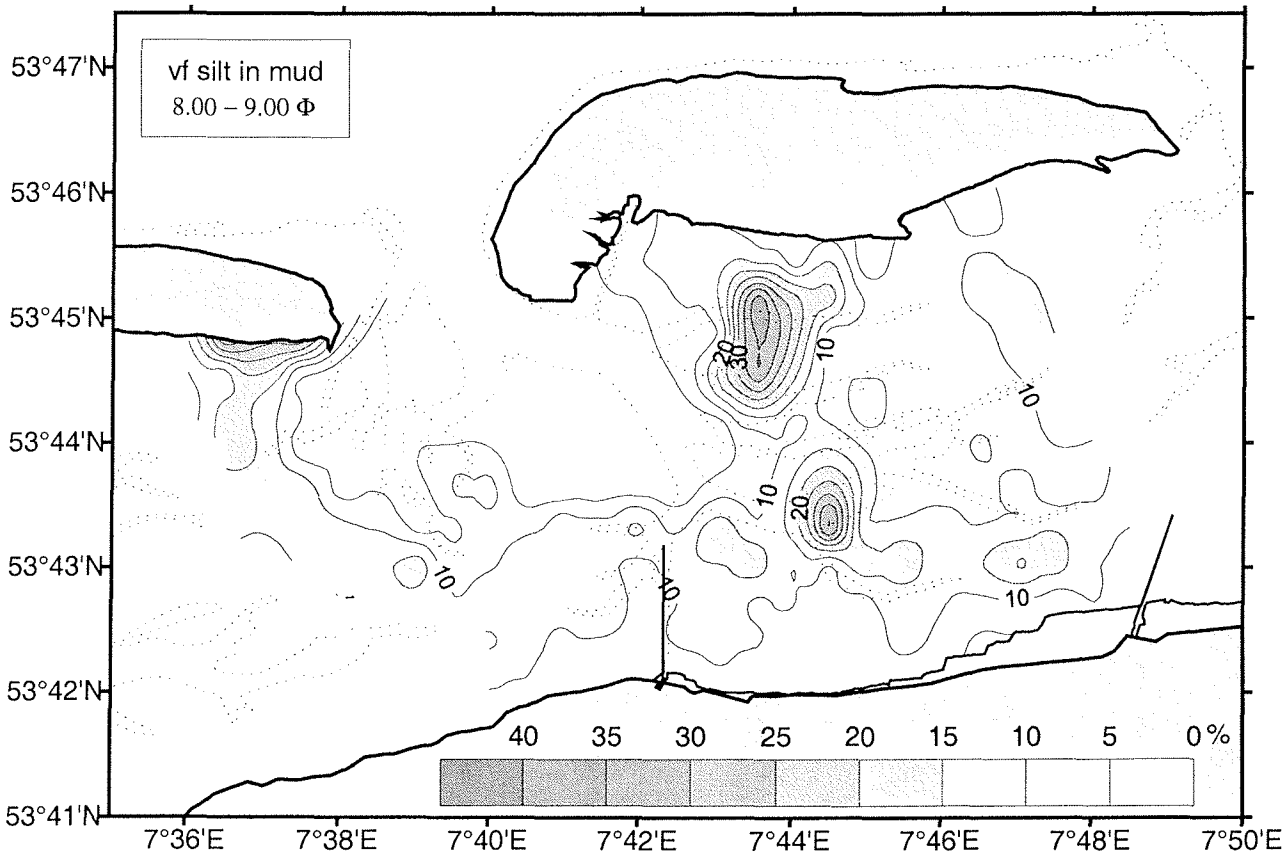

Figure 3-13 Distribution of very fine silt in the mud fraction

Very fine silts occur in the form of two semi-circles, one lining the wider inlet region, a second smaller semi-circle situated to the east which overlaps with the western one along a common branch defining two marked depocentres in the central part of the tidal basin (Fig. 3-13). Interestingly, this silt fraction is not enriched along the mainland shore, the southern arms of the two semi-circles being distinctly offset to the north. The contents vary between 2.94% and 45.88% with an average of 11.40%. The two depocentres, which reach very fine silt contents in excess of 30%, are distinctly offset from all previous depocentres defined by the coarser silt fractions. Only the northern one overlaps marginally with the eastern depocentre of the fine silt fraction.

3.1.2.6 Distribution of clay (>9.00Φ)

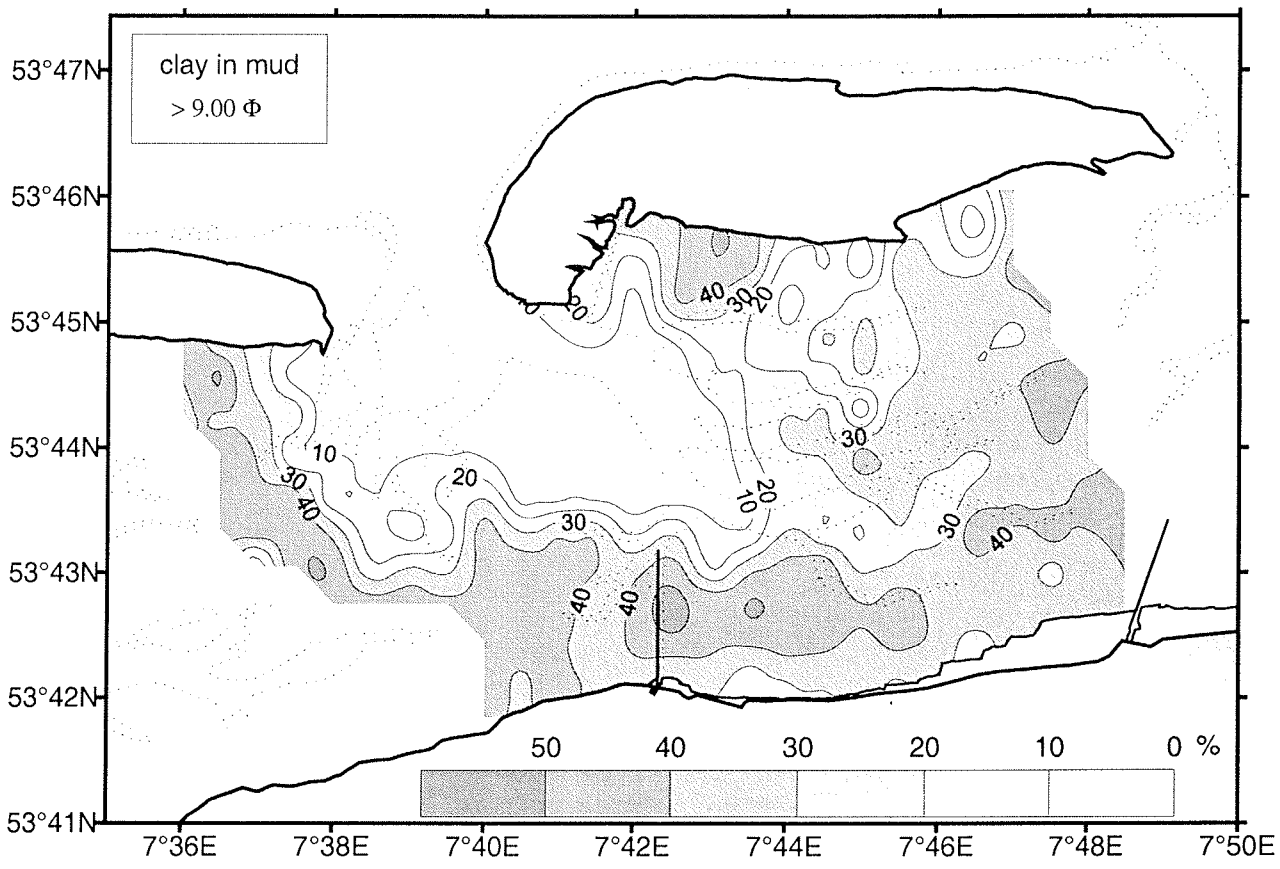

Figure 3-14 Distribution of clay in the mud fraction

The distribution pattern of the clay fraction is in some respects similar to that of the very fine silt fraction in that it also forms two broadly corresponding semi-circles (Fig. 3-14). The areas of highest enrichment, however, do not coincide with those defined by the very fine silt. In general, the clay fraction contributes more sediment to the mud fraction than any of the silt fractions. It reaches an average value of 34.58% and varies from 4.29% to 56.67%. Furthermore, the clay fraction only partly corresponds to the distribution pattern of the mud as a whole, e.g., along the watersheds where the highest mud contents are found the clay fraction contributes over 40% to the mud. High clay contents (>40%) occur in some parts of the island flats. A large clay depocentre is also found near the approach channel to Neuharlingersiel harbour, this accumulation being possibly associated with dredging activities as previously pointed out by Flemming and Davis (1994).

In summary, it can be stated that the individual size fractions of the mud show partly independent and partly associated distribution patterns. This demonstrates that the hydraulic sorting process is also active within the finest sediments of the tidal basin, although it is not clear at this stage what the grain size composition of individual hydraulic populations might look like. Considering that the clays and finer silt fractions are probably combined in flocs, faecal pellets and other aggregates, one would be inclined to postulate the existence of at least three, and possibly four hydraulic populations comprising the mud fraction.

3.2 Spatial distribution of shear strengths

Shear strengths were measured at every point of the sampling grid. In every case several measurements were averaged in order to avoid comparing extraneous measures with regular ones. The results were plotted into the map of the study area and contoured. As can be seen from Fig. 3–15, shear strengths of the surficial sediment in the Otzum tidal basin decrease in a general way from north to south. In this respect they trace the shore-normal energy gradient previously documented for the grain size pattern. The highest shear strengths lie over 75 kPa, the lowest ones under 15 kPa, the overall gradient covering a range of over 60 kPa. The lowest shear strengths (<30 kPa) are found along the watersheds and over large parts of the southern basin. An exception is a patch in the south-eastern part of the basin in which values >60 kPa are reached. These low shear strengths are, by and large, associated with high mud contents (cf. Fig. 3-8) which also explains the somewhat irregular pattern.

Sediments with high shear strengths (>60 kPa) line the northern part of the tidal basin which is characterized by the coarsest sediments (fine-medium sands), but also occur in a number of outliers further south. One of these is the Janssand in the west-central part of the basin, another one is situated in the south-eastern part of the basin. In these areas the shear strengths range from 45-65 kPa.

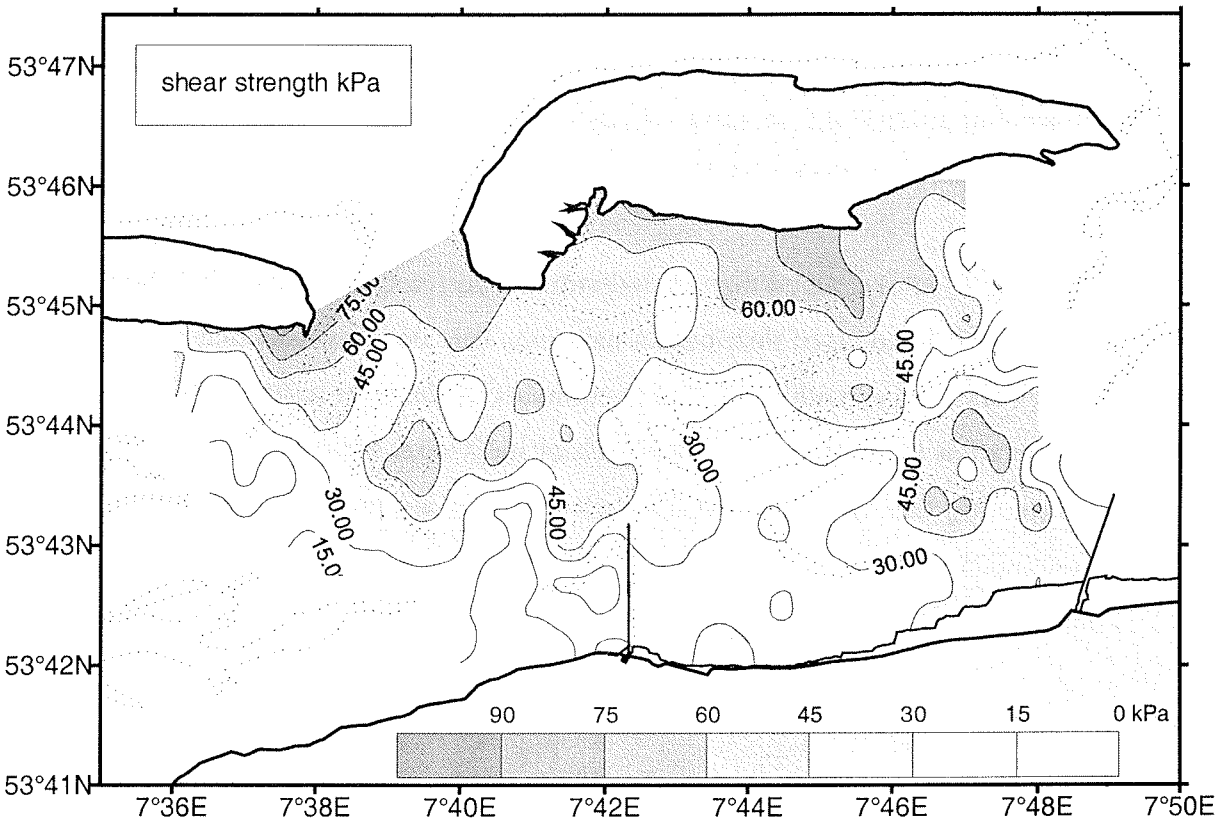

Figure 3-15 Distribution of shear strengths in the Otzum tidal basin

The overall north-south gradient in the distribution of shear strengths is particularly well documented in the latitudinal diagram of Fig. 3-16. Although there is a fairly large scatter in the data (about 30 kPa) resulting from the lateral (east-west) variability along each latitudinal transect, the range is almost uniform throughout.

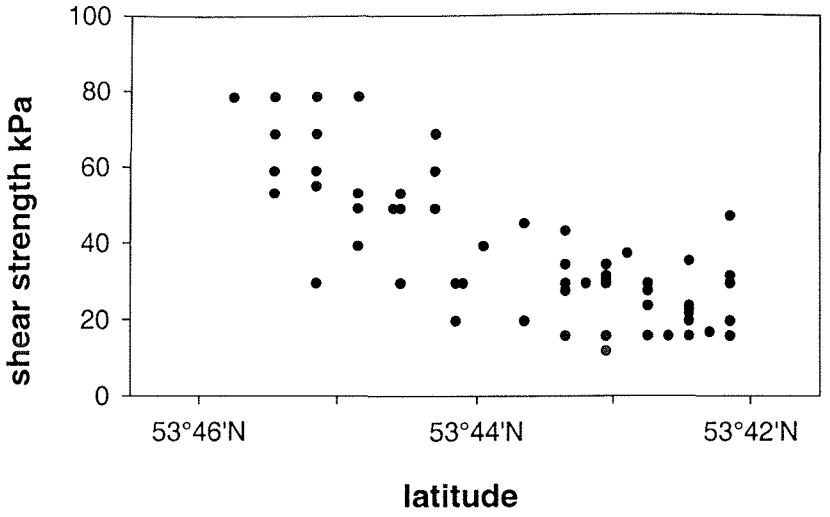

Figure 3-16 Latitudinal distribution of shear strengths in the Otzum tidal basin (7°42.5'E-7°45.5'E)

In summary, although there is a broad correlation between shear strength and mean grain size, there is no obvious single factor that can explain the high variability and often patchy distribution of shear strengths. Besides the obvious textural differences between sandy and muddy sediments, more subtle compositional aspects and associated mass physical properties evidently play an important role in defining shear strengths in sandy sediments. Thus, according to the protocol, most low shear strengths measured on the sand flats were located near tidal channels where the sediment is commonly very water-logged. On the other hand, in spite of the evidently overriding role played by physical factors, biological influences may be locally important and should therefore not be discounted altogether. They would in particular explain some of the scatter in the shear strength data.

3.3 Spatial distribution of bulk densities

As shown in section 2.5.1 (cf. Fig. 2-11), both wet and dry bulk density are inversely proportional to the mud content of the sediment. As a result, the distribution patterns produced by wet and dry bulk density in the Otzum tidal basin (Figs. 3-17 and 3-18) mirror the distribution patterns of sand and mud (cf. Figs. 3-1 and 3-8).

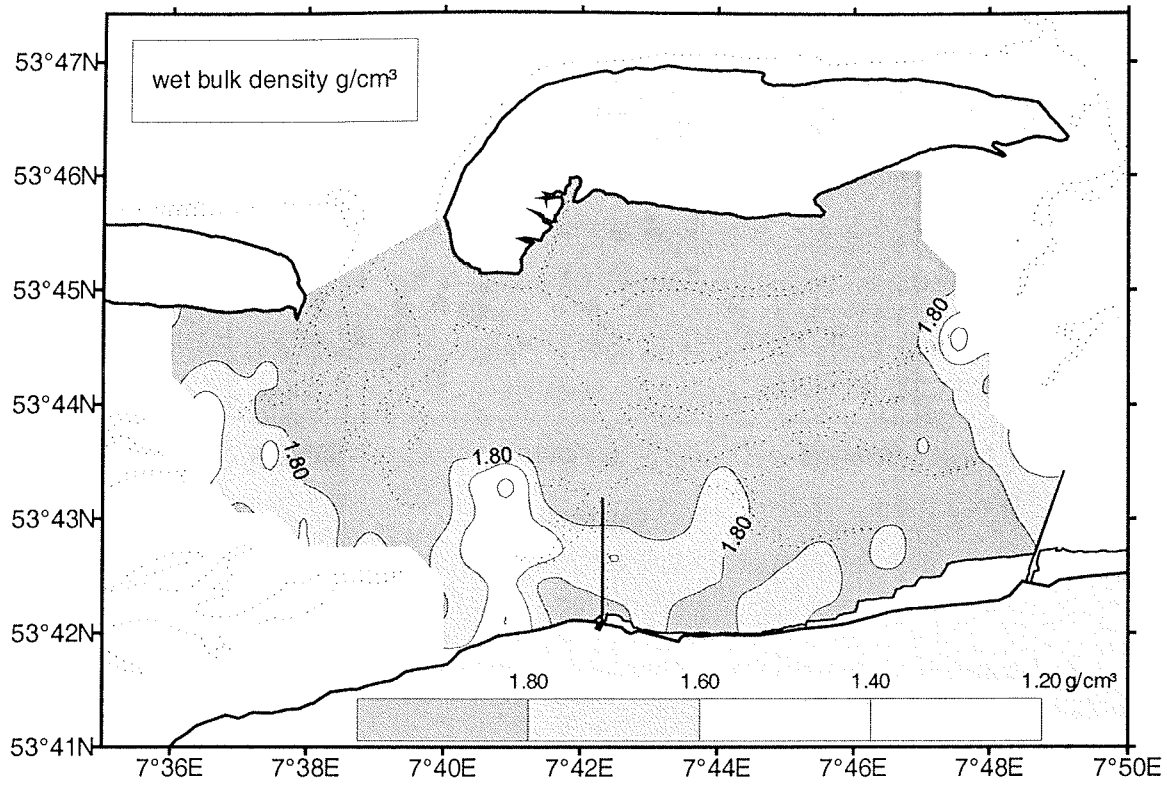

Figure 3-17 Variation of sediment wet bulk density in the Otzum tidal basin

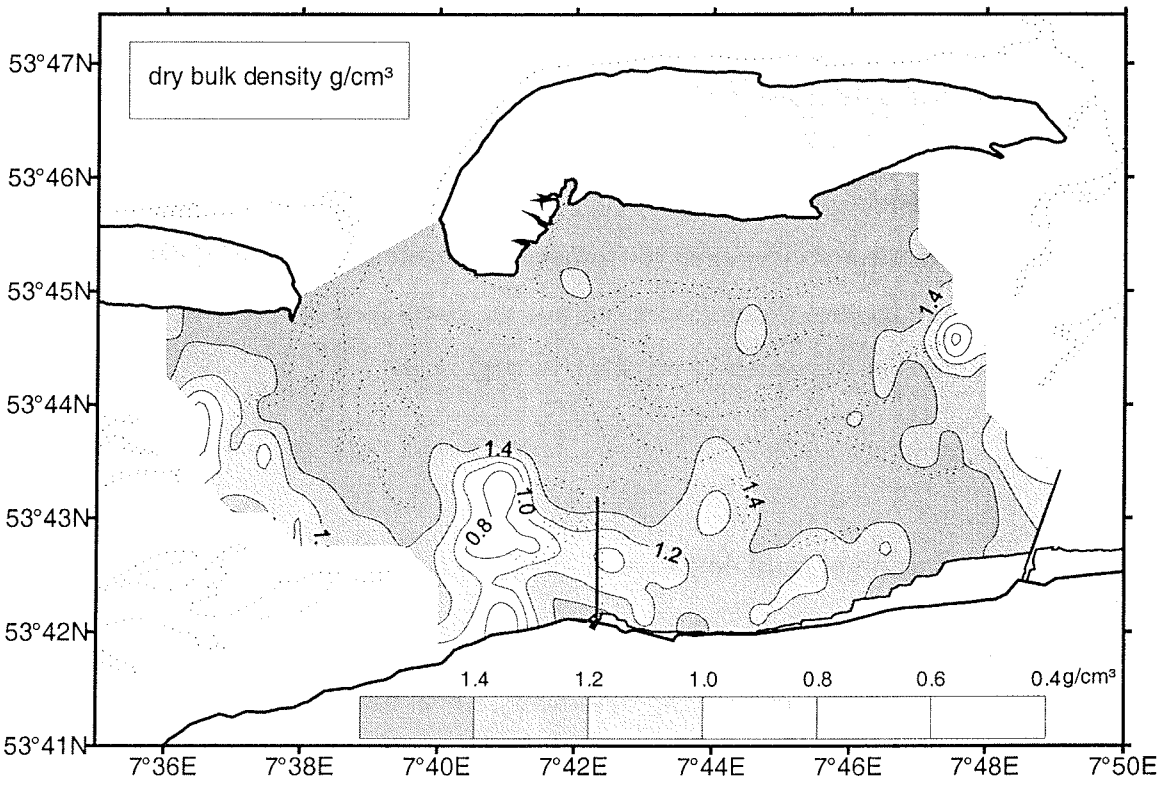

Figure 3-18 Variation of sediment dry bulk density in the Otzum tidal basin

Wet bulk density varies between 1.23 g/cm³ and 2.02 g/cm³, averaging at 1.82 g/cm³, whereas the dry bulk density varies from 0.42 g/cm³ to 1.66 g/cm³, the average being 1.37 g/cm³. In areas dominated by sand, the wet bulk density varies between 1.80 g/cm³ and 2.00 g/cm³, and the dry bulk density between 1.40 g/cm³ and 1.60 g/cm³. In muddy sediments, i.e. in the narrow zones along the watersheds and the mud depocentres near the mainland shore, bulk densities decrease rapidly with increasing mud content to values <1.60 g/cm³ in the case of wet bulk density, and <1.0 g/cm³ in the case of dry bulk density. The lowest bulk densities are associated with the highest mud contents which reach about 80% in the Otzum tidal basin, i.e. 1.25 g/cm³ in the case of wet bulk density and 0.4 g/cm³ in the case of dry bulk density.

3.4 Spatial distribution of porosities and void ratios

Both porosity and void ratio are inversely proportional to bulk density. Since bulk density is negatively correlated with mud content, it is to be expected that porosity and void ratio should be directly proportional to mud content. Indeed, as clearly evident from Fig. 3-19 and Fig. 3-20, the distribution patterns of the two parameters are almost identical to the pattern produced by the mud content (cf. Fig. 3-8).

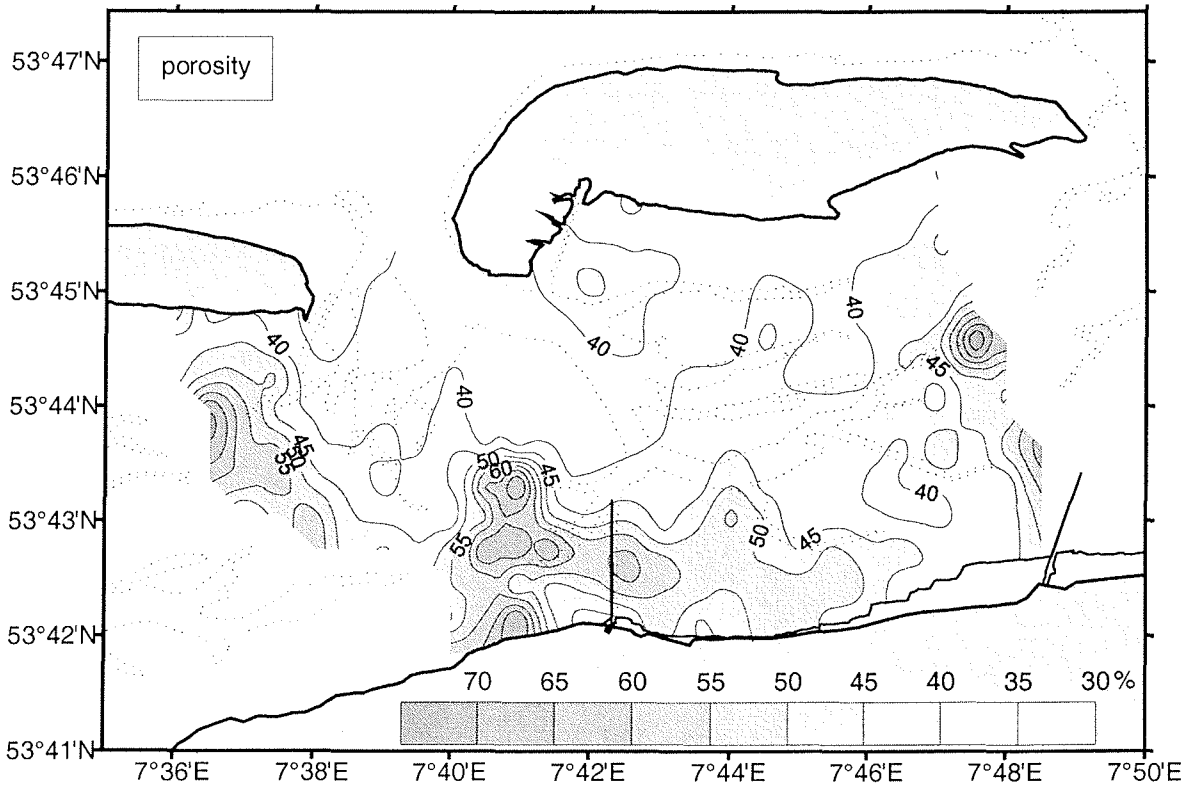

Figure 3-19 Distribution of sediment porosities in the Otzum tidal basin

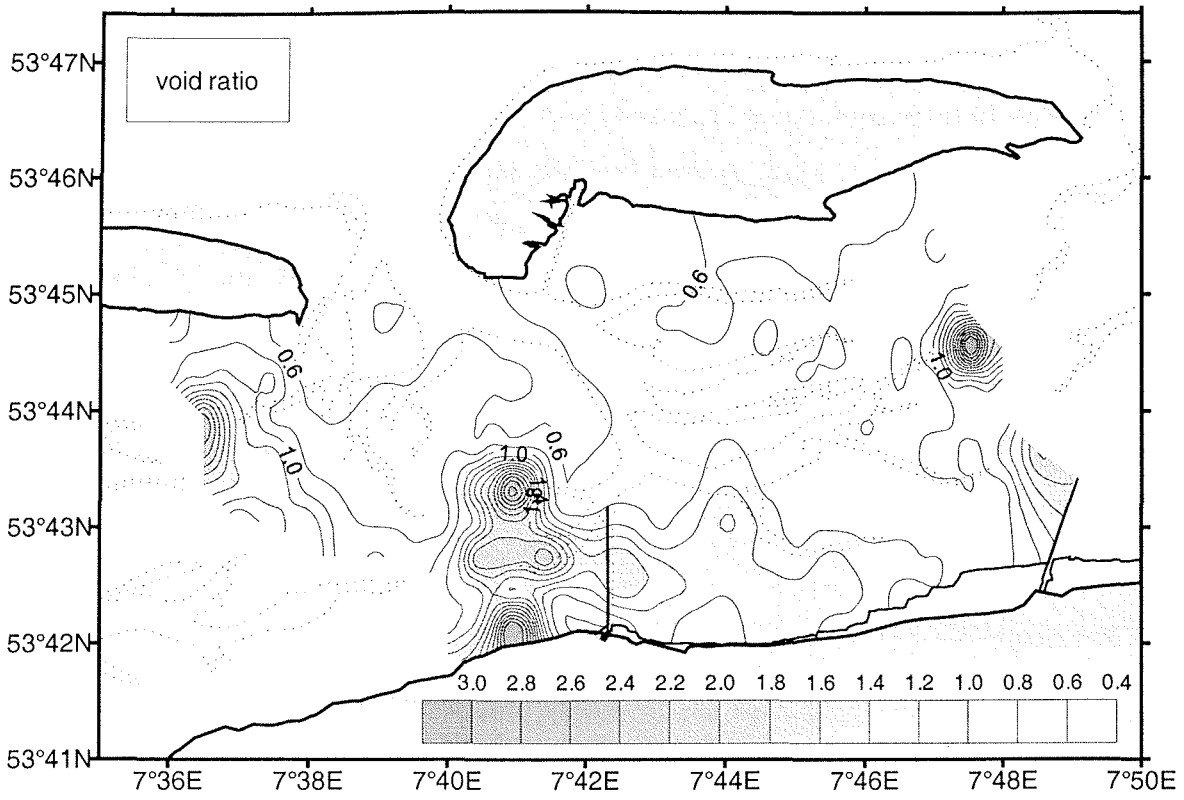

Figure 3-20 Distribution of sediment void ratios in the Otzum tidal basin

The porosity values in the study area vary between 34.25% and 79.35%, the average being 47.05%. The corresponding void ratios are 0.52 and 3.84 for minimum and maximum values respectively, the mean in this case being 0.92. Porosities, and hence void ratios, are lowest in the sand-dominated environments of the tidal basin, the porosity values fluctuating between 35% and 45%, those of the void ratios between 0.6 and 0.8. Where mud contents increase, i.e. in the narrow zones along the watersheds, in mussel beds, and along the southern margin of the tidal basin, porosities and void ratios increases rapidly to >60%, locally reaching >70%, in the case of porosity, and to >2.0, locally reaching >3.0, in the case of void ratio.

3.5 Spatial distribution of $CaCO_3$-contents in the mud fraction

The $CaCO_3$-contents of the mud fraction in the sediments of the Otzum tidal basin vary between 3.51% and 14.54%, the average being 9.15%. At first sight, the $CaCO_3$-contents in the study area appear to be very well correlated with the mud contents of the sediment (Fig. 3-21). In the sand-dominated tidal flats, the $CaCO_3$-contents are mostly <10%. Higher

contents are found along the watersheds where mud contents are also higher. Here, $CaCO_3$-contents are invariably >10%. A general trend of this type was also observed along the test transect. There, higher $CaCO_3$-contents always corresponded to higher mud contents in the sediment, both spatially and seasonally (see 2.7.3).

The distribution pattern of $CaCO_3$ in the muds of the Otzum tidal basin reveals two major features. Comparing the $CaCO_3$ map (Fig. 3-21) with the mud map (Fig. 3-8) reveals, firstly, a general increase of $CaCO_3$-content with increasing mud content, and secondly, that localities with highest $CaCO_3$-contents do not coincide with those having the highest mud contents. Instead, $CaCO_3$-contents appear to peak at intermediate mud values.

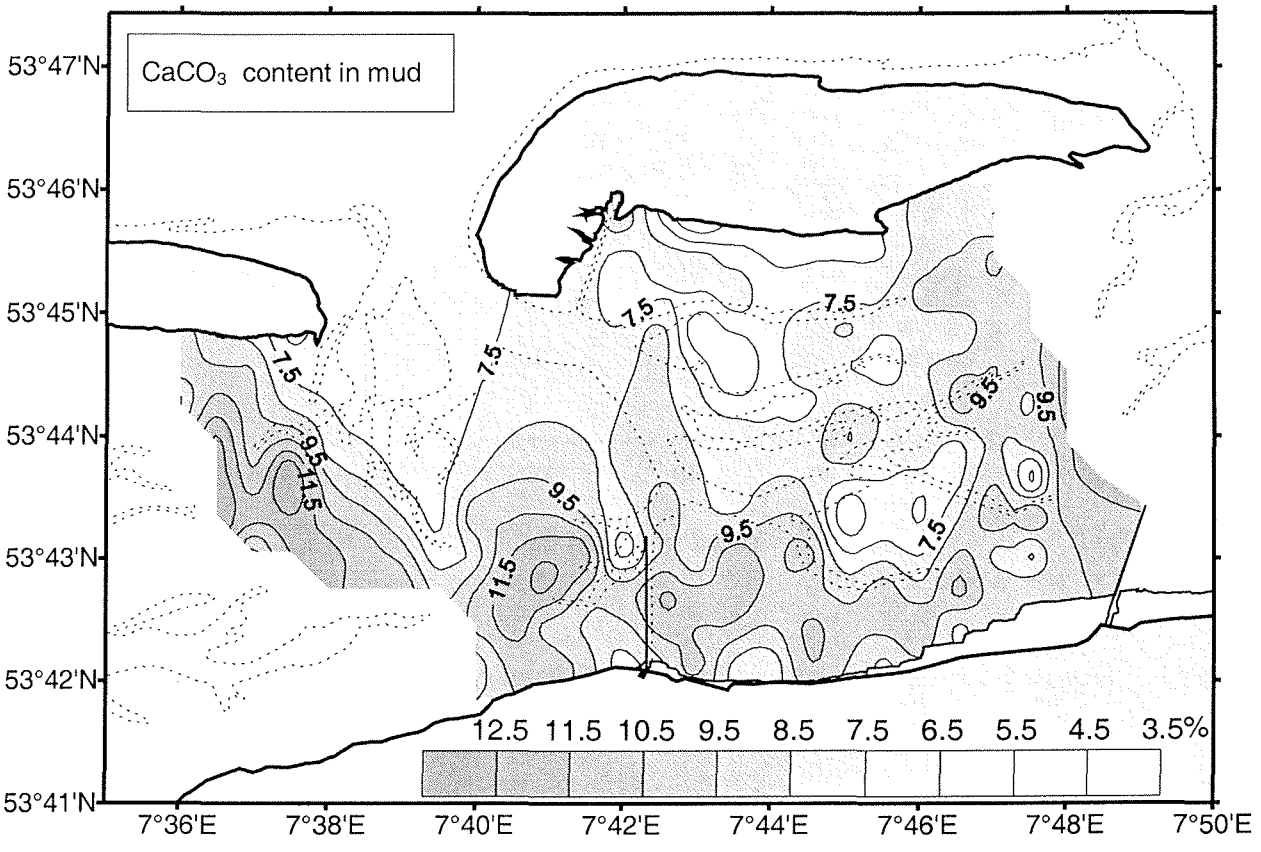

Figure 3-21 Distribution of $CaCO_3$-contents in the mud fraction

The disparity between $CaCO_3$-contents and high mud contents is highlighted in the scatter diagram of Fig. 3-22. In spite of considerable scatter in the data, the $CaCO_3$-content of the mud fraction clearly increases with increasing mud content up to a mud content of about

25%. Thereafter, the $CaCO_3$-contents appear to either remain constant or show a slight decline at very high mud contents, although the data is not conclusive in this respect. This peculiar trend must in some way be related to the local size composition of the muds. Thus, comparing the $CaCO_3$-map with the distribution maps of the individual silt fractions (Figs. 3-9 to 3-13), reveals a similar disparity, i.e. high $CaCO_3$-contents are invariably associated with low silt contents. Conversely, with the exception of the island flats, the $CaCO_3$-map almost perfectly matches the clay map (cf. Fig. 3-14). The fact that the highest clay contents in the mud fraction are also found at intermediate mud levels can only mean that the $CaCO_3$ in the mud is predominantly linked to the clay size fraction.

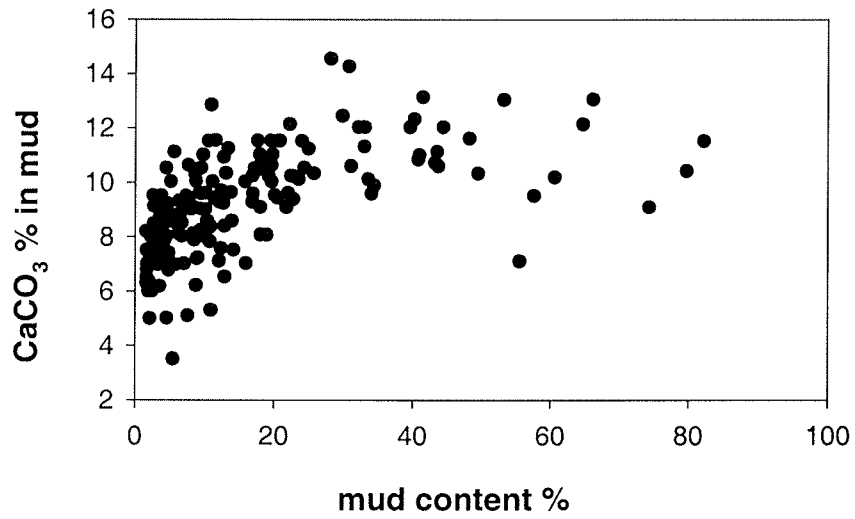

Figure 3-22 $CaCO_3$-content in the mud fraction versus mud content

3.6 Spatial distribution of organic matter in the mud fraction

The organic matter contents in the mud fraction of the sediments of the Otzum tidal basin vary from 2.24% to 10.46%, the average being 6.68%. Notably, the highest organic contents are recorded on the island flats where mud contents are very low (Fig. 3-23). From here the values at first decrease southwards into the tidal basin but pick up again about three-quarter way to the mainland shore before dropping once more to very low values adjacent to

the dike. Along the watersheds the trend is similar but the variation is far less pronounced than within the adjacent basin.

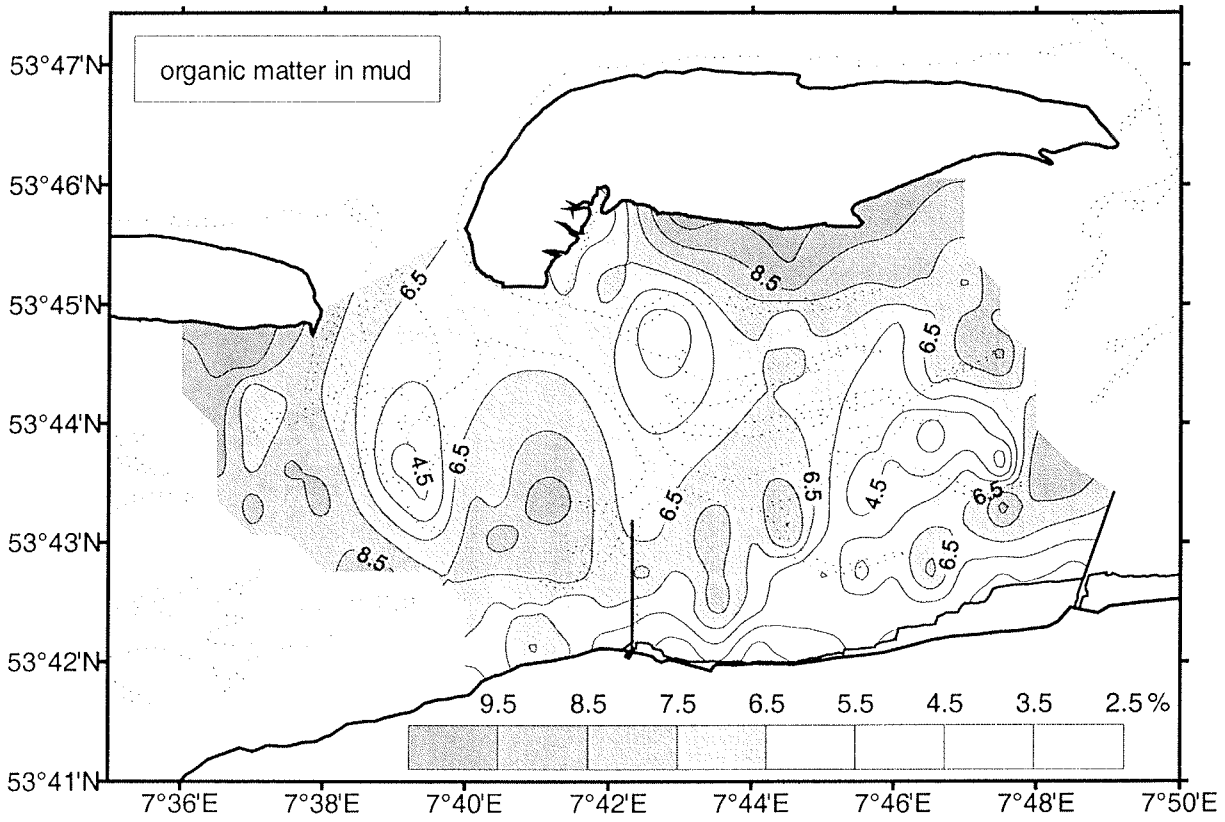

Figure 3-23 Distribution of organic matter in the mud fraction

At first sight, the distribution of organic matter in the muds of the Otzum tidal basin differs substantially from that of $CaCO_3$. Since the organic matter also shows little correlation with the bulk mud content (Fig. 3-24, left panel), it must evidently be linked to different size fractions than the carbonate. The largest difference between organic matter and carbonate is observed on the island flats where some of the lowest carbonate contents are associated with the highest organic matter contents. However, a somewhat better correlation between the two parameters appears to exist along the watersheds and in the southern parts of the tidal basin. Here the correlation with mud content also improves. This means that, like the carbonate, the organic matter must also be linked to the clay fraction but to a much lesser degree. The association of organic matter with specific size fractions is thus more complex than that of the carbonate. Comparing the organic matter contents with individual mud size fractions reveals a

clear affinity to the fine silt (7 – 8Φ), very fine silt (8 – 9Φ), and clay fractions (>9Φ). Combining these >7Φ size fractions and plotting the pooled data against the organic matter content finally reveals a distinct correlation (Fig. 3-24, right panel), although there is still considerable scatter. In summary, organic matter is preferentially associated with the finer size fractions of the mud.

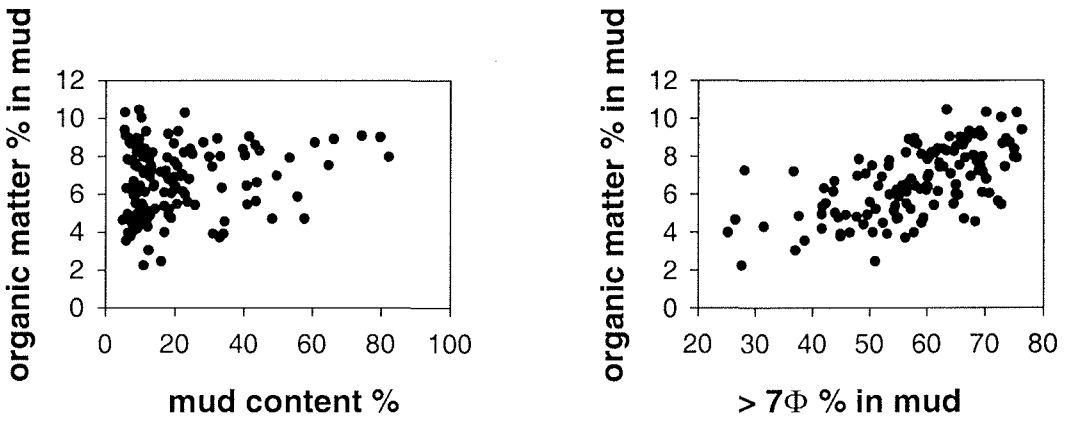

Figure 3-24 Organic matter content in the mud fraction versus mud content and the proportion of the >7Φ fraction in the mud fraction

3.7 Mechanisms of mud deposition

3.7.1 Biogenic processes

The spatial patterns of individual mass physical parameters have demonstrated that they are quite uniformly distributed in the sandy intertidal environments of the tidal basin. Pronounced changes are only observed in response to increasing mud contents. In the study area, elevated mud contents are restricted to isolated patches along the watersheds and to the southern parts of the tidal basin. As documented in the studies of Zens et al. (1997), Michaelis et al. (1995), and Hertweck (1995), many of these mud patches coincide with localities at

which the mussel *Mytilus edulis* preferentially settles to form beds of variable size in the long-term (Fig. 3-25).

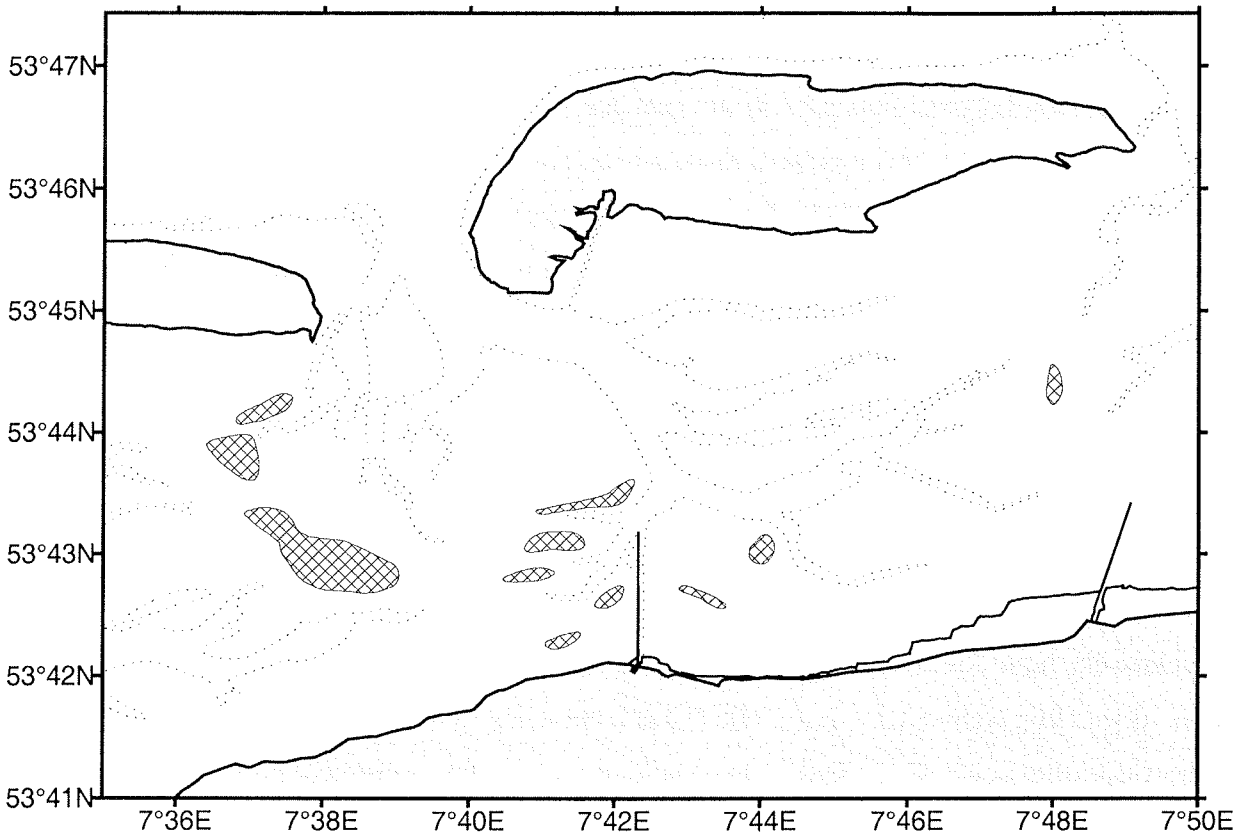

Figure 3-25 Distribution of *Mytilus edulis* beds in the study area (based on Zens et al., 1997; Michaelis et al., 1995; Hertweck, 1995)

Mussel beds have long been recognized as important mud traps in the Wadden Sea (e.g. Linke, 1954; Flemming and Delafontaine, 1994; Oost, 1995; Meadows et al., 1998). *Mytilus edulis* predominantly filters out suspended particles larger than 2-5 μm (Vahl, 1972; Bayne et al., 1976). After absorption of the food, the remaining material is excreted and deposited in the form of faeces. In addition, the mussels aggregate all the rejected material into so-called pseudo-faeces which are also deposited in and around the beds. In fact, pseudo-faeces make up as much as 80% of the biogenic muds. Due to their low bulk density and high water content, the biogenic muds are very soft and therefore very unstable, being easily resuspended by wave action. Nevertheless, the filtering activity of mussels is an important non-hydraulic mechanism of mud accumulation in the Wadden Sea, the deposits often occurring in areas

where non-biogenic muds would normally not accumulate because the hydrodynamic energy is too high.

Biogenic mud deposits must be viewed as temporary sinks which can bind large quantities of aggregated fine-grained material for extended periods of time. The actual volume or mass of such deposits depends on the number and size of the mussel beds present at any one time. At maximum development, mussel beds can occupy as much as 10% of the area of a tidal basin (e.g., Hertweck, 1995). However, since there was an exceptional dearth of mussel beds in the period of this study, the overall contribution of biogenic muds to the budget of fine-grained material in the Otzum tidal basin was correspondingly small.

3.7.2 Hydraulic processes

In comparison to the North Sea, the tidal waters of the Wadden Sea are characterized by relatively high concentrations of suspended matter. In addition, the asymmetry of a tidal wave in shoaling waters (cf. Groen, 1967) has a tendency of moving suspended sediments in a shoreward direction. As a result, hydraulically controlled sedimentation of fine-grained sediment should be a common phenomenon in tidal basins. A depositional mechanism associated with this phenomenon was first proposed by Van Straaten and Kuenen (1957) in the form of the so-called "settling lag" and "scour lag". Settling lag refers to the time interval between the moment at which a decelerating current can no longer keep a particle in suspension and the moment at which the settling particle reaches the bottom. Scour lag, in turn, refers to the time interval between the moment at which an accelerating current begins to exceed the settling velocity of a particle and the moment at which it reaches the critical resuspension velocity. The net effect of the two processes results in a gradual shoreward displacement of a particle until it reaches a position at which the current is unable to resuspend it. The settling lag/scour lag mechanism can thus only come into effect if the mean current velocity and the water depth both decrease.

According to the marine charts NIEDERSÄCHSISCHE KÜSTE, TOPOGRAPHISCHE WATTKARTE 1:25000 and DEUTSCHE KÜSTE, OSTFRIESISCHE INSELN 1:50000 as well as BUNDESAMT FÜR SEESCHIFFAHRT UND HYDROGRAPHIE (1995, 1996, 1997), the mean high-water level at spring tide (MSpHW) lies at about 1.5 m NN, and

at neap tide (MNpHW) at about 1.1 m NN, the term NN denoting the topographic chart datum. On the island flats the MNpHW level defines the lowest elevation at which pioneer salt marsh plants (*Salicornia* and *Spartina*) can survive. Due to the continuous natural slope of the seabed, the energy of the tidal wave is progressively attenuated up to the high water level. Such an environment is particularly favourable to the settling lag/scour lag effect. Along the mainland shore, on the other hand, the MNpHW level is situated near the foot of the dike. As a result, the energy attenuation zone is much narrower and hydrodynamic energy levels are thus much higher than on the island flats. In such circumstances the settling lag/scour lag effect is much less efficient and deposition of fine-grained material is thus inhibited.

Kranck (1973, 1975), studying flocculation processes of suspended sediment in seawater and the deposition from flocculated suspensions, found that suspended sediments from tidal inlets, narrow straits, and the bottom waters of muddy seabed areas had characteristic particle size spectra composed of regular and almost symmetrical frequency distributions with well-developed modes. Optical studies revealed that the particles forming these distributions consist of unsorted mixtures of flocs and single grains. When sediments with such regular spectra were deflocculated and the single grain distributions measured, the size spectra changed to flatter frequency distributions having much lower modal peaks. The relationship between the deflocculated modal size and the floc modal size was expressed by the equation (Kranck, 1973, 1975):

$$\log(\text{grain mode}) = -0.58 + 1.30 \log(\text{floc mode})$$

This means that at 64μm (4Φ) the floc mode is equal to the grain mode. At sizes below this the floc mode is larger than the grain mode, and at sizes over this the floc mode is smaller than the grain mode. Thus, if the hydrodynamic energy is so high as to only allow particles <4Φ to settle out from suspension, then particles >4Φ will not settle out, even if the finer particles are partly flocculated. As the hydrodynamic energy decreases with decreasing water depth, more and more flocculated particles will settle out together with the single particles which results in a more poorly sorted sediment. When the point is reached where the number of particles settling out as flocs begins to exceed that of the particles settling out as single grains, the sediment no longer gets hydraulically sorted.

On the basis of these observations it can be concluded that in the course of transport and deposition hydraulic particle sorting will take place at least in the coarser fractions even if

they are partly flocculated and aggregated. As a result, the finest particles are kept in suspension for a longer time, being ultimately deposited when the hydrodynamic energy has dropped to a very low level. In the Dutch Wadden Sea it has long been noted that in similar depositional environments fine-grained sediments have constant ratios between the amounts of grains below and above about 16μm (6Φ) (e.g., Doeglas, 1946; Favejee, 1951; van Straaten, 1963). A similar phenomenon was also noted in the Danish Wadden Sea (Bartholdy, 1985; Bartholdy and Pheiffer Madsen, 1985; Pejrup, 1988). As described in section 2.1.2, a marked change in sediment composition was observed at about 7Φ (8μm) in the fine-grained sediments of the Otzum tidal basin. The ratio between the proportions of the >7Φ and the >4Φ size fractions in the surficial sediments should therefore be a sensitive indicator for relative energy levels in the tidal basin.

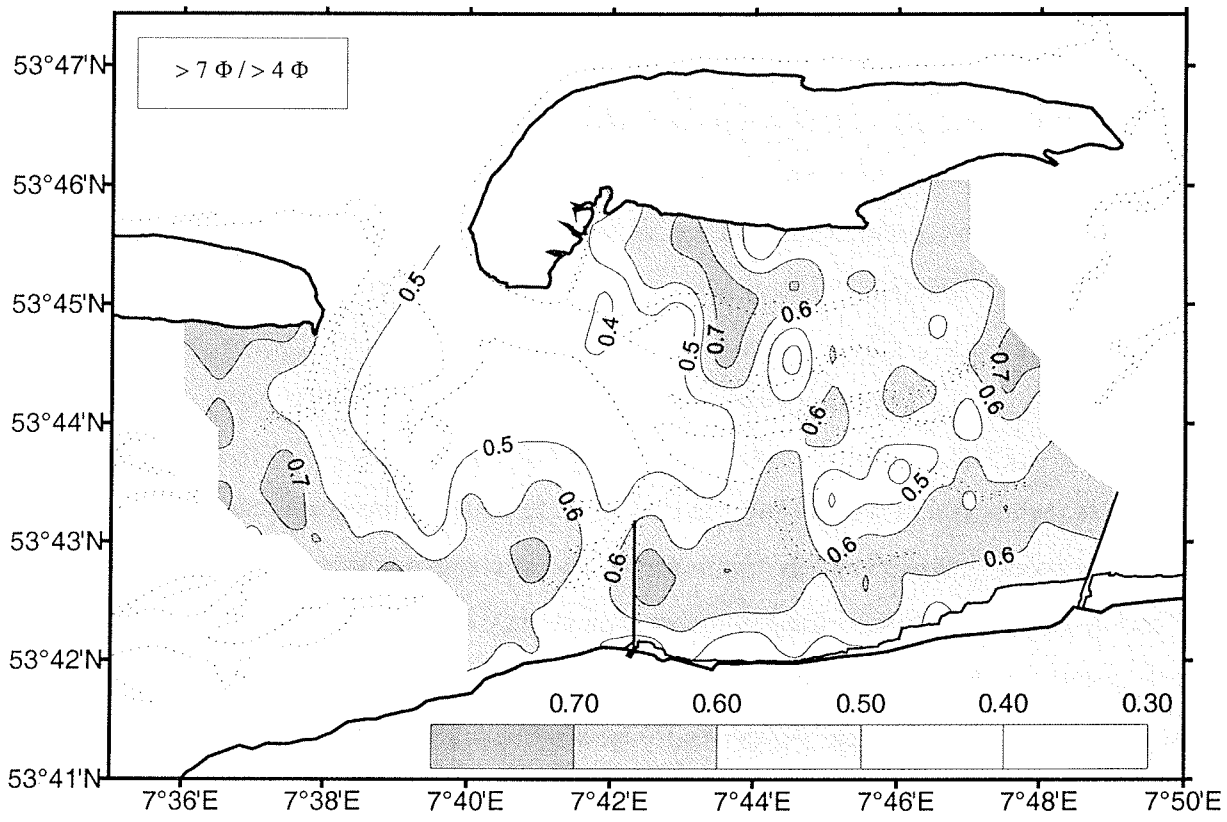

Figure 3-26 Distribution of (>7Φ / >4Φ) ratios in the Otzum tidal basin

From the spatial pattern formed by the (>7Φ/>4Φ) ratios in the Otzum tidal basin (Fig. 3-26) it can be seen that, with the exception of areas occupied by biogenic muds along the watersheds, the (>7Φ/>4Φ) ratio is slightly higher on the island flats than along the mainland coast. This would suggest that energy levels are slightly lower on the island flats than elsewhere in the basin. The pattern produced by the (>7Φ/>4Φ) ratio therefore supports the conclusion reached earlier with respect to the local effectiveness of the settling lag/scour lag mechanism in the Otzum tidal basin.

4 Textural sediment parameters

4.1 Statistical methods

4.1.1 Moment statistics

Statistical grain size parameters, namely the mean, median, mode, sorting, skewness, and kurtosis are commonly used to describe grain size distributions of a sediment. Such textural parameters can be generated by different statistical procedures. One of these is the method of moments. In contrast to selective percentile statistics, the moment method takes all the available size frequency data, i.e. the whole size distribution, into consideration (cf. Table 4-1).

Table 4-1 Equations defining the moment measures of grain size distributions (after Marsal, 1979)

Mean	$\bar{x} = \frac{\sum f_i x_i}{\sum f_i}$
Sorting	$\sigma = \sqrt{\frac{\sum f_i (x_i - \bar{x})^2}{\sum f_i}}$
Skewness	$\frac{\sum f_i (x_i - \bar{x})^3}{(\sum f_i) \cdot \sigma^3}$
Kurtosis	$\frac{\sum f_i (x_i - \bar{x})^4}{(\sum f_i) \cdot \sigma^4}$

where x_i is the midpoint of every size interval in Φ; f_i is the frequency percentage of every size interval; $\sum f_i$ is the sum to 100 (in practice it may be <100 if the sample is very fine, and part of the fine fraction is truncated due to technical limitations of the grain size measuring technique).

A normal distribution can be defined by two moments, the mean and the standard deviation. The mean is the arithmetic average of a frequency distribution. In sedimentological

terms it denotes the mean grain size of a sediment. In general, it is thought to reflect a combination of source and transport related features. For sediments deposited in the course of hydraulic transport, the mean diameter is an average measure of the maximum kinetic energy of the fluid and is commonly represented by a current velocity (e.g., Inman, 1949; Menard, 1950; Bagnold, 1968).

The mode or modal diameter is the most frequent grain size occurring in a frequency distribution, whereas the median denotes the grain size at which a frequency distribution is divided into two equal parts, i.e. at the 50th percentile. In normal distributions the mean, median, and mode (expressed in Φ) coincide, i.e. they all have the same grain size. Most natural sediments, however, do not have normal grain size distributions and the mode thus becomes more important than the mean. This is especially relevant when dealing with multi-modal sediments because the presence of more than one mode implies that the sediment is composed of several grain size populations, each of which may have been derived from a different sediment source (e.g., Curray, 1960; Flemming, 1988).

In combination with the first moment, the second moment expresses the standard deviation which is a measure of the "spread" of a distribution around a mean. In sedimentological terms it describes the degree of sorting, low standard deviations denoting better sorted (e.g., curve A in Fig. 4-1a), high standard deviations more poorly sorted sediments (e.g., curve C in Fig. 4-1a).

In combination with the mean and the standard deviation, the third and the fourth moments define the skewness and the kurtosis of a grain size distribution, respectively. Skewness relates to the symmetry of a distribution curve, the median and mode lying to the right of the mean in a positively skewed distribution (left curve in Fig. 4-2), and to the left of the mean in a negatively skewed distribution (right curve in Fig. 4-2). In a normal distribution the skewness is zero and the mean, mode and median coincide (centre curve in Fig. 4-2). Kurtosis, by contrast, defines the peakedness of a size frequency distribution. However, symmetrical distribution curves may be quite differently peaked (cf. Fig. 4-1b). Normal distribution curves would have a kurtosis of 3, leptokurtic curves a kurtosis >3, being characterized by more peaked distributions than the normal curve, and platykurtic curves a kurtosis <3, being characterized by flatter distributions than the normal distribution.

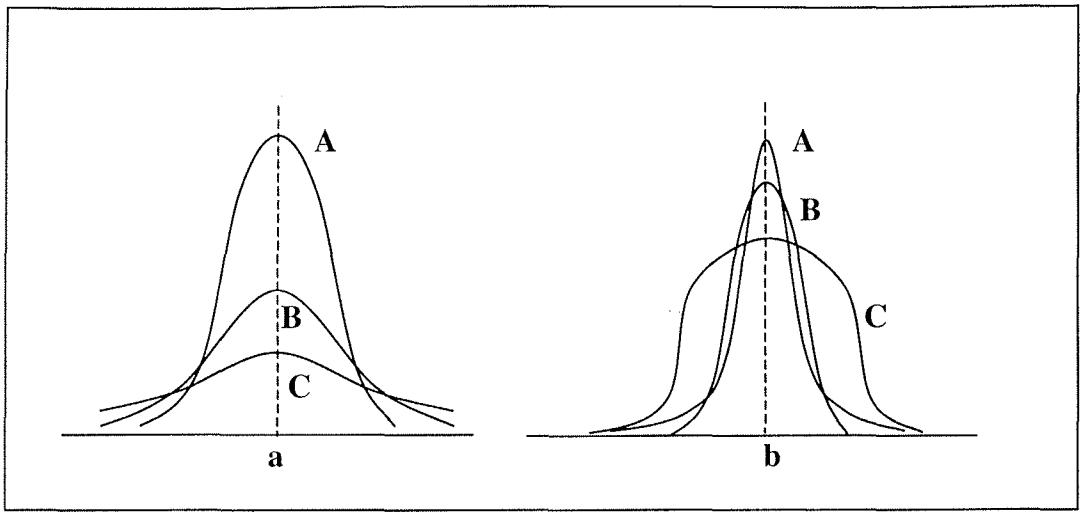

Figure 4-1 a: Normal distributions with different standard deviations; b: Symmetrical distributions with different kurtoses. A - leptokurtic distribution with kurtosis >3, B – normal distribution with kurtosis = 3, C – platykurtic distribution with kurtosis <3.

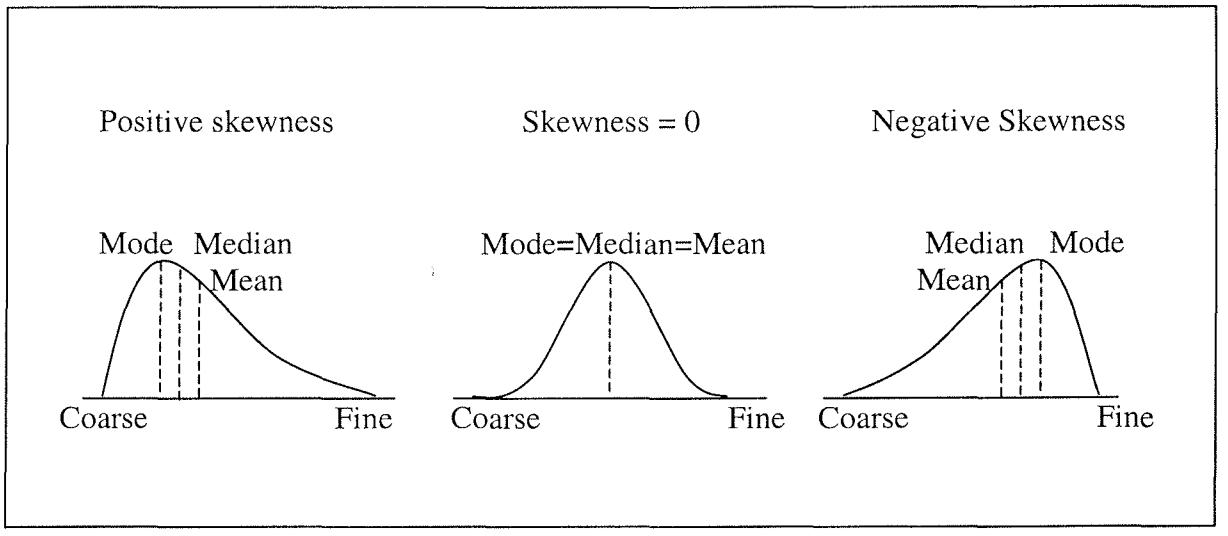

Figure 4-2 The relative positions of mode, mean, and median in positively skewed (left) and negatively skewed (right) distributions relative to a normal distribution (centre)

In practice, a frequency distribution may be considered to have a normal distribution if it has a skewness of 0 and a kurtosis of 3. Since a distribution theoretically has an infinite number of moments and the moments are not an inherent property of normal distributions only, it is not uncommon that non-normal distributions have a skewness of 0 or a kurtosis of 3. In total, the different moment measures provide unique descriptions of grain size distributions which can hence be used to compare individual samples with each other or to plot spatial patterns of large sample suites, thereby revealing systematic changes related to the depositional process.

4.1.2 Percentile statistics

Besides the statistical moment method, there are various percentile methods which commonly use different combinations of graphically determined percentile values to calculate textural parameters. The first graphic procedure, based on the millimetre scale, was developed by Trask (1932). A few years later Krumbein (1934, 1936) introduced the Φ-scale which represents the binary logarithmic transformation of the millimetre scale. This transformation was prompted by the fact that many sediments were found to have uni-modal grain size distributions which could be described by a lesser or greater departure from a log-normal distribution. Using Φ-values in place of mm-values greatly simplified the arithmetic involved in computing grain size parameters, and the Φ-based graphic procedure is today still being widely applied in geology. In the pre-computer age, the statistical parameters had to be individually calculated by hand (later by pocket calculator). This was a time-consuming and tedious procedure, in particular when large sample numbers were involved. In each case the percentile values had to be manually picked out of a graphic cumulative grain size distribution plotted on probability paper. It is for this reason that the term graphic statistics is sometimes used in place of percentile statistics.

The two most commonly used percentile-based procedures are those by Inman (1952) and Folk and Ward (1957). The former author developed a number of simple equations using up to five percentiles, whereas the latter authors expanded the equations using up to seven percentiles to allow a better description of grain size distributions which depart more strongly from normal distributions (Table 4-2).

Table 4-2 Percentile procedures for the calculation of textural parameters

	Inman (1952)	Folk and Ward (1957)
Mean	$M_\phi = \frac{\Phi_{16} + \Phi_{84}}{2}$	$M_z = \frac{\Phi_{16} + \Phi_{50} + \Phi_{84}}{3}$
Sorting	$\sigma_\phi = \frac{\Phi_{84} - \Phi_{16}}{2}$	$\sigma_I = \frac{\Phi_{84} - \Phi_{16}}{4} + \frac{\Phi_{95} - \Phi_5}{6.6}$
Skewness	$\alpha_\phi = \frac{\Phi_{84} + \Phi_{16} - 2\Phi_{50}}{\Phi_{84} - \Phi_{16}}$	$SK_I = \frac{\Phi_{84} - \Phi_{16} + 2\Phi_{50}}{2(\Phi_{84} - \Phi_{16})} + \frac{\Phi_{95} - \Phi_5 + 2\Phi_{50}}{2(\Phi_{95} - \Phi_5)}$
Kurtosis	$\beta_\phi = \frac{(\Phi_{95} - \Phi_5) - (\Phi_{84} - \Phi_{16})}{\Phi_{84} - \Phi_{16}}$	$K_G = \frac{\Phi_{95} - \Phi_5}{2.44(\Phi_{75} - \Phi_{25})}$

4.2 A systematic comparison of moment measures with percentile measures

There are few detailed studies in which textural parameters generated by a percentile method have been systematically compared with those derived from moment statistics. Friedman (1962a) discussed the relationships and differences between percentile and moment measures of about a thousand sediment samples of sandstones and recent sands. He found that for recent sands the sorting coefficients derived by the two methods were systematically related to each other. Nyandwi (1995) compared mean diameter, sorting, skewness, and kurtosis values of a large sample set from the Spiekeroog tidal flats derived by the method of moments with those generated by the percentile method of Inman (1952). He found good correlations for mean diameters and sorting but no correlation for skewness and kurtosis. These studies only dealt with sands or the sand fractions of a sediment. However, an equivalent comparison which also incorporates the mud fractions in the sediment has thus far not been carried out.

To shed more light on this question and, in particular, to derive at a decision about which method, if any, should preferentially be applied, a systematic investigation was carried out using the data set generated in the course of this study (321 samples). The comparison

involved the total size distributions (sand and mud) resolved at 0.25Φ intervals, applying the percentile methods by Inman (1952) and Folk and Ward (1957) as well as the method of moments. The textural parameters were computed by newly developed FORTRAN77 program using the equations listed in Table 4-1 and Table 4-2.

4.2.1 A comparison of textural parameters generated by the two percentile methods

A systematic comparison of the results obtained by the percentile methods of Inman (1952) and Folk and Ward (1957) reveals a fairly good correlation between the mean diameters and the sorting values (upper two plots in Fig. 4-3). In the case of the mean diameters (upper left plot in Fig. 4-3), the values are almost identical at about 2Φ but then progressively diverge the finer the sediment gets. At about 6.5Φ the Inman mean is about one whole Φ-value finer than the Folk and Ward mean. Then, between 6.5Φ and 7Φ, there is a sudden vertical displacement in the progression, the two means being identical once more at about 7Φ. At values >7Φ the relationship is not entirely clear because of the few data points but the new regression appears to proceed with a slope which parallels the slope at coarser mean diameters, i.e. the mean diameters again begin to diverge in the same manner as before.

In the case of sorting, the relationship between the two percentile methods is characterized by two trends (upper right plot in Fig. 4-3). At values >1Φ the trend is ill-defined, the Inman sorting values being either identical or lower than the Folk and Ward sorting values. At an Inman sorting of about 0.5Φ (corresponding to a Folk and Ward sorting of about 1.2Φ) the slope in the trend line changes dramatically, the Inman sorting now improving at a much lower rate than the Folk and Ward sorting, the two reaching identical values at about 3Φ, the Folk and Ward sorting being marginally better thereafter.

In the case of skewness, the Inman and the Folk and Ward values are almost identical in the range from negatively skewed to near-symmetrical distributions up to a skewness of about +0.05. At this point the scatter suddenly increases from identical values to +0.5 values in the case of the Folk and Ward skewness. The point scatter then progressively converges to again reach identical values at a skewness of about +0.9.

Kurtosis values, by contrast, are overall poorly correlated, the scatter rapidly diverging from a common origin at an Inman kurtosis of about 0 and a Folk and Ward kurtosis of about 0.5. In some cases the Inman kurtosis values are considerably lower than the Folk and Ward values, in other cases the two are identical, and in yet others they are higher. The upper and lower limits, however, are defined by straight line relationships.

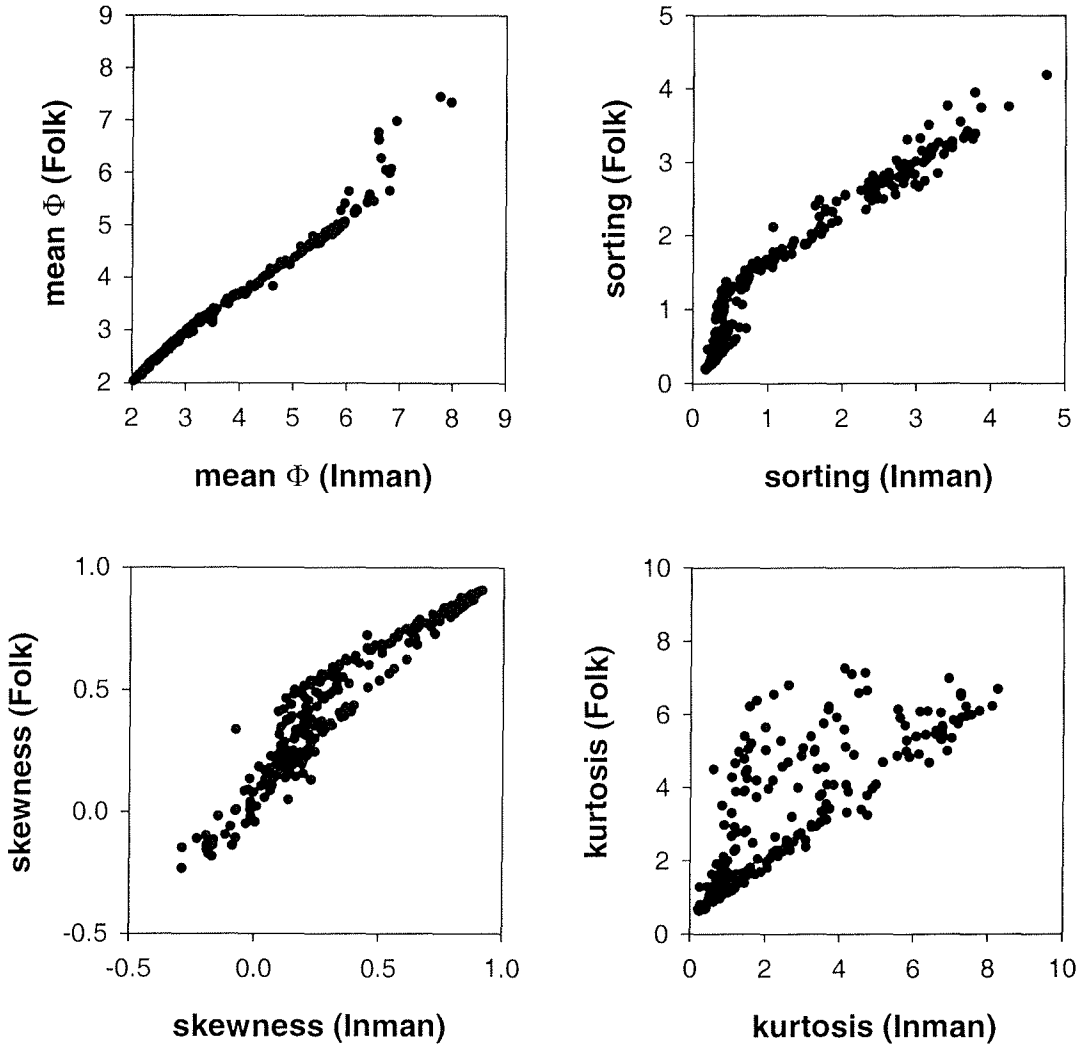

Figure 4-3 Comparing grain-size parameters between Inman's method and the method of Folk and Ward

In summary it can be concluded that, with the exception of kurtosis, the textural parameters calculated by different percentile methods are broadly comparable in that the overall textural trends are similar. In a sample to sample comparison, however, there can be substantial differences with respect to kurtosis values.

4.2.2 Moment statistics versus percentile statistics

4.2.2.1 The total sediment concept

Theoretically, a so-called total sediment refers to all the grain-size fractions from the coarsest to the finest endmembers in a frequency distribution. In the case of gravel-sand or sand-mud mixtures, the grain-size measurements are often truncated due to technical limitations, one part being measured by one technique, the second part by another technique. In the present case, the sediments were composed either of sand or of sand-mud mixtures, the grain size distributions of the sands (or sand fractions) being measured by settling tube, the mud fractions by Sedigraph. To optimise the time required for the analysis of the fine fractions, the distributions were arbitrarily truncated at 11Φ. This appeared justified because 305 of the 321 samples (i.e. 95 %) had less than 1 % of its material finer than 11.00Φ, and only one sample had more than 5 %.(cf. Table 4-3). The distortions introduced at the fine end of the distribution by this procedure were thus minimal.

Table 4-3 Weight-% material finer than 11.00Φ in all analysed samples

Fractions finer than 11.00Φ	<1 %	1 - 2 %	2 –3 %	3 –4 %	> 5 %
Percentage in all samples %	95.00	4.06	0.31	0.31	0.31

Comparing both the textural parameters of the Inman and the Folk and Ward percentile methods with the results of the moment statistics (Fig. 4-4 and Fig. 4-5) demonstrates that, of the four parameters, the mean diameters and the sorting of the total sediment show reasonably good correlations, particularly at the coarser-grained ends and in the better sorted parts of the scatter diagrams (upper panels in Figs. 4-4- and 4-5). Of the two percentile methods, the Folk and Ward procedure produces less variable trends with respect to these parameters. In sediments with mean diameters <4Φ (sandy sediments) the percentile

means are slightly coarser than the moment means, whereas at mean grain sizes >4Φ (muddy sediments) the percentile means are slightly finer than the moment means. With respect to sorting, both percentile methods show poor correlation with their moment counterparts in all better sorted sediments. Due to the larger range covered by the moment sorting in this crucial range, the moment method evidently provides a much better distinction between individual samples of generally well sorted sediments.

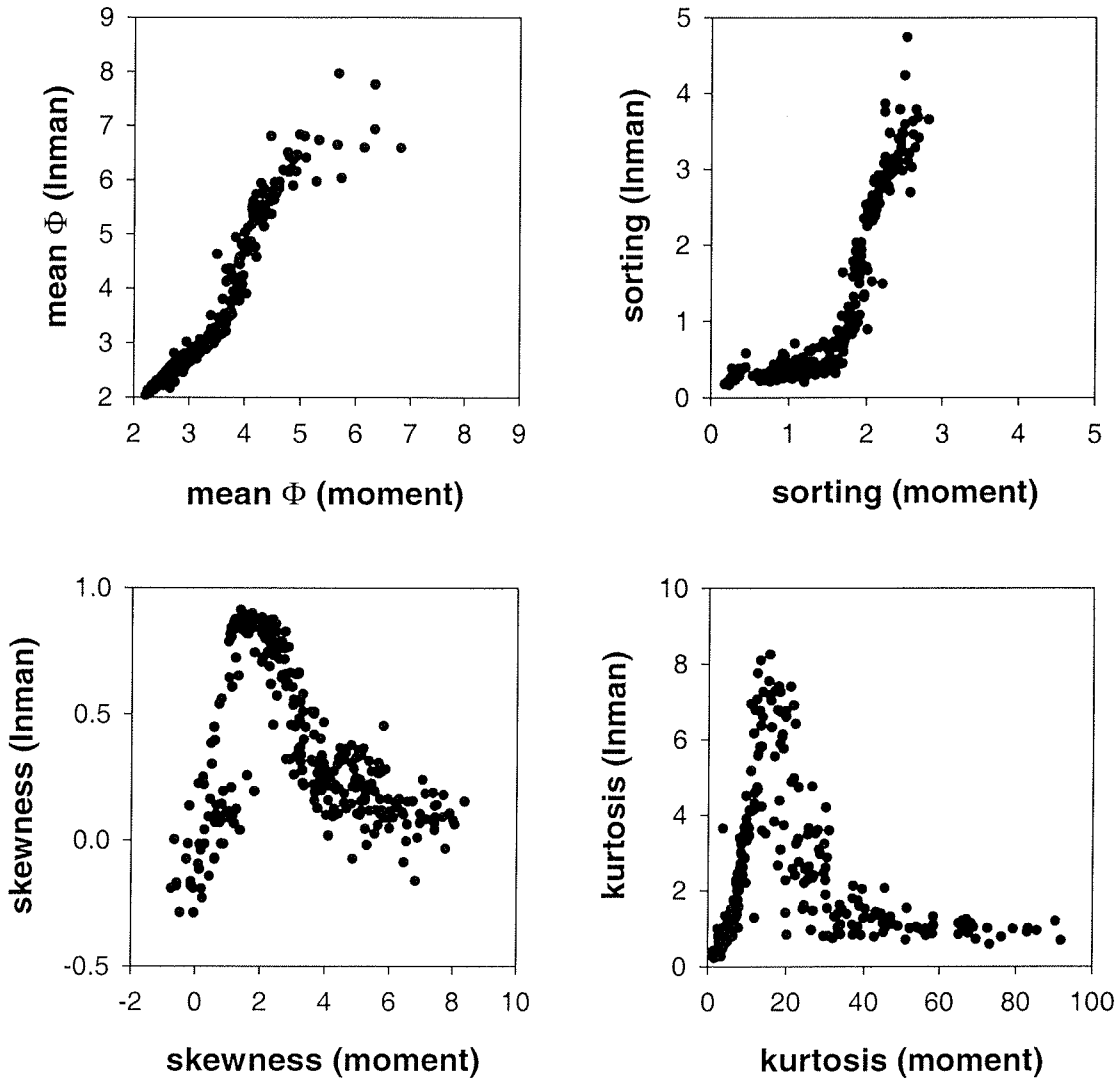

Figure 4-4 Moment measures versus percentile measures after Inman (1952)

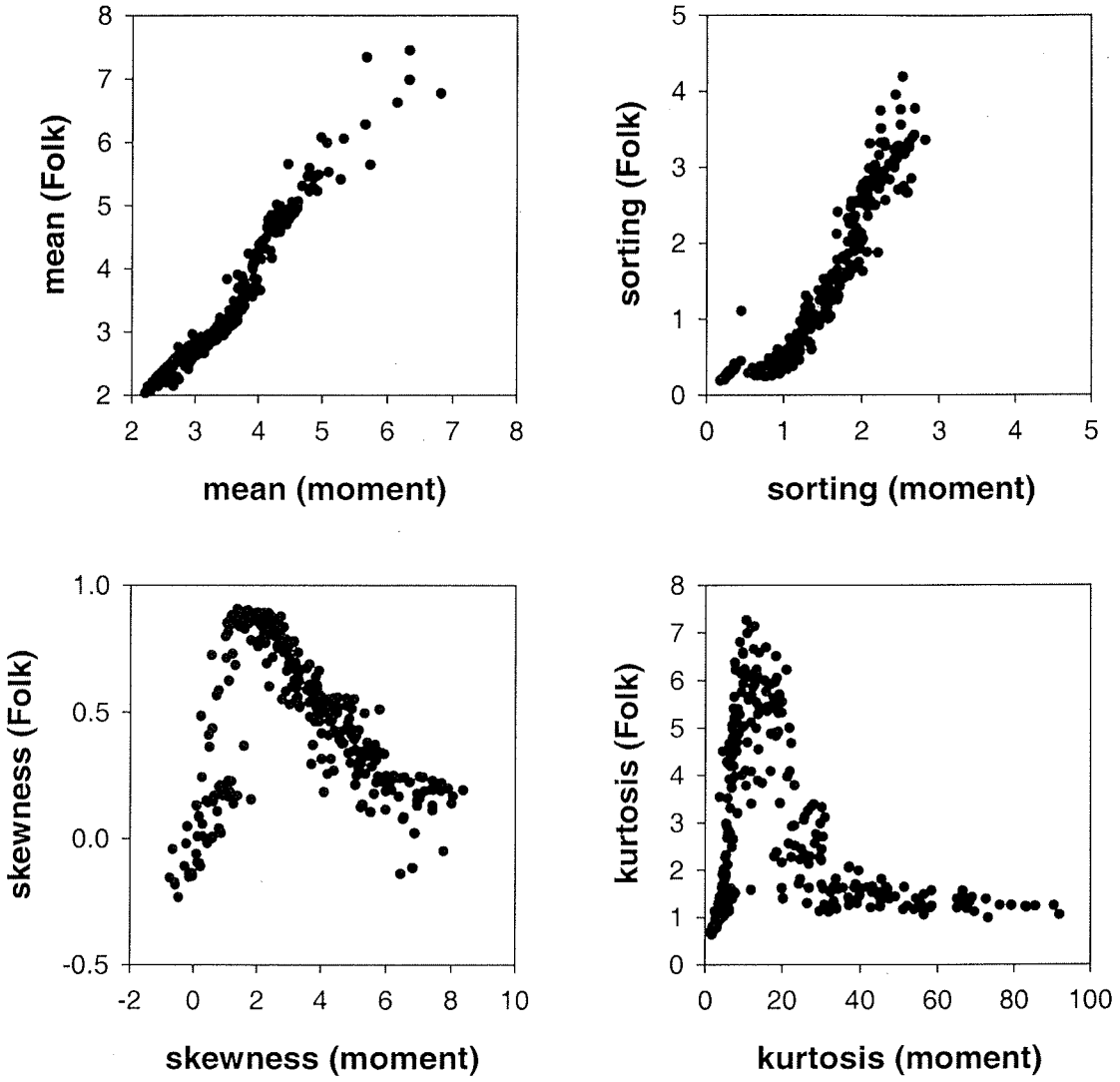

Figure 4-5 Moment measures versus percentile measures after Folk and Ward (1957)

In comparison with the mean diameters and sorting values, the relationships between percentile skewness and kurtosis, on the one hand, and moment skewness and kurtosis, on the other, are rather different (lower panels in Figs. 4-4 and 4-5). In each case the point scatter can be divided into two different groups, one being positively correlated, the other being negatively correlated with their respective moment counterparts. In both percentile methods

the dividing points between the two trends lie at a moment skewness of 2, and a moment kurtosis of 15, respectively. As a result of this twofold trend the relationships are ambiguous, there being two moment measures for every percentile measure.

In summary, as far as skewness and kurtosis are concerned, the moment measures are clearly more consistent than their percentile counterparts. As a consequence, percentile values of skewness and kurtosis of sand-mud mixtures should be treated with caution regarding their usefulness in reflecting hydraulic size-sorting processes. On the other hand, it has to be remembered that muds are commonly deposited in the form of flocs, faecal pellets, and other aggregates which are destroyed when processing samples for laboratory analysis. This breaking down of the larger, compound particles into their much smaller constituents obviously distorts the true hydraulic nature of the sediment (cf. section 3.7). As a result, even the textural parameters generated by application of the moment method must be viewed with reservation regarding their hydraulic relevance.

4.2.2.2 The sand fraction concept

Having highlighted some inconsistencies in the generation and interpretation of textural parameters calculated on the basis of total sediment distributions (sand-mud mixtures), it might now be useful to compare the percentile method with the moment method using the sand fractions only. Both methods were applied to the same data set generated by using a settling tube for grain size analysis.

As illustrated in Fig. 4-6, the textural relationships between the percentile method (here after Inman, 1952) and the moment method clearly produce far more coherent trends when based on the sand fractions alone. Significantly, the data scatter increases the more complex the moment measures become. Thus, the mean diameters generated by the two methods are virtually identical. Moment sorting is fairly well correlated with Inman's sorting, the latter appearing slightly less well sorted than the former. Skewness and kurtosis, in turn, show more scatter but are nevertheless positively correlated, thus strongly departing from the ambiguous trends observed when comparing the same parameters based on the total sediment.

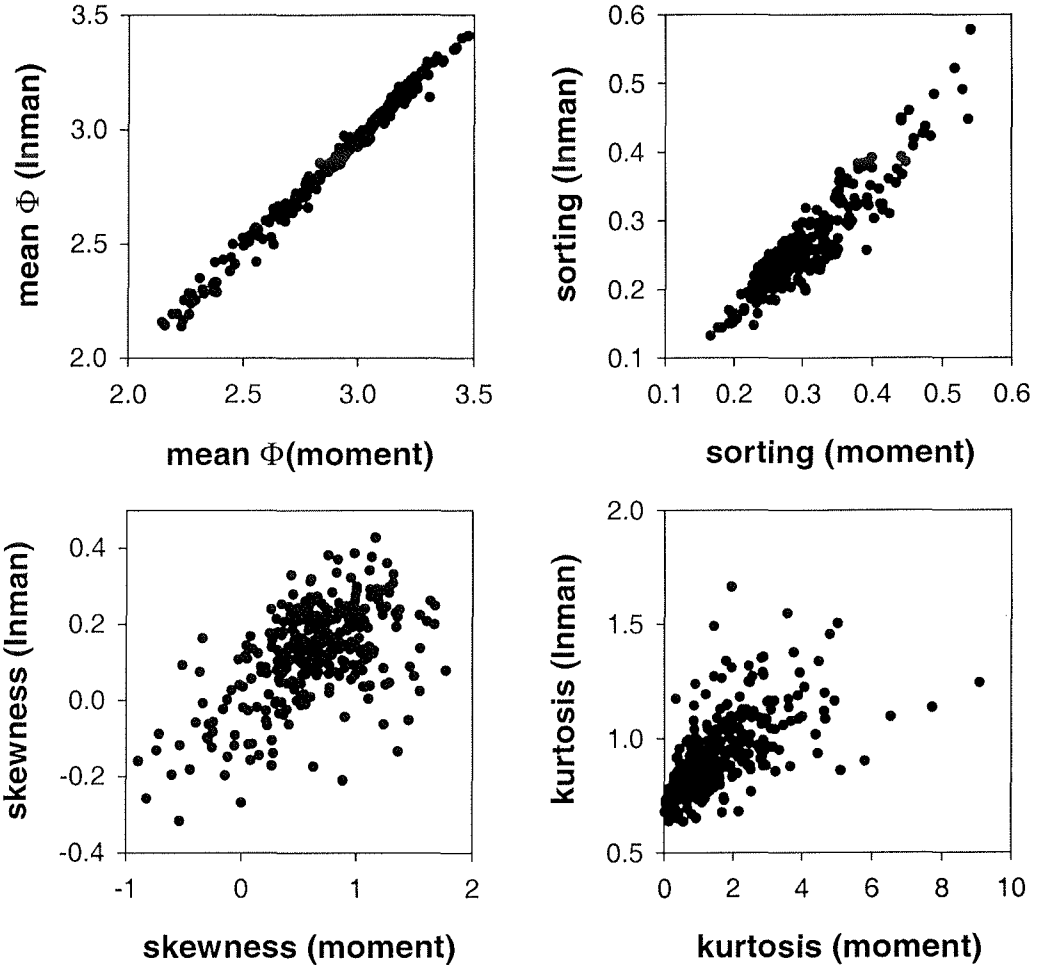

Figure 4-6 A comparison of textural parameters generated by the Inman percentile method and the moment method

Looking at the respective scales along the x and y axes, a feature must now be addressed which was ignored in the previous comparisons. It will be noted that in the case of skewness and kurtosis (i.e. in the more complex moment measures) the scale intervals are completely different. This means that the numeric values of the one method are not directly comparable to the other. Indeed, this may also apply to the sorting scales, and the apparent difference in sorting highlighted above may therefore simply be a mathematical artefact. It will be noted that the difference in the scales increases with increasing complexity of the

moment measure. Thus, at the level of the first moment (mean diameter) the difference is negligible, at the level of sorting it amounts to a small offset, while at the levels of skewness and kurtosis the differences increase in non-linear fashion. As a consequence, with the exception of the first moment, all the other moments require newly adapted subdivisions if the same descriptive terminologies are to be used as those developed for the percentile measures.

Table 4-4 Sorting classification of sands based on moment statistics (after Friedman, 1961)

Sorting Interval	Terminology
< 0.35	Very well sorted
0.35 – 0.50	Well sorted
0.50 – 0.80	Moderately well sorted
0.80 – 1.40	Moderately sorted
1.40 – 2.00	Poorly sorted
2.00 – 2.60	Very poorly sorted
> 2.60	Extremely poorly sorted

In terms of moment statistics, the sand fractions of the sediments in the study area are fine to very fine grained, the mean grain sizes lying between 2.15 - 3.48Φ. The sorting coefficients range from 0.17 – 0.54. According to classification of Friedman (1961) (Table 4-4), 81.93% of the samples would be very well sorted, 16.82% well sorted, and 1.25% moderately well sorted. Skewness, in turn, ranges from -0.90 to +1.77, most of the sands (90.97%) being positively skewed.

4.2.3 Relationships between individual grain-size parameters

4.2.3.1 Moment measures

According to the statistical procedure (see section 4.1.1), the mean grain size is the reference point in the grain size frequency distribution relative to which the sorting coefficient, the skewness and the kurtosis are calculated. Due to the response of grain size distributions to hydraulic size-sorting processes, similar textural features should reflect similar hydrodynamic conditions, whereas different textural features should relate to different hydrodynamic regimes. Progressive changes in the spatial arrangement of such textural relationships should thus reflect systematic hydrodynamic changes. This theoretical concept was tested by comparing the relationships between the textural parameters of all the sediment samples in individual scatter diagrams, and then transferring tagged data points forming obvious groupings to their respective geographic positions on textural maps of the study area to check whether they formed coherent spatial patterns in the Otzum tidal basin as required by the theoretical concept.

As illustrated in Fig. 4-7, the textural relationships between the mean diameters and the other three parameters allows a clear distinction of at least three sample groups, here highlighted by different symbols (group A: open circles; group B: solid circles; and group C: inverted open triangles). Group A represents pure sands, whereas group B and C represent sediments composed of different sand-mud mixtures. Transposing these groups onto a map of the study area (Fig. 4-8) confirms that the groups indeed form coherent spatial patterns which are quite clearly controlled by different hydrodynamic regimes. Thus, group A samples form a large patch stretching from the inlet some 5 km towards the south-east, thus occupying the highest energy zone of the tidal basin. Group C samples are found exclusively on the two island flats, whereas group B samples are restricted to the watersheds and the dike flats along the mainland shore. The coherent spatial arrangement of the individual sample groups into different hydrodynamic zones therefore provides strong support for the validity of the hydraulic size-sorting concept outlined above.

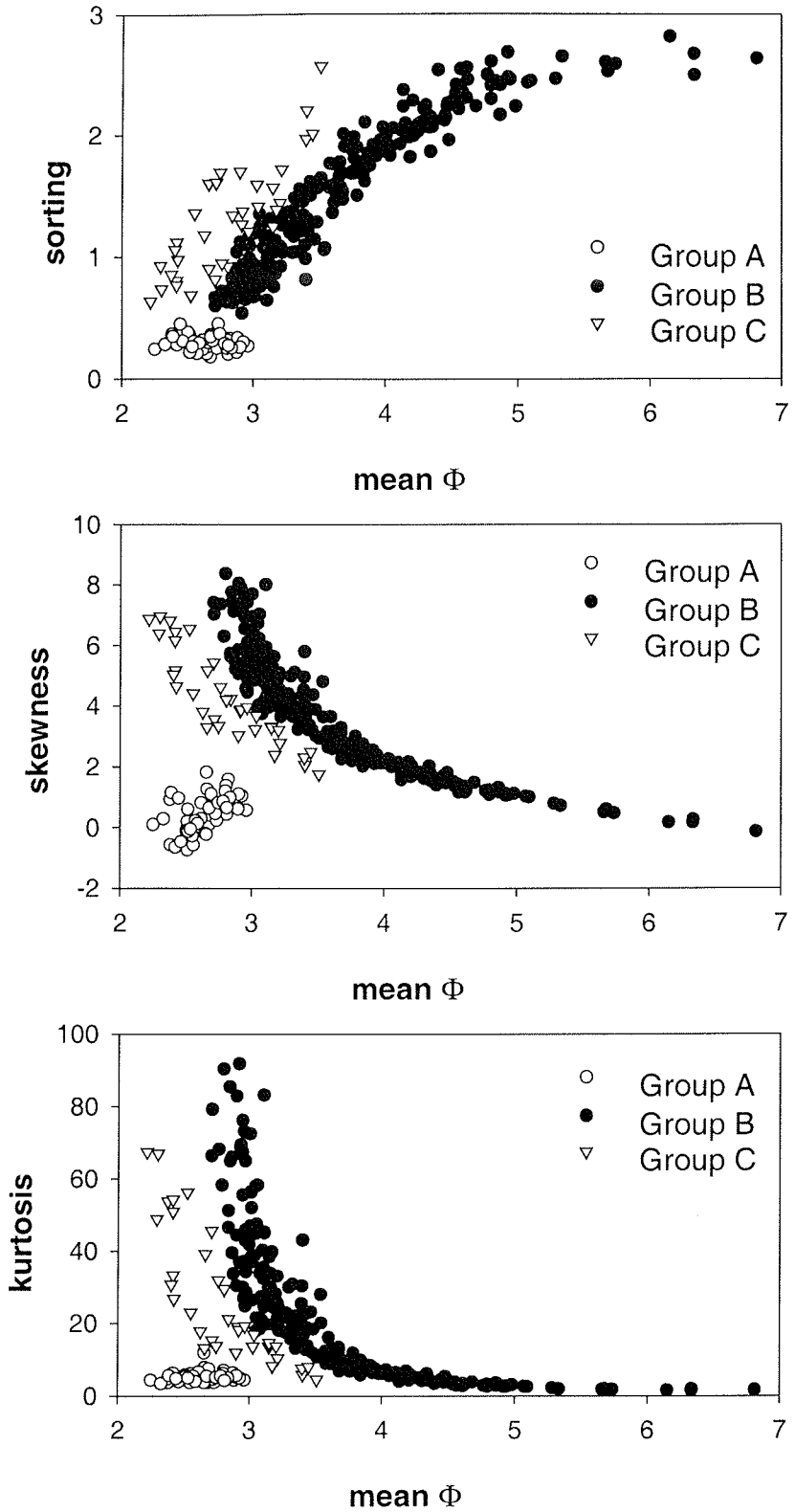

Figure 4-7 Moment mean versus moment sorting, skewness and kurtosis

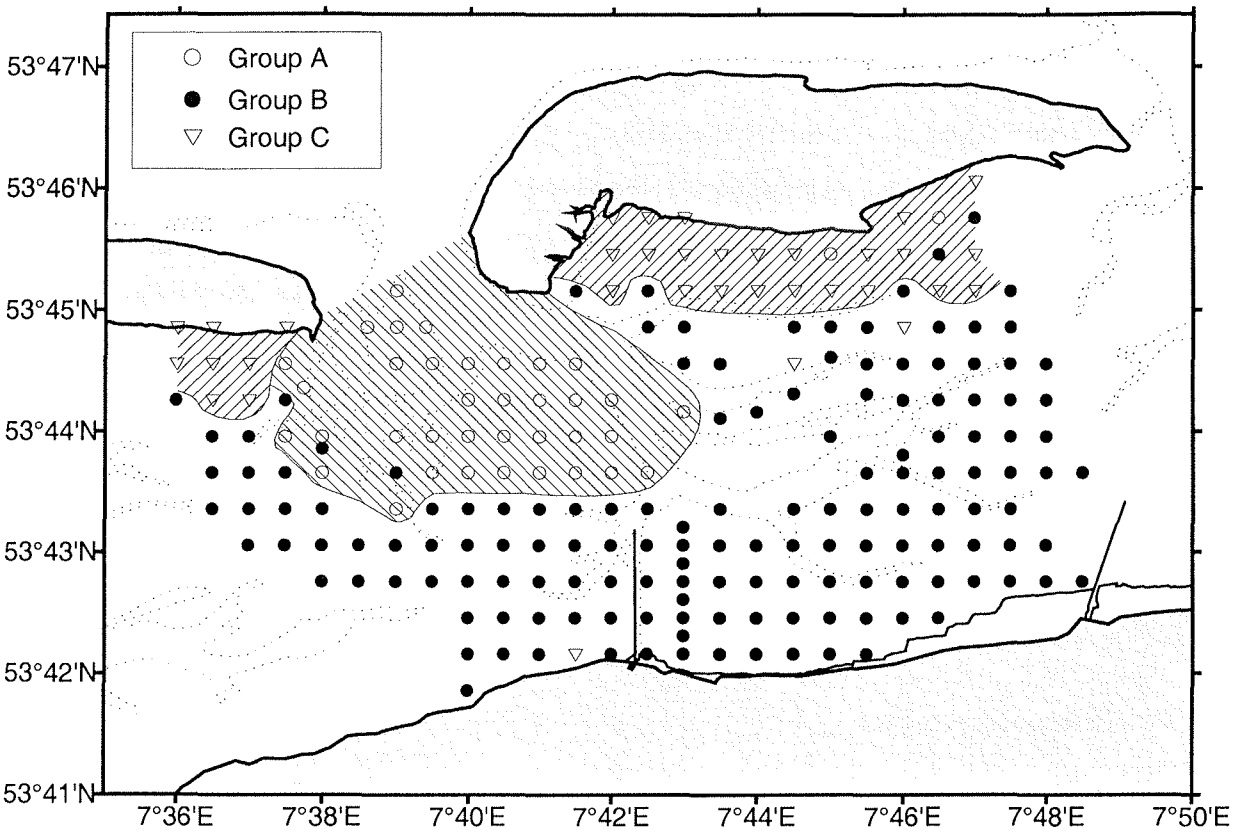

Figure 4-8 The spatial patterns of group A, B and C sediments in the study area

Of the three groups, the pure sands (group A) have the lowest sorting coefficients (0.18 - 0.45) and the smallest kurtosis values (3.40 - 11.89). The skewness values are concentrated around 0, ranging from -0.74 to +1.81. These samples are thus the best sorted, their grain-size distributions being mostly near-symmetrically distributed. Besides the differences between group A and group B and C samples, the mean versus sorting, mean versus skewness, and mean versus kurtosis relationships of group B and C samples have broadly similar trends, being merely offset by large enough amounts to separate them from each other. The group C samples are on the whole somewhat coarser than the group B samples. Furthermore, as in the case of group C samples, the group B sediments become progressively more poorly sorted as the mean grain size decreases, while changing from very positively skewed and very leptokurtic distributions to almost negatively skewed, somewhat platykurtic distributions.

The textural differences of the sediments comprising group A, B and C samples must evidently be related to the hydrodynamic processes controlling their deposition. Thus, group B sediments are composed of fine sand, very fine sand, and mud which can be considered to reflect tide-controlled sedimentation along the watersheds and the mainland shore. Group C sediments, which occur on the island flats and comprise fine sands with small admixtures of medium sand and mud, are predominantly deposited in the course of settling lag/scour lag activity in the wake of vigorous wave resuspension processes. In accordance with the historical evolution of the East Frisian barrier islands (Fitzgerald et al., 1984a, 1984b; Fitzgerald and Penland, 1987; Flemming, 1991), the pure sands of the group A sediments reflect the influence of both high wave action and strong current velocities (cf. section 1.2.2.2) which both prevent the deposition of fine sediments. Many of these samples have a negative skewness, thus conforming with the textural character of typical beach sands (e.g., Friedman, 1961, 1962a, 1979).

4.2.3.2 Percentile measures

In comparison to the results of the moment measures, the corresponding textural scatter diagrams using the Inman and Folk and Ward percentile measures do not show such clear differences between the group A, B and C sediments (Fig. 4-9). Even though the general trends of the mean versus sorting and mean versus kurtosis diagrams are similar to those of the moment measures, they do not even separate the pure sands (group A) efficiently from the mixed sand-mud samples (group B and C), the latter two groups also showing considerable overlap. In contrast to the moment mean versus the moment skewness, both the corresponding diagrams of the Inman and Folk and Ward percentiles not only show a poor spatial resolution of the different groups but, in addition, have completely different trends.

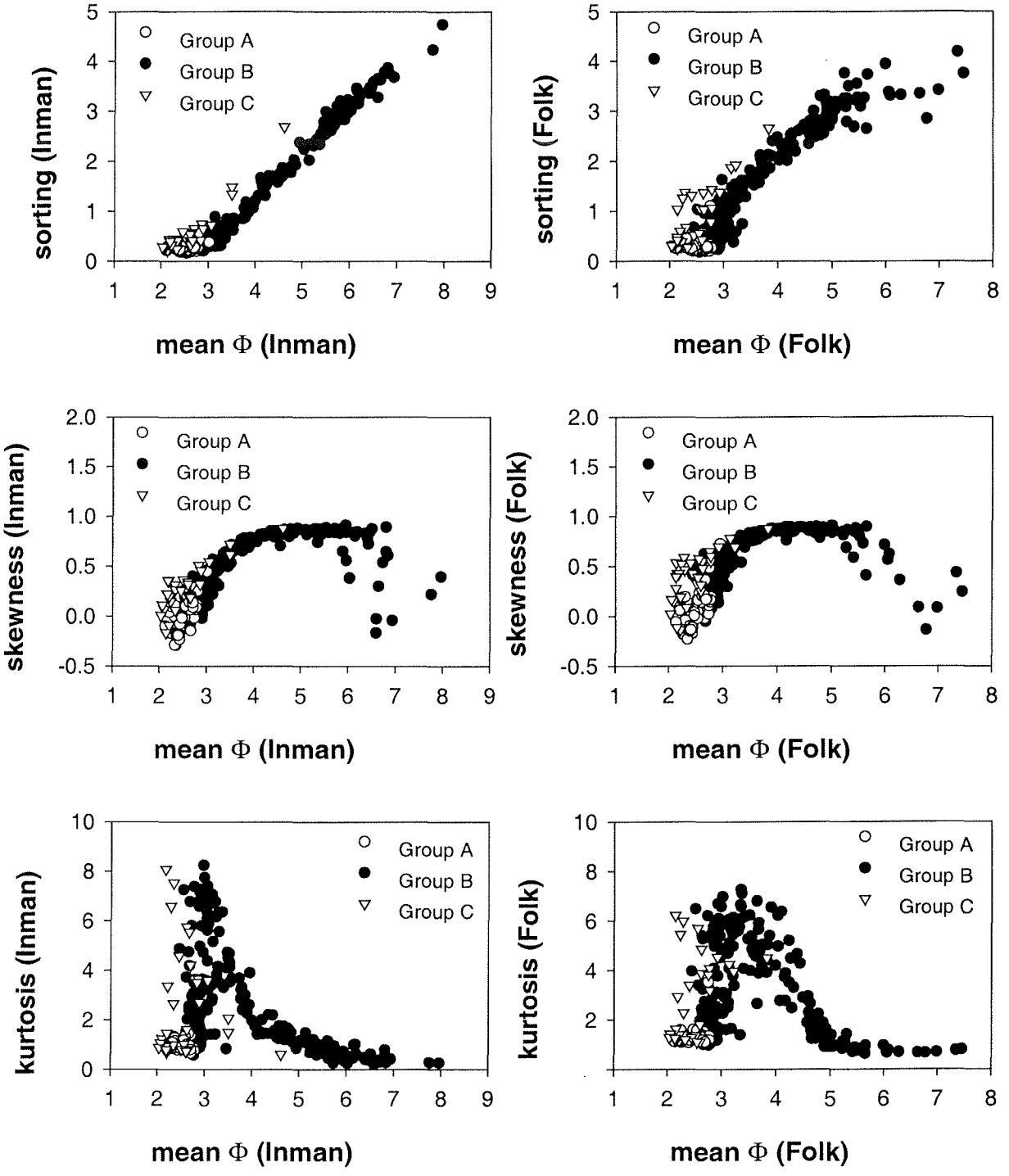

Figure 4-9 Percentile means versus percentile sorting, skewness and kurtosis

4.3 A critique of methods

The comparison of the relationships between the textural parameters generated by the method of moments and the percentile method has clearly demonstrated the superiority of the moment method in distinguishing specific hydrodynamically controlled sediment groups in the Otzum tidal basin. The only plausible reason for this is the fact that the percentile method describes grain size distributions on the basis of a small number of selected percentiles, whereas the moment method takes the entire grain size distribution into consideration. This evidently results in a much better textural characterisation of individual grain size distributions. To illustrate this, let us consider three samples, one comprising pure sand, another a mixture of 96% sand and 4% mud, and the third a mixture of 96% sand and 4% gravel. In this case the percentile method would give all three samples an identical textural description because it ignores the finest and coarsest 5% of the frequency distributions. On account of their composition the three sediments would clearly be associated with different hydrodynamic regimes which would result in spatially separated deposits. The comparison has shown that the percentile method does correctly reveal the relationship between mean grain size and sorting of the sediments, but that it does not correctly describe the effects of skewness and kurtosis on the grain-size distribution. This conclusion underlines the findings of Friedman (1962b) and Middleton (1962) who stated that the moment method described different properties of a grain size distribution than the percentile method.

Grain-size parameters are widely and frequently used to describe sedimentary facies, and even to define sediment transport pathways (e.g., McLaren, 1981; McLaren and Bowels, 1985; Gao and Collins, 1991, 1992; Gao et al., 1994; Masselink, 1992; McLaren et al., 1993; Teeter, 1993; Stevens et al., 1996; McLaren et al., 1998; Asselman, 1999; Zhou, 1999). In the context of this study, and as previously pointed out by Friedman (1962a) and Middleton (1962), it should again be emphasized that grain-size parameters determined by the method of moments and by the percentile method produce different results. They describe different textural features, depending on the composition of the sediment.

The percentile method considers up to 95% of a grain-size distribution but does so on the basis of only a few selected percentile measures. If the tails of a distribution can not be resolved due to technical limitations, they can be extrapolated without great difficulty from the cumulative curve if considered necessary. Considering technical limitations and resolution problems, the different methods each have their advantages and drawbacks. Thus, Folk (1966)

pointed out that the range of geological information in a sediment sample was so large that every analytical method was equally valid for comparing a suite of samples. As shown in the present study, this does not mean that every method will provide the same answer. A lower spatial resolution will obviously obscure information and hence impair genetic interpretations. Thus, in spite of the truncation at the fine tails of some muddy samples, the moment method described the properties of the grain size distributions with a far higher resolution than the percentile method. The results of this study thus strongly favour the use of the mathematical moment method in calculating and interpreting textural grain size parameters.

4.4 Spatial patterns produced by mean diameters and modal diameters

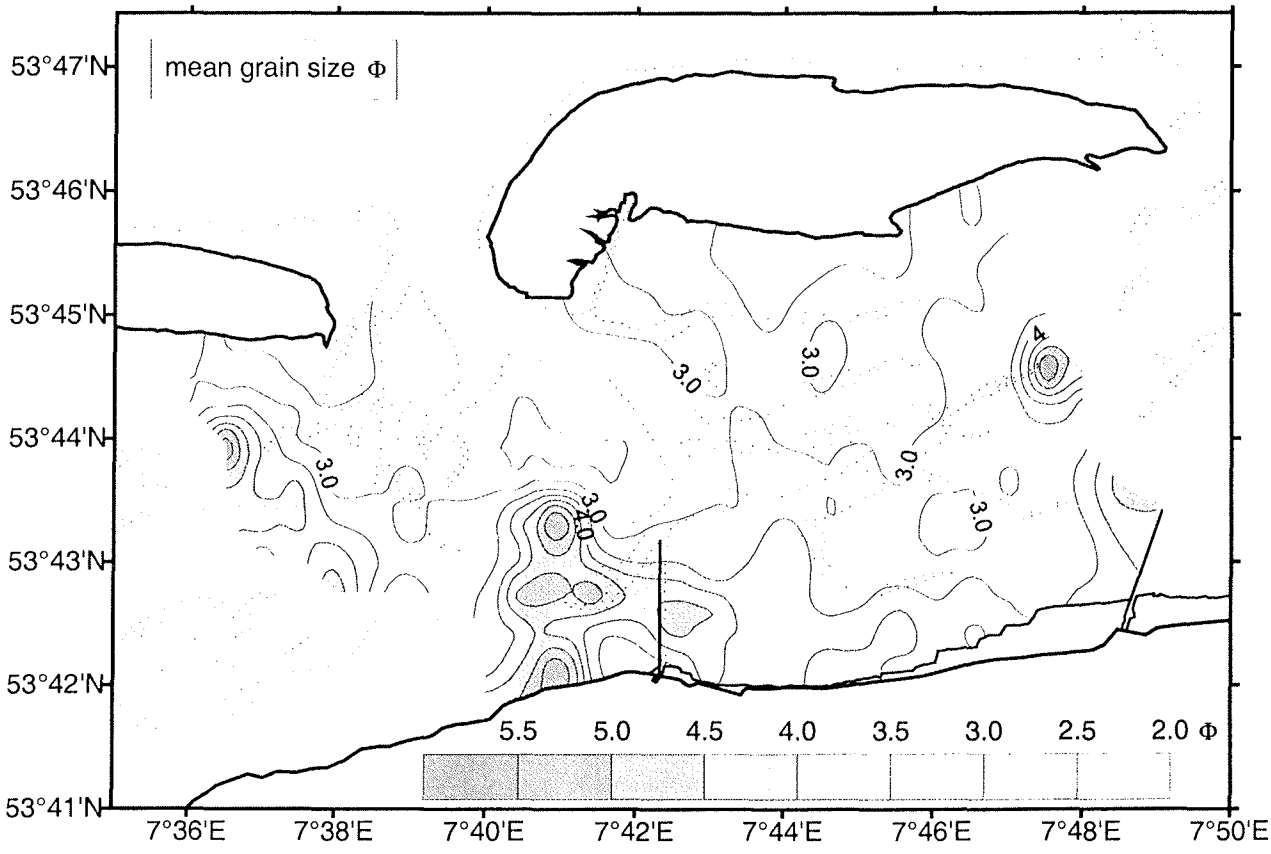

Figure 4-10 Distribution pattern of mean diameters in the Otzum tidal basin

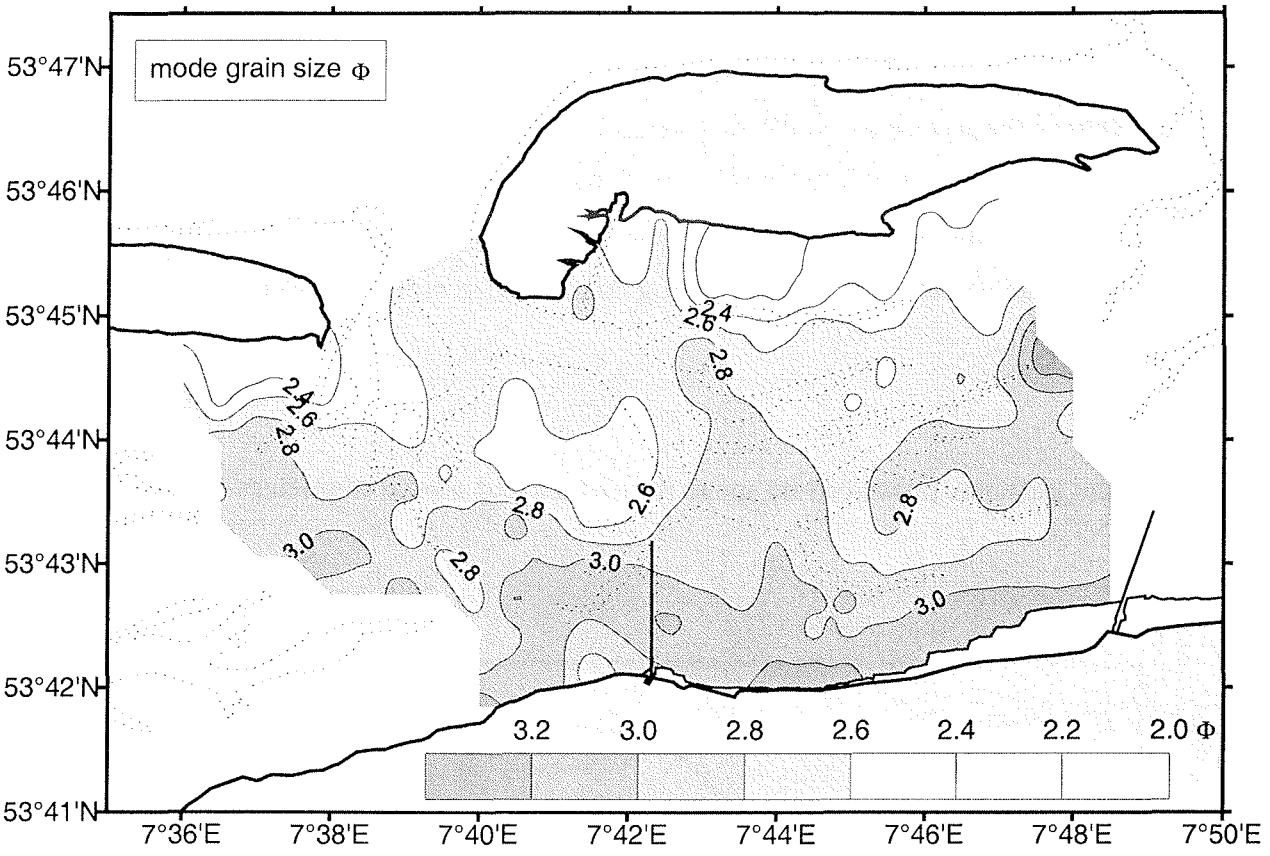

Figure 4-11 Distribution pattern of modal diameters in the Otzum tidal basin

The spatial pattern produced by the mean grain diameters of the total sediment in the Otzum tidal basin is illustrated in Fig. 4-10. Not withstanding some irregularities, the mean grain size decreases from north to south, i.e. from the barrier islands to the mainland shore. The coarsest sediments have mean grain diameters of 2.00Φ to 2.50Φ and are distributed along the backbarrier island shores and in the inlet. In an isolated patch on the Janssand mean diameters of 2.40Φ to 2.60Φ are found. The finest sediments are found in narrow belts or a number of patches along the watersheds where the mean grain size reaches values of up to 6.50Φ. The seaward half of the tidal basin is covered by fine sand (2.00Φ - 3.00Φ), the landward half by very fine sand (3.00Φ - 4.00Φ).

The spatial pattern produced by the modal grain size differs markedly from that of the mean diameter. The shore-parallel trend of individual size classes is more clearly defined than in the case of the mean grain size (Fig. 4-11). The coarsest mode is found in a single large

patch on the backbarrier island flats of Spiekeroog, the diameter being essentially the same as that of the mean (2.00Φ - 2.50Φ). This patch is associated with a large overwash fan which has deposited beach sediments on the island flats. The finest mode occurs in a narrow belt along the mainland dike, the grain sizes varying between 3.00Φ and 3.40Φ. Over most of the remaining tidal basin the modal diameter is coarser than 3.00Φ. The modal pattern traces the shore-normal energy gradient postulated by Nyandwi (1995), Nyandwi and Flemming (1995), Flemming and Ziegler (1995), and Mai (1999) much better than the mean diameter. In addition, the mode shows much coarser sediments along the watersheds than the mean, the difference reflecting the strong influence of biogenic muds on the textural composition of the sediments.

4.5 Spatial patterns produced by sorting, skewness and kurtosis

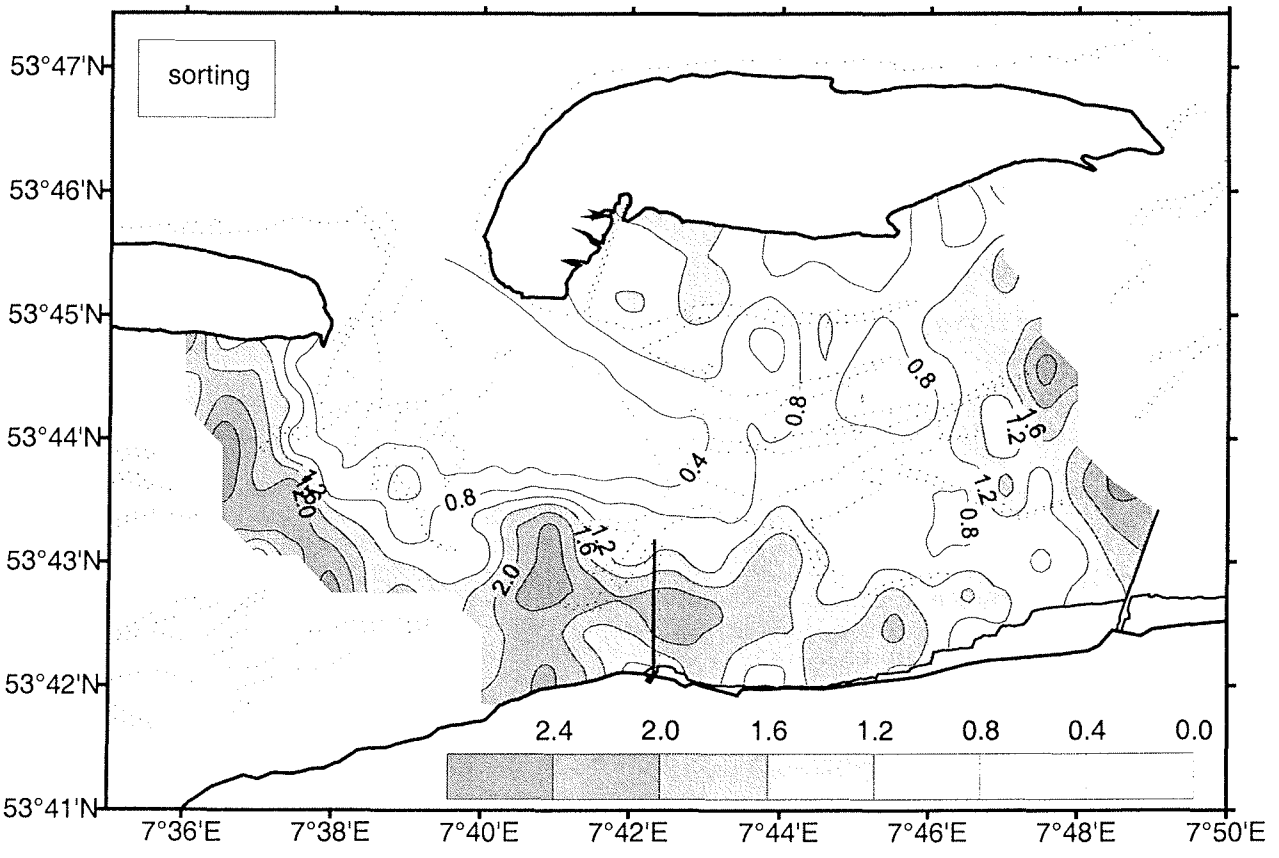

Figure 4-12 Distribution pattern of sorting coefficients in the Otzum tidal basin

The spatial distribution pattern produced by sorting coefficients in the Otzum tidal basin is illustrated in Fig. 4-12. There is substantial variability in the pattern, sorting coefficients ranging from very well sorted (0.15) to very poorly sorted (>2.40). The pattern broadly traces the shape of the tidal basin, the sediments being very well sorted in and around the inlet, followed by well and moderately well sorted sediments. Moderate and poor sorting is observed along the margins of the basin, i.e. along the watersheds and along the mainland shore. The sorting pattern of the total sediment is remarkably similar to that of mud distribution (cf. Fig. 3-8), as well as the inverse pattern produced by the fine sand fraction (Fig. 3-4) which occupies the largest area of the tidal basin centred around the inlet region. This indicates that the distribution of sorting coefficients is evidently a function of energy dissipation, good sorting reflecting efficient, poor sorting less efficient size-sorting processes.

Since the disaggregation of mud flocs and faecal pellets during laboratory processing will have distorted the true sorting of the sediment, rendering muddy sediments more poorly sorted than they would have been with intact aggregates, it is interesting to note that it still allows recognition of the basic energy dissipation pattern. This means that, with the exception of local biogenic mud deposits, the more muddy sediments formed by mud flocs and aggregates still occupy a lower energy zone than, for example, the less muddy sands. This is, in fact, borne out by the gradient produced in the distribution of mean grain sizes (cf. Fig. 4-10) because mean grain size, in contrast to the modal diameter, responds very sensitively to changes in the tails of a grain size distribution. Nevertheless, it also means that the energy gradient reflected in the strong sorting gradient is an exaggeration of the true situation.

The distribution patterns of skewness and kurtosis differ from the sorting pattern in that the strongest gradients are observed in the eastern half of the tidal basin (Figs. 4-13 and 4-14). Skewness ranges from -0.50 to 7.50, sediments with positively skewed grain size distributions dominating the depositional system. Negative skewness is only observed near the inlet and on the Janssand. Kurtosis, in turn, ranges from 0 to 75, indicating that the size frequency distributions progressively change from near-normal (mesokurtic) distributions in and around the inlet to very peaked (leptokurtic) distributions in the eastern half of the basin and, to a lesser degree, also along the western margin of the basin. However, the areas displaying highest skewness and kurtosis values are distinctly offset from those displaying poorest sorting, indicating that these parameters not only reflect energy gradients but also differential mixing of different size fractions or hydraulic populations.

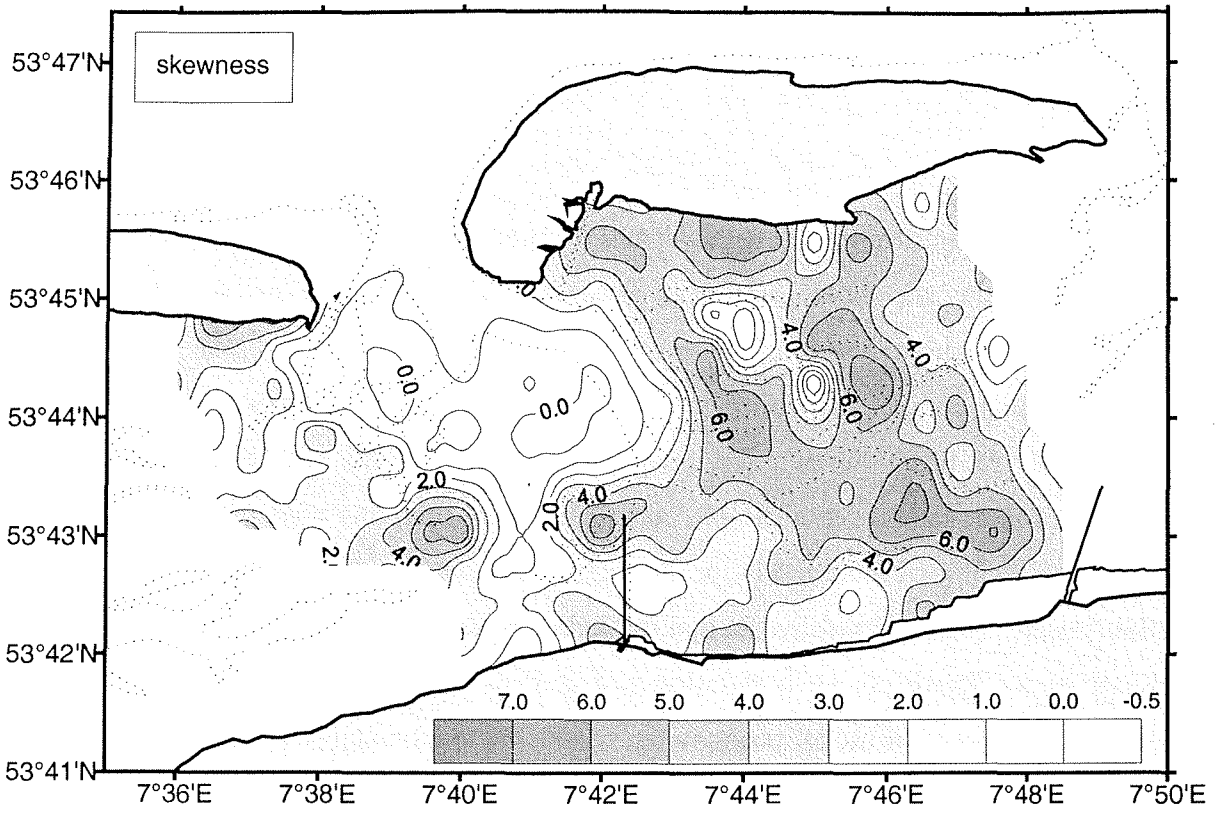

Figure 4-13 Distribution of skewness values in the Otzum tidal basin

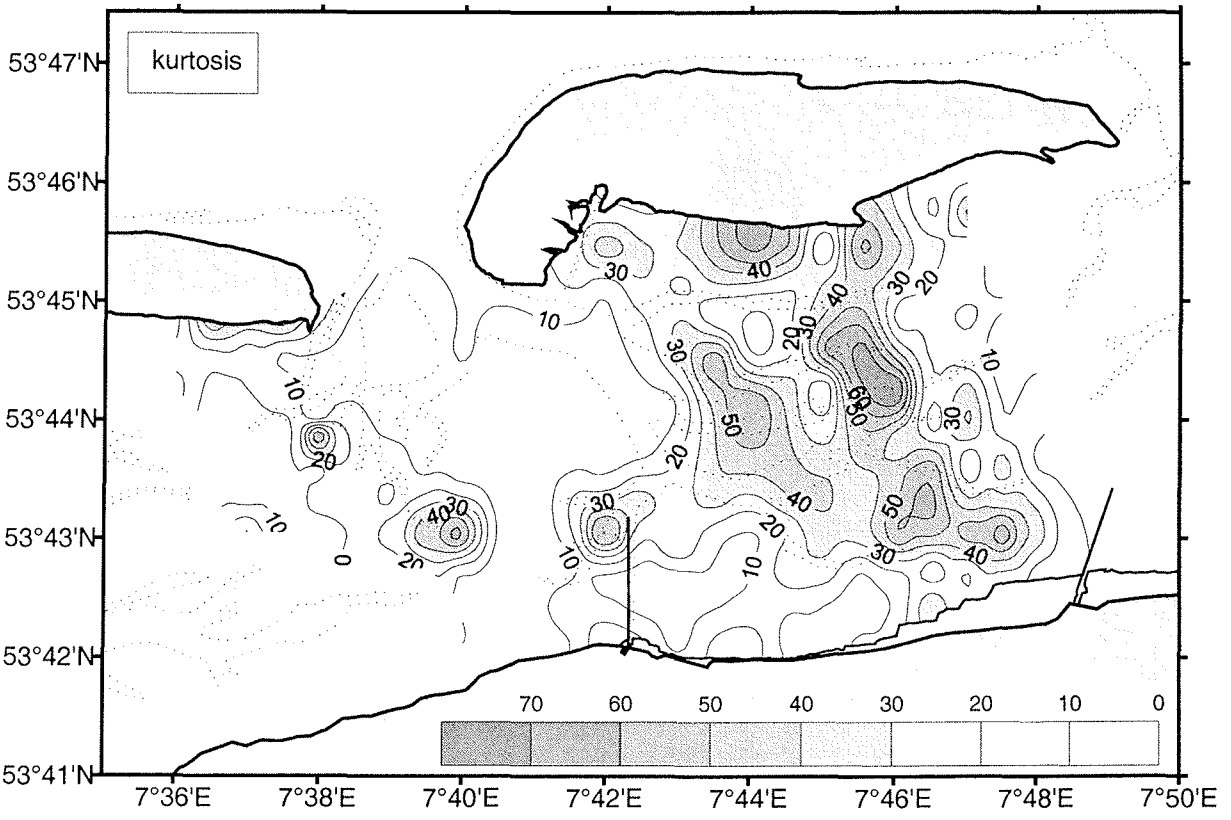

Figure 4-14 Distribution of kurtosis values in the Otzum tidal basin

4.6 Relationships between textural parameters of different sediment fractions

4.6.1 Total sediment

As clearly evident from the textural scatter diagrams and the spatial distribution patterns discussed above, the statistical grain size parameters alone do not disclose their spatial relationships in the study area. In order to investigate major trends, e.g. modal groupings, in the grain size distributions, all unimodal size distributions were superimposed in a single diagram (Fig. 4-15). From this diagram it can be seen that, with the exception of the discrete distributions of pure sands, every sample containing some mud has a very long and flat fine tail. In order to emphasize both modal peaks and the tail sections, the y-axis has been given a logarithmic scale. The diagram reveals that the sediment as a whole is composed of a mixture of a single better sorted coarse population and at least one poorly sorted fine population. Furthermore, the spread of modal peaks in the coarse population suggests that this population has undergone a size-sorting process which has resulted in a progressive modal shift from coarser to finer grain sizes.

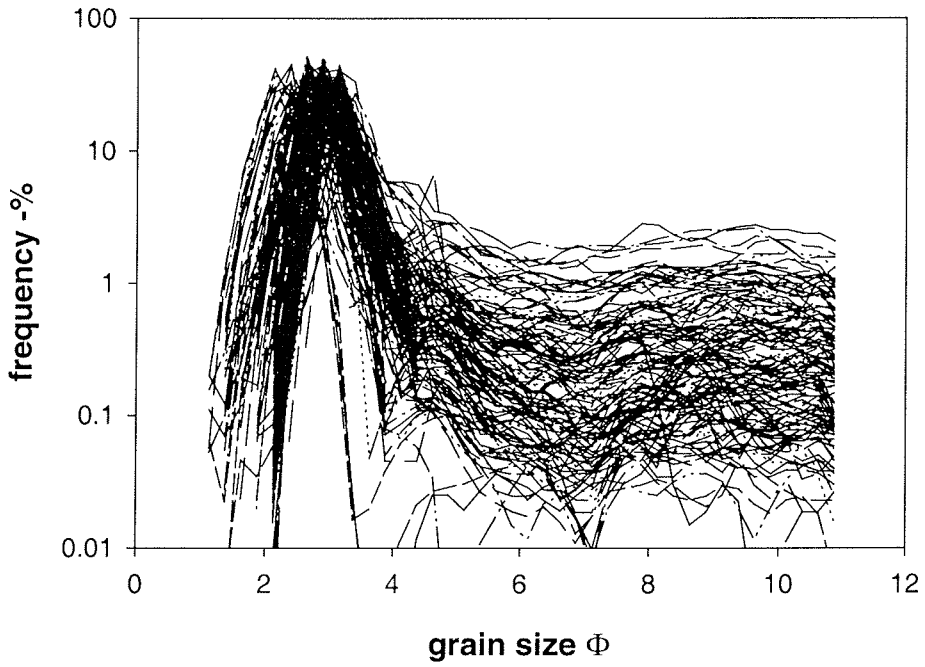

Figure 4-15 Pooled grain-size frequency distributions of the sediments in the Otzum tidal basin

In order to assess the relationships between the grain-size frequency distributions and the grain-size parameters of the individual samples in each of the groups identified earlier, textural parameters were calculated for differently truncated size spectra, i.e. for the <4Φ, <7Φ and <11Φ size ranges. The resulting trends are illustrated in Fig. 4-16. The diagrams can be considered to represent the patterns produced when a basic sand fraction is mixed with different fine fractions. The plots clearly reveal that the sand fractions of all three sediment groups are very well sorted, have near-symmetrical distributions, and have mesokurtic shapes (left-hand panels in Fig. 4-16). Incorporating all grain sizes up to 7Φ (centre panels in Fig. 4-16), reveals that this part of the size spectrum contributes marginally to a poorer sorting, especially in group B sediments, introduces more positive skewness into some samples, especially into most of group B and all group C samples, and begins to emphasize the peakedness of the distributions, especially of some of the group B and the group C samples. This pattern becomes even more enhanced when incorporating every size fraction up to 11Φ (right-hand panels in Fig. 4-16). Clearly, only when including all size fractions do the diagrams achieve maximum clarity, in particular highlighting the fact that individual size distributions plotted in Fig. 4-15 can, in spite of their apparent similarity, have quite different textural expressions.

As fine material is mixed into the sediment, the size ranges change and mean grain sizes become finer. Thus, as the size-sorting process proceeds and coarser size classes drop out, the finer size classes begin to increasingly dominate the distribution, causing the sorting to decrease, in this case from 0.17 to 2.81. At the same time, the size frequency curves become skewed towards more positive values, in this case from –0.74 to +8.37, the peakness of the distributions increasing from mesokurtic to extremely leptokurtic shapes in proportion to the amount of fine particles added, in this case from 1.76 to >90.

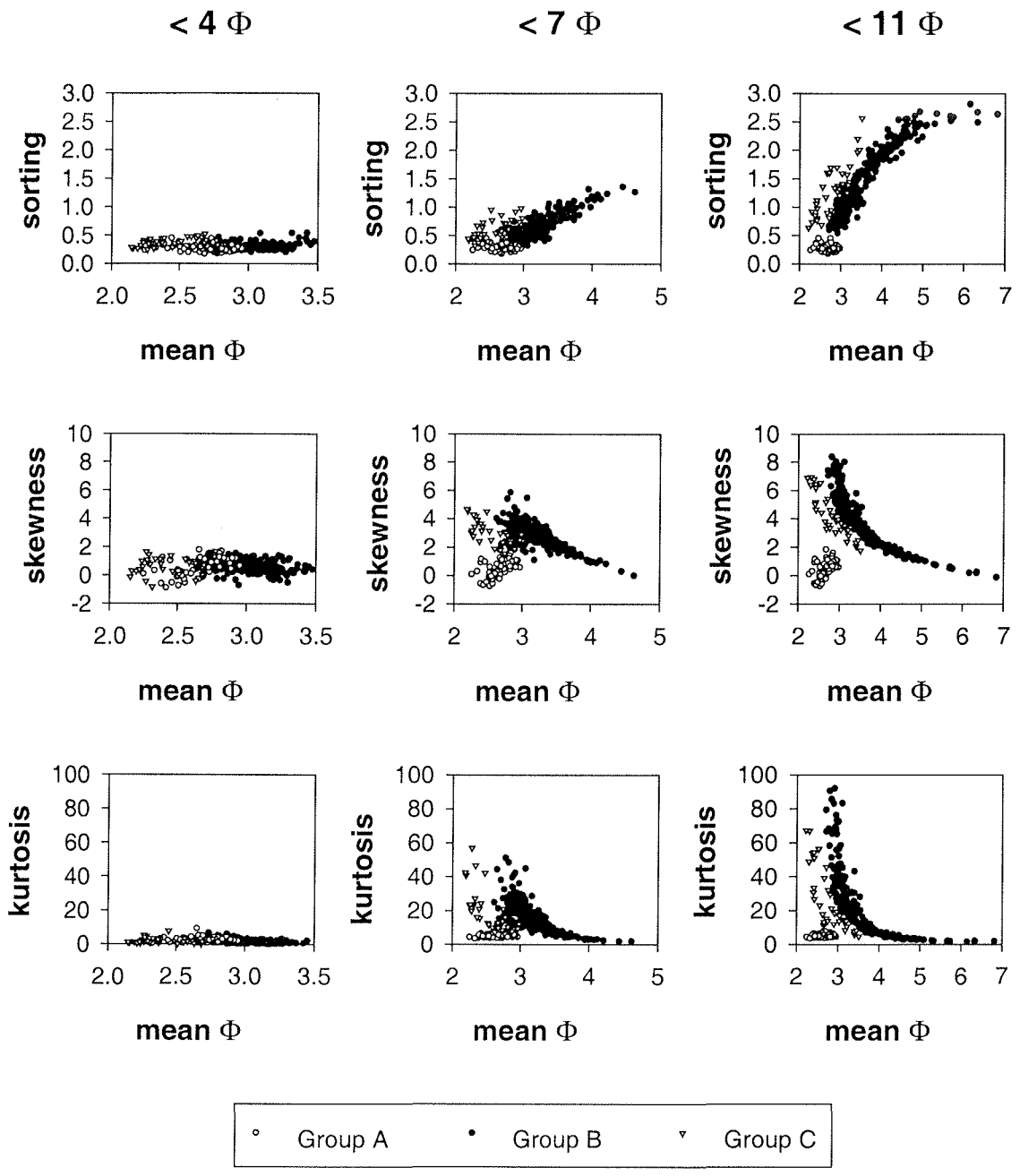

Figure 4-16 Relationships between textural parameters of different size fractions

4.6.2 The mud fraction

4.6.2.1 Relationships between textural parameters in different mud fractions

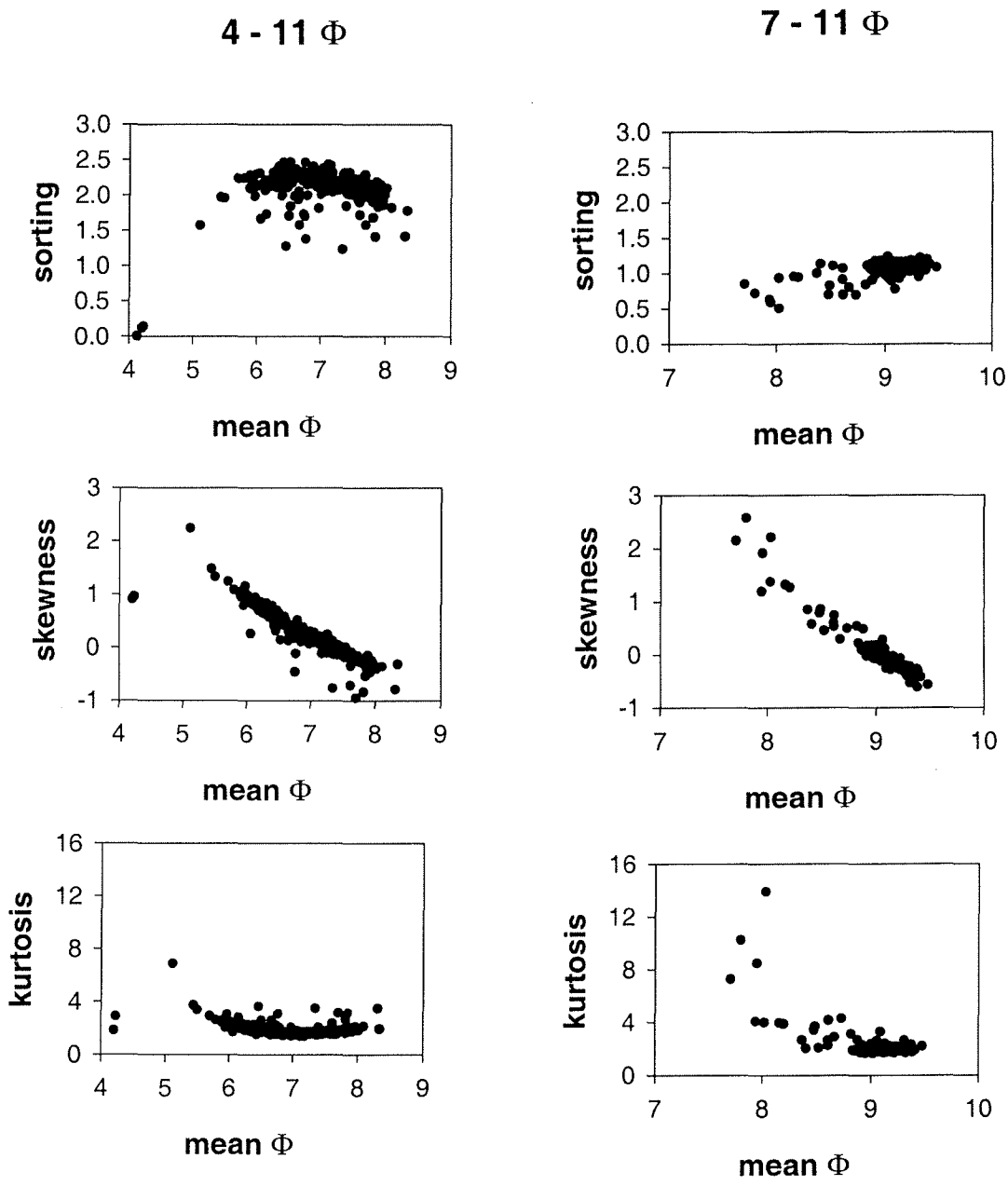

Figure 4-17 Relationships between the textural parameters of different mud fractions

As discussed in section 2.1.2, the mud fraction of the sediment is composed of a better sorted coarser population and a less well sorted finer population. When comparing the textural attributes of different mud size fractions, the same overall picture emerges (Fig. 4-17). Sorting coefficients, skewness, and kurtosis all change with changing mean diameter of the investigated mud fraction. This is particularly well documented in the mean versus sorting relationship of the 4 - 11Φ fraction. As the mean changes from 4Φ to 6Φ, the sorting of the material decreases rapidly, but remains more or less constant after that (upper left panel in Fig. 4-17). On the other hand, when considering the 7 - 11Φ fraction only (upper right panel in Fig. 4-17), the sorting decreases more gradually over the whole range of mean diameters. This is in agreement with the evidence that the mud fraction is divided into two subpopulations at a grain size of about 7Φ. Skewness and kurtosis, by contrast, do not show any substantial differences in their trends between the two fractions (middle and lower panels in Fig. 4-17).

4.6.2.2 Suspended muds

To compare the textural characteristics between deposited muds and suspended muds, quantitative samples of the latter were collected by means of a pump centrifuge at different tidal phases and in different seasons. The disaggregated size distributions are illustrated in Fig. 4-18. Even a cursory glance at the diagram confirms that the size distributions of the muds in suspension are very similar to those in the sediments. This is particularly evident in the finer fractions (7 - 11Φ) which all have a mode around 9Φ. As in the case of the deposited muds, the coarser mud fractions (4 - 6.5Φ) show the biggest variability.

Looking at the relationships between the mean diameters and the other textural parameters of different size fractions in the suspended muds, it is abundantly clear that the sorting, skewness, and kurtosis change systematically with mean grain size in the total mud fraction (left panels in Fig.4-19) but remain constant in the >7Φ fractions. The documented variations in the textural parameters in the total mud fraction are thus evidently linked to the coarser mud fractions.

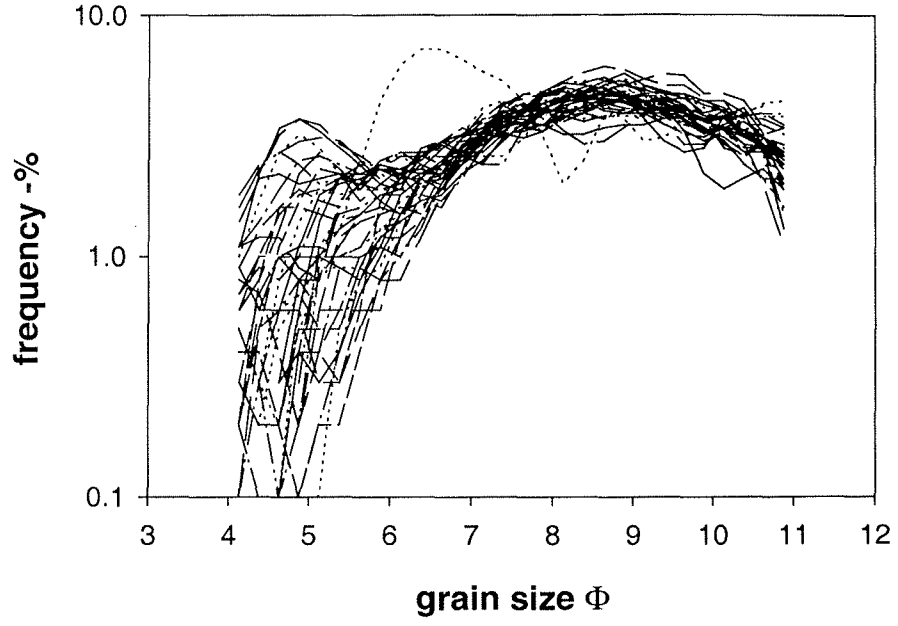

Figure 4-18 Grain size distributions of mud in suspension

In comparison to the suspended muds, the mud in the sediment is clearly much coarser and more poorly sorted. In addition, the >7Φ fractions of the suspended muds are finer and better sorted than the same fractions in the sediment. If the mud in the sediment is thus considered to be composed of particles which have settled out from a suspended parent population, then the mud remaining in suspension should have the sorting characteristics demonstrated by Kranck (1973, 1975), even if the fine-grained particles are partly flocculated and aggregated. At first sight, the uniformly good sorting observed in the >7Φ fractions of both the suspended and deposited muds appear to contradict the model. However, as can be shown, the good sorting of the fine subpopulation is in this case a mathematical artefact produced by the exclusion of the coarser mud fractions. The apparently good sorting in the finer mud fractions observed in this and other studies (e.g., Griffiths, 1967; Sly et al., 1983; Steven et al., 1996) is therefore not a good indicator of the sorting of the mud as a whole.

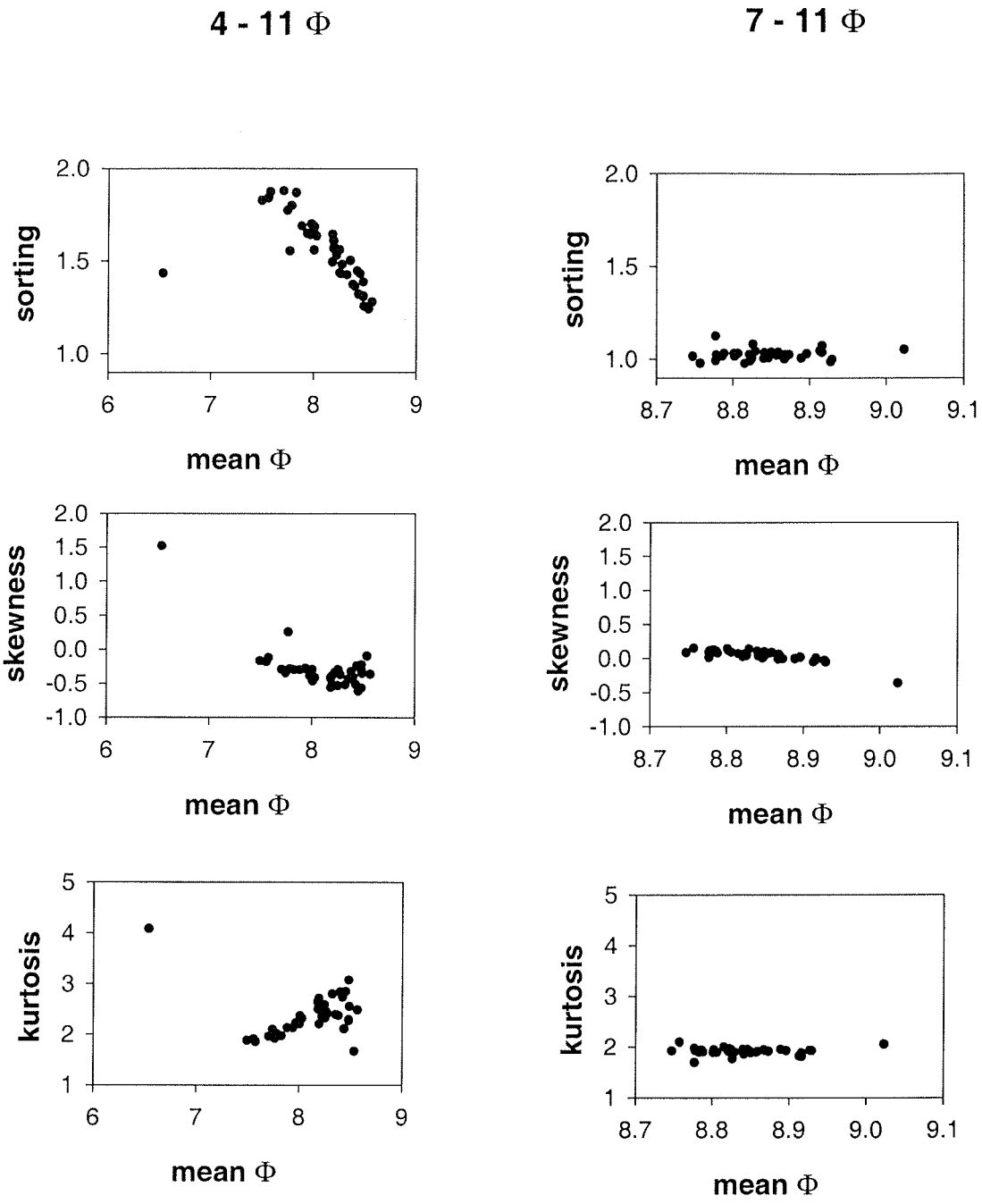

Figure 4-19 Relationships between the textural parameters in different size fractions of suspended muds

4.6.3 Sediment mixing

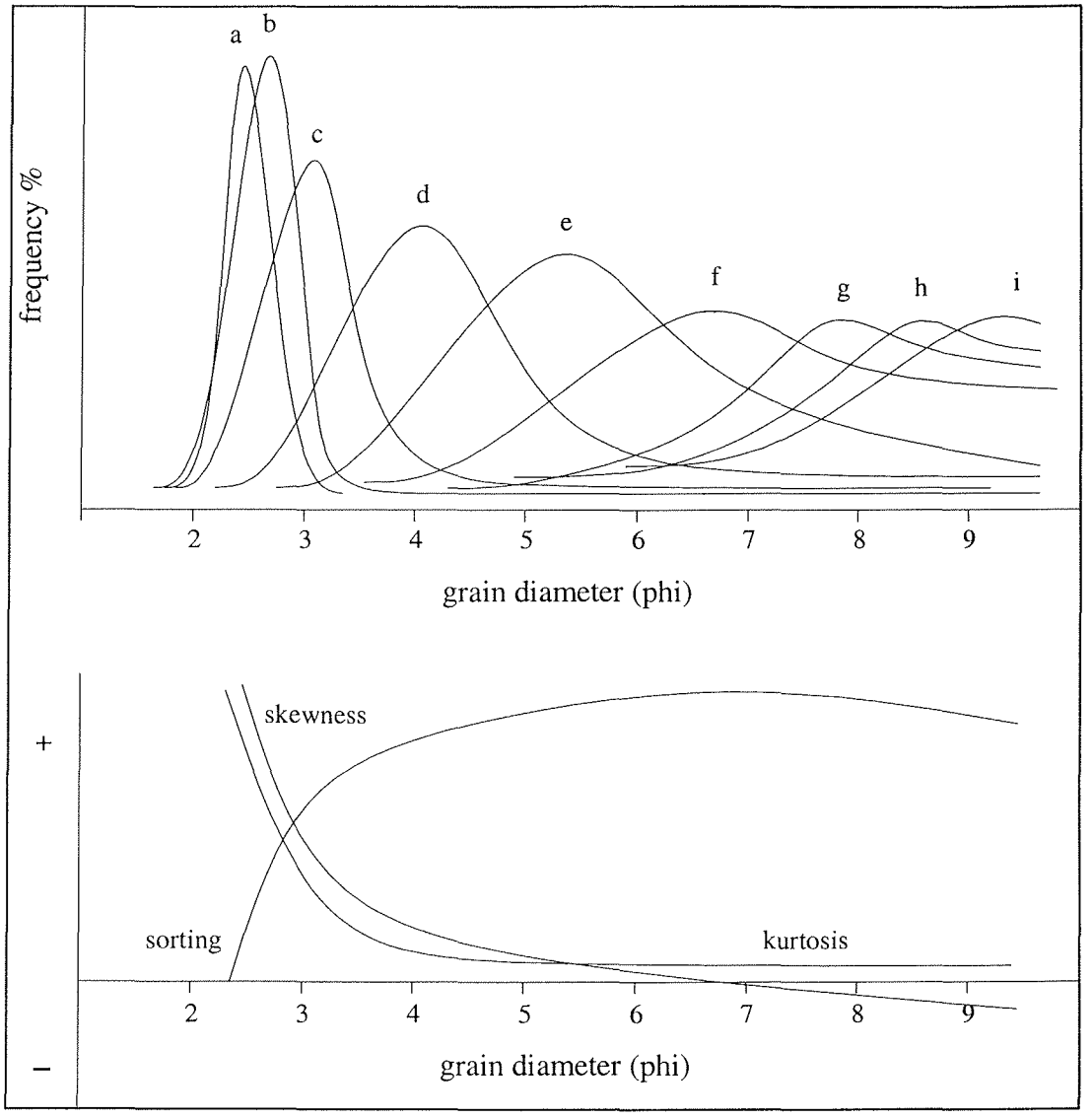

Figure 4-20 Evolution of grain-size frequency distributions and textural parameter in the course of size-sorting and mixing

From the above discussion it can be concluded that in the course of a progressive size-sorting process along an energy gradient, the textural attributes of the deposited sediment will change in a systematic manner the finer the sediment gets. This is illustrated by the grain size distribution curves in Fig. 4-20. Pooled together they would represent the original parent

population of the source material. As the coarser, better sorted size fractions settle out, the remaining suspension initially gets finer grained and increasingly more poorly sorted, the distribution becoming less positively skewed and more platykurtic in shape. Only when the finest endmembers are reached, does the sorting improve again as a result of the truncation at the fine tail. Only if a subpopulation derived from another depositional process, e.g. from bedload flux or aeolian input, is mixed into the sediments deposited from suspension will the textural relationships carry an overprint. In the case of the Otzum tidal basin this is documented by the slight differences observed between the group B and group C sediments. In conclusion, therefore, the interrelationships between various textural grain size parameters of systematically sampled sediments can provide important information about the depositional process.

5 Conclusions

5.1 Mass physical state of the sediments

The muddy sediments in the Otzum tidal basin are structurally very different from the sandy sediments. A pronounced change in the mass physical properties of the sediment is observed at a mud content of about 50%. In a given volume of sediment the volume of the voids, and hence the mass of the interstitial water, increases with increasing mud content. In sand-dominated sediments the mass of mud in a given volume initially increases with increasing mud content. However, when a mud content of about 50% is reached the mass of mud either remains constant or it begins to decrease as the void ratio in the sediment increases more rapidly. This speciality of muddy sediments has great significance because compaction (loss of interstitial water) can dramatically alter the mass physical state of a mud. Thus, at constant mud contents the mass of mud in a given volume of sediment will differ substantially as a function of compression (decrease in water content) or expansion (increase in water content). Applying this principle to rare elements, heavy metals, or contaminants of various sorts, it can be demonstrated that their concentrations in the sediment will vary in accordance with the mass physical sediment state, although their contents (mass per unit mass) may have remained unchanged.

5.2 Bulk density

On the basis of systematic sampling in the Otzum tidal basin, universal relationships between water content and bulk sediment densities were derived. These can be expressed as:

$$WBD = (0.37949017 + 0.0065738815 \cdot W)^{-1} \qquad (r = 0.9711,\ N = 321)$$

and

$$DBD = -0.37768025 + 2.8854035 \cdot e^{\left(\frac{-W}{49.613606}\right)} \qquad (r = 0.9939,\ N = 321)$$

with WBD as the wet bulk density (g/cm³); DBD as the dry bulk density (g/cm³); W as the water content in weight-% (weight of water divided by the weight of the whole sediment with water and salt, multiplied by 100)

These relationships can be used as quick and simple methods to obtain the bulk densities of surficial sediments if the water contents are known, provided the sediment is composed of average terrigenous material (e.g. quartz, rock fragments, carbonates). This certainly applies to the entire Wadden Sea, and larger North Sea for that matter. They should not be used if the solid material has different densities (e.g., in the case of diatomaceous oozes).

5.3 Shear strength

The shear strength of the sediment is not only controlled by the mass physical properties but also by other factors influencing the sediment. A pronounced decrease in shear strength with increasing mud content of the sediment was observed in the Otzum tidal basin. The shear strengths of the muddy sediments are very low, usually below 20 kPa which corresponds to the porous structure characterizing muds. In the sandy sediments, by contrast, the shear strengths can vary between 10 kPa and about 100 kPa, scatter decreasing with increasing mud content. On the one hand, this may simply reflect textural changes in the sediment. On the other hand, in sediments containing <20% mud the shear strength may be the result of other factors also, since it was observed that the same sediments could have different shear strengths, whereas different sediments sometimes had the same shear strength. Biological influences, for example, can stabilize or destabilize sediment surfaces and thereby affect the shear strength of the sediment. However, natural compaction due to water drainage or very loosely packed, water-logged deposits (e.g., bubble sands) will also dramatically influence the shear strength of a sediment.

5.4 Textural sediment parameters

Textural grain-size parameters, namely mean grain size, sorting coefficient, skewness, and kurtosis are basicly and widely applied descriptors of sediments, being also used to explain depositional processes. In most studies to date, simplified percentile statistics are used for the description of grain size distributions of sediments. In this study it was demonstrated that the results of moment statistics are superior to percentile statistics when using textural data for the interpretation of depositional processes. While percentile statistics are adequate when dealing with sands, they fail to adequately resolve the textural relationships in sand-mud mixtures. The moment method, by contrast, was able to distinguish subtle differences between

different sediment groups in the Otzum tidal basin. The textural relationships between mean diameter and sorting, mean diameter and skewness, and mean diameter and kurtosis in systematically sampled sediments can clearly provide important information about the hydrodynamic processes involved in their deposition.

5.5 Mechanisms controlling depositional processes

Most sediments in the Otzum tidal basin were deposited by the prevailing tidal current regime. This applies in particular to the coarser sand fractions. The tidal basin was formed during the Holocene sea-level rise against the background of a shore-normal energy gradient (Nyandwi, 1995; Nyandwi and Flemming, 1995; Flemming and Ziegler, 1995; Mai, 1999). With the formation of the barrier islands and the backbarrier tidal basins, the hydrodynamic conditions changed in accordance with the changed morphology. This, and especially human intervention in the form of land reclamation and dike construction along the mainland coast, had a strong influence on the recent sedimentation processes. Modern sedimentation is mainly controlled by the dynamics of the fine-grained sediments in the tidal basin, especially the production and storage of biogenic muds by the filtering activity of the mussel *Mytilus edulis*, and the effects of storm action coupled with low water temperatures during the cold season.

The systematic grain-size analysis of the fine sediment fractions in the bed sediment and in the suspended sediments have revealed a general dearth of particles around 7Φ (8μm). The mud is usually composed of a better sorted coarse population (<7Φ) and poorly or unsorted fine population (>7Φ). Even though the fine-grained sediments are usually transported and deposited in the form of flocs and aggregates, the muds tend to get better sorted as the grain size increases. With the exception of the biogenic muds, the content of the fine population in the mud fraction is strongly controlled by the energy regime in the tidal basin. As the result of the diking along the mainland coast, this part of the tidal basin is today exposed to much higher energy conditions than the island flats on the other side of the basin. This is supported by the distribution patterns of the fine fractions and the variations of both the $CaCO_3$-contents and organic matter contents of the mud fractions. The main differences in the depositional processes governing the sediment distribution patterns are clearly evident in the mass physical sediment properties and the relationships between individual textural grain-size parameters.

References

Allen, J. R. L. (1977). Physical processes of sedimentation. George Allen and Unwin, London, 248 pp.

Antia, E. E. (1993). Sedimentology, morphodynamics and facies association of a mesotidal barrier island shoreface (Spiekeroog, Southern North Sea). Berichte. Fachbereich Geowissenschaften. Universität Bremen, Nr.32, 370 pp.

Antia, E. E., Flemming, B. W. and Wefer, G. (1994). Transgressive facies sequence of a high-energy wave-tide-storm influenced shoreface, a case study from the East Frisian barrier islands (southern North Sea). Facies, 30:15-24.

Asselman, N. E. M., (1999). Grain-size trends used to assess the effective discharge for floodplain sedimentation, River Waal, The Netherlands. J. Sediment. Petrol., 69(1): 51-61.

Backhaus, H. (1943). Die Ostfriesischen Inseln und ihre Entwicklung. Ein Beitrag zu den Problemen der Küstenbildung im südlichen Nordseegebiet. Schr. Wirt.-Wiss. Ges. Studium Niedersachsens, Reihe A, 12, Hannover.

Bagnold, R. A. (1968). Deposition in the process of hydraulic transport. Sedimentology, 10: 45-56.

Barckhausen, J., Lang, H. D., Meyer. K.-D., Streif, H. J. and Elwert, D. (1973). Geologische Übersichtskarte 1:200 000, Blatt CC 2310 Helgoland. Bundesanst. für Bodenforsch., Hannover.

Bartholdy, J. (1985). Dynamic interpretation of grain size relations in silt. Geo-Marine Letters, 5: 67-70.

Bartholdy, J. and Pheiffer Madsen, P. (1985). Accumulation of fine-grained material in a Danish tidal area. Marine Geology, 67: 121-137.

Bates, R. L. and Jackson, J. A. (1980). Glossary of geology. American Geological Institute, Falls Church, Virginia, second edition, 751 pp.

Bayne, B. L., Thompson, R. J. and Widdows, J. (1976). Feeding and digestion. In: Bayne, B. L. (Ed.), Marine mussels: their ecology and physiology. Int. Biol. Progr. 10. Cambridge Univ. Press, Cambridge, 121–158.

Behre, K.-E., Menke, B. and Streif, H. (1979). The Quaternary geological development of the German part of the North Sea. In: E. Oele, R. T. E., Schüttenhelm and A. J. Wiggers (Eds.), The Quaternary history of the North Sea. Acta Univ. Ups. Symp. Univ. Ups. Annum Quingentesium Celebrantis: 2, Uppsala, 85-113.

Bennett, R. H., Lambert, D. N. and Grim, P. J. (1971). Tables for determining unit weight of deep-sea sediments from water content and average grain density measurements. National Oceanic and Atmospheric Administration Tech. Memo, ERL AOML-13.

Black, C. A., Evans, D. D., Ensminger, L. E., White, J. L. and Claric, F. E. (1965). Methods of Soil Analysis, Part 1, Physical and Mineralogical Properties, Including Statistics of Measurement and Sampling. American Society of Agronomy, Wisconsin, 770pp.

Brezina, R. E. (1979). Particle size and settling rate distributions of sand-sized materials. PARTEC 79, 2nd European Symposium on Particle Characterisation, Nürnberg, 21 pp.

Brezina, R. E. (1980). Korngrössenanalyse sandkörniger Materialien. Labor u. Prax., 4:18-26.

Brezina, R. E. (1986). Macrogranometer MC86 Laboratory Manual. Granometry, Heidelberg, 33 pp. (unpublished).

Bundesamt für Seeschiffahrt und Hydrographie. (1995). Gezeiten Tafeln für 1996.

Bundesamt für Seeschiffahrt und Hydrographie. (1996). Gezeiten Tafeln für 1997.

Bundesamt für Seeschiffahrt und Hydrographie. (1997). Gezeiten Tafeln für 1998.

Carver, R. E. (1971). Procedures in sedimentary petrology. Wiley-Interscience, New York, 653 pp.

Curray, J. R. (1960). Tracing sediment masses by grain-size modes. Intern. Geol. Congr., 21st, Copenhagen, Repot. Session, Norden, 119-130.

Davis R. A. and Flemming, B. W. (1995). Stratigraphy of a combined wave- and tide-dominated intertidal sand body: Martens Plate, East Frisian Wadden Sea, Germany. Spec. Publs int. Ass. Sediment., 24: 121-132.

Delafontaine, M. T., Bartholomä, A, Flemming, B. W. and Kurmis, R. (1996). Volume-specific dry POC mass in surficial intertidal sediments: a comparison between biogenic muds and adjacent sand flats. Senckenbergiana marit., 26(3/6): 167-178.

Delft Hydraulics (1995). Europipe development project-Monitoring measurements 1994 of waves, tides, currents, turbidities and wind. Data report, Delft, 12 pp.

Doeglas, D. J. (1946). Interpretation of the results of mechanical analysis. J. Sediment. Petrol., 16: 19-40.

Driscoll, M. L., Tucholke, B. E. and McCave, I. N. (1985). Seafloor zonation in sediment texture on the Nova Scotian Lower Continental Rise, Marine Geology, 66: 25-41.

Dunn, D. A. (1980). Revised techniques for quantitative calcium carbonate analysis using the "Karbonat-Bombe", and comparisons to other quantitative carbonate methods. J. Sediment. Petrol., 50(2): 631-637.

Ehlers, J. (1988). The morphodynamics of the Wadden Sea. Balkema, Rotterdam, 297 pp.

Fairchild, I. J., Hendry, G., Quest, M. and Tucker, M. (1988). Chemical analysis of sedimentary rocks. In: M. Tucker (Ed.), Techniques in Sedimentology, Blackwell Scientific Publications, 274–354.

Favejee, J. C. L. (1951). The origin of the "Wadden" mud. Meded. Landb. Hoegesch. Wageningen, 51: 113-141.

Ferk, U. (1995). Folgen eines beschleunigten Meeresspiegelanstiegs für die Wattgebiete der niedersächsischen Nordseeküste. Die Küste, 57: 135-156.

Figge, K., Köster, R., Thiel, H. and Wieland, P. (1980). Schlickuntersuchungen im Wattenmeer der Deutschen Bucht. Die Küste, 35:147-186.

Figge, K. (1981). Sedimentverteilung in der Deutschen Bucht, Blatt Nr. 2900. Deutsches Hydrographisches Institut, Hamburg.

Fitzgerald, D. M., Penland, S. and Nummedal, D. (1984a). Changes in tidal inlet geometry due to backbarrier filling: East Frisian Islands, West Germany. Shore and Beach, 52 (4): 2-8.

Fitzgerald, D. M., Penland, S. and Nummedal, D. (1984b). Control of barrier island shape by inlet sediment bypassing: East Frisian Islands, West Germany. Marine Geology, 60: 355-376.

Fitzgerald, D. M. and Penland, S. (1987). Backbarrier dynamics of the East Frisian Islands. J. Sediment. Petrol., 54(4): 746-754.

Flemming, B. W. and Thum, A. B. (1978). The settling tube - a hydraulic method for grain size analysis of sand. Kieler Meereforsch., Sonderh. 4: 82-95.

Flemming, B. W. (1988). Process and pattern of sediment mixing in a microtidal coastal lagoon along the west coast of South Africa. In: de Boer, P. L., van Gelder, A. and Nio, S. D. (Eds.), Tide-Influenced Sedimentary Environments and Facies. D. Reidel Publ. Co., Dordrecht, 275-288.

Flemming, B. W. (1991). Zur Holozänen Entwicklung, Morphologie und faziellen Gliederung der ostfriesischen Insel Spiekeroog (südliche Nordsee). Senckenberg am Meer, Bericht 91/3, 51pp.

Flemming, B. W., Schubert, H., Hertweck, G. and Müller, K. (1992). Bioclastic tidal-channel lag deposits: a genetic model. Senckenbergiana marit., 22: 109-129.

Flemming, B. W. and Davis, R. A. (1994). Holocene evolution, Morphodynamics and sedimentology of the Spiekeroog barrier island system (Southern North Sea). Senckenbergiana marit., 24(1/6): 117-155.

Flemming, B. W. and Delafontaine M. T. (1994). Biodeposition in a juvenile mussel bed of the East Frisian Wadden Sea (Southern North Sea). Netherlands J. Aquat. Ecology, 28(3-4): 289-297.

Flemming, B. W. and Nyandwi, N. (1994). Land reclamation as a cause of fine-grained sediment depletion in backbarrier tidal flats (Southern North Sea). Netherlands J. Aquat. Ecology, 28(3-4): 299-307.

Flemming, B. W. and Ziegler, K. (1995). High-resolution grain size distribution patterns and textural trends in the backbarrier environment of Spiekeroog Island. Senckenbergiana marit., 26(1/2): 1-24.

Flemming, B.W. and Bartholomä, A. (1997). Response of the Wadden Sea to a rising sea level: a predictive empirical model. German J. Hydrogr., 49: 343-353.

Flemming, B. W. and Delafontaine M. T. (2000). Mass physical properties of muddy intertidal sediments: some applications, misapplications and non-applications. Continental Shelf Research (in press).

Folk, R. L. and Ward, W. C. (1957). Brazos river bar. A study in the significance of grain size parameters. J. Sediment. Petrol., 27, pp3-26.

Folk, R. L. (1966). A review of grain-size parameters. Sedimentology, 6: 73-93.

Friedman, G. M. (1961). Distinction between dune, beach, and river sands from their textural characteristics. J. Sediment. Petrol., 31: 514-529.

Friedman, G. M. (1962a). On sorting, sorting coefficients, and the lognormality of the grain-size distribution of sandstones. J. Sediment. Petrol., 70: 737-753.

Friedman, G. M. (1962b). Comparison of moment measures for sieving and thin-section data in sedimentary petrological studies. J. Sediment. Petrol., 32:15-25.

Friedman, G. M. and Sanders, J. E. (1978). Principles of sedimentology. John Wiley and Sons, New York., 792 pp.

Friedman, G. M. (1979). Address of retiring President of the International Association of Sedimentologists: Differences in size distributions of populations of particles among sands of various origins. Sedimentology, 26: 3-32.

Führböter, A. (1979). Warscheinlichkeiten und Häufigkeiten von Extremsturmfluten. Die Küste, 34: 40-52.

Gao, S. and Collins, M. (1991). A critique of the "McLaren method" for defining sediment transport paths - discussion. J. sediment. Petrol., 61(1): 143-146.

Gao, S. and Collins, M. (1992). Net sediment transport patterns inferred from grain-size trends, based upon definition of "transport vectors". Sedimentary Geology, 80: 47-60.

Gao, S., Collins, M., Lanckneus, J., De Moor, G. and Van Lancker, V. (1994). Grain size trends associated with net sediment transport patterns: an example from the Belgian continental shelf. Marine Geology, 121: 171-185.

Gibbs, R. J.,Mathews, M. D. and Link, M. D. (1971). The relationship between sphere size and settling velocity. J. Sediment. Petrol., 41: 7-18.

Griffiths, J. C. (1967). Scientific method in analysis of sediment. McGraw – Hill, New York, 508 pp.

Groen, P. (1967). On the residual transport of suspended matter by an alternating tidal current. Neth. J. Sea Res., 3: 564-574.

Grotjahn, M. (1990). Sedimente und Makrofauna der Watten bei der Insel Spiekeroog-Untersuchung im Rahmen des Sensitivitätsrasters Deutsche Nordseeküste. Jahresbericht der Forschungsstelle Norderney, 39: 97-119.

Hamilton, E. L. (1974). Prediction of deep-sea sediment properties: state-of-the art. In: A. L. Inderbitzen (Ed.), Deep-sea sediment, physical and mechanical properties. Plenum Press, New York and London. 1- 43.

Hanisch, J. (1980). Neue Meeresspiegeldaten aus dem Raum Wangerooge. Eiszeitalter u. Gegenwart, 30: 221-228.

Hertweck, G. (1978). Die Bewohner des Wattenmeeres in ihren Auswirkungen auf des Sediment. In: Reineck, H.-E. (Ed.), Das Watt – Ablagerungs- und Lebensraum. Kramer, Frankfurt a.M. 145–172.

Hertweck, G. (1995). Verteilung charakteristischer Sedimentkörper und Benthossiedlungen im Rückseitenwatt der Insel Spiekeroog, südliche Nordsee. I. Ergebnisse der Wattkartierung 1988-92. Senckenbergiana marit., 26(1/2): 81-94.

Hertweck, G. and Liebezeit, G. (1996). Biogenic and geochemical properties of intertidal biosedimentary deposits related to *Mytilus* beds. Marine Ecology, 17(1-3): 131-144.

Homeier, H. and Luck, G. (1969). Das Historische Kartenwerk 1:50 000 der Niedersächsischen Wasserwirtschaftsverwaltung als Ergebnis historisch-topographischer Untersuchungen und Grundlage zur kausalen Deutung der Hydrovorgänge im Küstengebiet. Göttingen.

Homeier, H. (1979). Die Verlandung der Harlebucht bis 1600 auf der Grundlage neuer Befunde. Jahresbericht der Forschungsstelle Norderney, 30:105-115.

Hübner, U. and Backhaus, J. O. (1997). Der küstennahe Gezeitenstrom im Gebiet der östlichen Ostfriesischen Inseln. Berichte, Forschungszentrum Terramare, Nr.4, 65 pp.

Huntley, D. A. (1980). Tides on the north-west European continental shelf. In: Banner, F. T., Collins, M. B. and Massie, K. S. (Eds.), The North-West European shelf seas: the sea bed and the sea in motion II. Physical and chemical oceanography, and physical resources. Elsevier, Amsterdam, 301-351.

Inman, D. L. (1949). Sorting of sediment in the light of fluid mechanics. J. of Sediment. Petrol., 19: 51-70.

Inman, D. L. (1952). Measures for describing the size distribution of sediments. J. Sediment. Petrol., 22: 125-145

Jelgersma, S. (1979). Sea-level changes in the North Sea basin. In: E. Oele, R. T. E., Schüttenhelm and A. J. Wiggers (Eds.), The Quaternary history of the North Sea, Acta Univ. Ups. Symp. Univ. Ups. Annum Quingentesium Celebrantis: 2, Uppsala, 233-248.

Jepsen, R., Roberts, J. and Lick, W. (1997). Effects of bulk density on sediment erosion rates. Water, Air and Soil Pollution, 99: 21-31.

Keil, K. (1954). Ingenieurgeologie und Geotechnik. Veb Wilhelm Knapp Verlag, Halle (Saale), 1132 pp.

Keller, G. H. (1974). Marine geotechnical properties: interrelationships and relationships to depth of burial. In: Inderbitzen, A. L. (Ed.), Deep-sea sediment, physical and mechanical properties. Plenum Press, New York and London, 77-100.

Koch, M. and Niemeyer, H. D. (1978). Sturmtiden-Strommessungen im Bereich des Norderneyer Seegats. Jahresbericht der Forschungsstelle Norderney, 29: 91 -108.

Kranck, K. (1973). Flocculation of suspended sediment in the sea. Nature, 246: 348-350.

Kranck, K. (1975). Sediment deposition from flocculated suspensions. Sedimentology, 22: 111 – 123.

Krumbein. W. C. (1934). Size frequency distribution of sediments. J. Sediment. Petrol., 4: 65-77.

Krumbein. W. C. (1936). Application of logarithmic moments to size frequency distribution of sediments. J. Sediment. Petrol., 6: 35-47.

Lambert, D. N. and Bennett, R. H. (1972). Tables for determining porosity of deep-sea sediments from water content and average grain density measurements. National Oceanic and Atmospheric Administration Tech. Memo., ERL AOML-17.

Linke, O. (1954). Die Bedeutung der Miesmuscheln für die Landgewinnung im Wattenmeer. Natur und Volk, 84: 253-261.

Liu, C and Evett, J. B. (1984). Soil Properties: Testing, Measurement, and Evaluation. Prentice-Hall, New Jersey, 315 pp.

Lozán J. L., Rachor, E., Reise, K., Westernhagen, H. von und Lenz, W. (Eds.), (1994). Warnsignale aus dem Wattenmeer. Blackwell, Berlin 387 pp.

Luck, G. (1976). Protection of the littoral and seabed against erosion. Jahresbericht der Forschungsstelle Norderney, 27: 9-78.

Mai, S. (1999). Die Sedimentverteilung im Wattenmeer: Ein Simulationsmodell. Berichte, Fachbereich Geowissenschaften, Universität Bremen, Bremen, Nr. 142, 114 pp.

Marsal, D., 1979. Statistische Methoden für Erdwissenschaftler. E. Schweizerbart'sche Verlagsbuchhandlung, Stuttgart, 2. Auflage, 192 pp.

Masselink, G. (1992). Longshore variation of grain size distribution along the coast of the Rhone Delta, Southern France: a test of the "McLaren model". J. Coast. Res., 8(2): 286-291.

McCave, I. N. (1985). Sedimentology and stratigraphy of box cores from the HEBBLE site on the Nova Scotian Continental Rise. Marine Geology, 66: 59-89.

McCave, I. N., Manighetti, B. and Robinson, S. G. (1995). Sortable silt and fine sediment size/composition slicing: Parameters for palaeocurrent speed and palaeoceanography. Paleoceanography, 10(3): 593-610.

McLaren, P. (1981). An interpretation of trends in grain size measures. J. Sediment. Petrol., 51(2): 611-624.

McLaren, P. and Bowles, D. (1985). The effects of sediment transport on grain-size distributions. J. Sediment. Petrol., 55(4): 457-470.

McLaren, P., Cretney, W. and Powys, R. (1993). Sediment pathways in a British Columbia fjord and their relationship with particle-associated contaminants. J. Coast. Res., 9(4): 1026-1043.

McLaren, P., Steyaert, F. and Powys, R. (1998). Sediment transport studies in the tidal basins of the Dutch Waddenzee. Senckenbergiana marit., 29(1/6): 53-61.

Meadows, P. S., Meadows, A., West, F. J. C., Shand, P. S. and Shaikh, M. A. (1998). Mussels and mussel beds (*Mytilus edulis*) as stabilizers of sedimentary environments in the intertidal zone. In: Black, K. S., Paterson, D. M. and Cramp, A. (Eds.), Sedimentary Process in the Intertidal Zone. Geological Society, London, Special Publication, 139, 331-347.

Menard, H. W. (1950). Sediment movement in relation to current velocity. J. Sediment. Petrol., 55(4): 457–470.

Michaelis, H., Obert, B., Schultenkötter, I. and Böcker, L. (1995). Die Miesmuschelbestände der niedersächsischen Watten, 1989-1991. Jahresbericht der Forschungsstelle Norderney, 40: 55-70.

Middleton, G. V. 1962. On sorting, sorting coefficients, and the lognormality of the grain-size distribution of sandstones - a discussion. J. Sediment. Petrol., 70: 754-756.

Middleton, G. V. (1976). Hydraulic interpretation of sand distributions. Journal of Geology, 84: 405-426.

Müller, G. (1967). Methods in sedimentary petrology. Stuttgart (Schweizerbart), 283 pp.

Müller, G. and Gastner, M. (1971). The "Karbonat-Bombe", a simple device for the determination of the carbonate content in sediments, soils and other materials. Neues Jahrb. Miner. Mh., 10: 466-469.

Niemeyer, H. D. (1986). Ausbreitung und Dämpfung des Seeganges im See- und Wattengebiet von Norderney. Jahresbericht der Forschungsstelle Norderney, 37: 49-96.

Nyandwi, N. (1995). The nature of the sediment distribution pattern in the Spiekeroog backbarrier area, the East Frisian Islands. Berichte, Fachbereich Geowissenschaften, Universität Bremen, Bremen, No. 66, 162 pp.

Nyandwi, N. and Flemming, B. W. (1995). A hydraulic model for the shore-normal energy gradient in the East Frisian Wadden Sea (Southern North Sea). Senckenbergiana marit., 25(4/6): 163-171.

Oost, A. P. (1995). Dynamics and sedimentary development of the Dutch Wadden Sea with emphasis on the Frisian inlet. Chapter 6: The influence of biodeposits of the blue mussel *Mytilus edulis* on fine-grained sedimentation in the temperate-climate Dutch Wadden Sea. Geologia Ultraiectina, Utrecht, 126: 359-400.

Passega, R. (1957) Texture as characteristic of clastic deposition. Am. Ass. Petrol. Geol. Bull., 41: 1952-1984.

Passega, R. (1964) Grain size representation by CM patterns as a geological tool. J. Sediment. Petrol., 34: 830-847.

Passega, R. (1977) Significance of CM diagrams of sediments deposited by suspensions. Sedimentology, 24: 723-733.

Pejrup, M., 1988. The triangular diagram used for classification of estuarine sediments: a new approach. In: de Boer, P. L., van Gelder, A. and Nio, S. D. (Eds.), Tide-Influenced Sedimentary Environments and Facies. D. Reidel Publ. Co., Dordrecht, 289-300.

Ragutzki, G. (1982). Verteilung der Oberflächensedimente auf den niedersächsischen Watten. Jahresbericht der Forschungsstelle Norderney. 32: 55-67.

Roberts, J., Jepsen, R., Gotthard, D. and Lick, W. (1998). Effects of particle size and bulk density on erosion of quartz particles. Journal of Hydraulic Engineering, 124(12): 1261-1268

Shepard, F. P. (1954). Normenclature based on sand-silt-clay ratios. J. Sediment. Petrol. 24: 151-158.

Siefert, W. und Lassen, H. (1985). Gesamtdarstellung der Wasserstandsverhältnisse im Küstenvorfeld der Deutschen Bucht nach neuen Pegelauswertungen. Die Küste, 42: 1-77.

Silva, A. J. and Brandes, H. G. (1998). Geotechnical properties and behaviour of high-porosity, organic-rich sediments in Eckernförde Bay, Germany. Continental Shelf Research, 18: 1917–1938.

Sindowski, K.-H. (1966). Geologische Karte von Niedersachsen 1:25 000, Blatt 2212 Spiekeroog. Niedersächs. Landesamt Bodenforsch., Hannover.

Sindowski, K.-H. (1970). Das Quartär im Untergrund der Deutsch Bucht (Nordsee). Eiszeitalter und Gegenwart. 231: 33–46.

Singer, J. K., Anderson, J. B., Ledbetter, M. T., McCave, I. N., Jones, K. P. N. and Wright, R. (1988). An assessment of analytical techniques for the size analysis of fine-grained sediments. J. Sediment. Petrol., 58(3): 534-543.

Sly, P. G., Thomas, R. L. and Pelletier, B. R. (1983). Interpretation of moment measures derived from water-lain sediments. Sedimentology, 30: 219-233.

Stein, R. (1985). Rapid grain-size analyses of clay and silt fraction by SEDIGRAPH 5000D: comparison with coulter counter and Atterberg methods. J. Sediment. Petrol., 55(4): 590-615.

Stephan, H.-J. (1982). Seegangsleistung und Verweilzeit im Bereich der ostfriesischen Inseln zur Deutung morphologischer Vorgänge. Jahresbericht der Forschungsstelle Norderney, 32: 27-39.

Stevens, R. L., Bengtsson, H. and Lepland, A. (1996). Textural provinces and transport interpretations with fine-grained sediments in the Skagerrak. J. Sea Res., 35(1-3): 99-110.

Teeter, A. M. (1993). Suspended transport and sediment-size transport effects in a well-mixed, meso-tidal estuary. In: Mehta, A. J. (Ed.), Nearshore and estuarine cohesive

sediment transport. Coastal and Estuarine Studies, 42. American Geophysical Union, Washington, D.C., 411–429.

Trask, P. D. (1932). Origin and environment of source sediments of petroleum. Houston, Texas, Gulf Pub. Co., 67 pp.

Unesco (1981). Unesco Tech. Pap. in Mar. Sci., No. 38. Paris: Unesco, 192 pp.

Vahl, O. (1972). Efficiency of particle retention in *Mytilus edulis*. Ophelia, 12: 42–52.

van Straaten, L. M. J. U. and Kuenen, PH. H. (1957). Accumulation of fine grained sediments in the Dutch Wadden Sea. Geol. en Mijnbouw, 19: 329–354.

van Straaten, L. M. J. U. (1963). Aspects of Holocene sedimentation in The Netherlands. Ver. K. ned. geol.-mijnb. Genoot. Geol. Ser. 21(1): 149-172.

Wang, H., and McCave, I. N., (1990). Distinguishing climatic and current effects in mid-Pleistocene sediments of Hatton and Gardar Drifts, NE Atlantic. J. Geol. Soc. London, 147: 373-383.

Wehrmann, A. und Hertweck, G. (1998). Lebensspuren. In: M. Türkay (Ed.), Wattenmeer. Kleine Senckenberg-Reihe, Nr. 29, 53–57.

Zens, M., Michaelis, H. Herlyn, M. and Reetz, M. (1997). Die Miesmusselbestände der niedersächsischen Watten im Frühjahr 1994. Jahresbericht der Forschungsstelle Norderney, 41: 141-155.

Zhou, D. (1999). Statistical analysis of dispersion and geochemical patterns of sedimentary system in northern shelf of the South China Sea. In: J. Harff, W. Lemke and K. Stattegger (Eds.), Computerized Modeling of Sedimentary Systems. Springer, Berlin, 401-412.

Publications of this series:

No. 1 **Wefer, G., E. Suess and cruise participants**
Bericht über die POLARSTERN-Fahrt ANT IV/2, Rio de Janeiro - Punta Arenas, 6.11. - 1.12.1985.
60 pages, Bremen, 1986.

No. 2 **Hoffmann, G.**
Holozänstratigraphie und Küstenlinienverlagerung an der andalusischen Mittelmeerküste.
173 pages, Bremen, 1988. (out of print)

No. 3 **Wefer, G. and cruise participants**
Bericht über die METEOR-Fahrt M 6/6, Libreville - Las Palmas, 18.2. - 23.3.1988.
97 pages, Bremen, 1988.

No. 4 **Wefer, G., G.F. Lutze, T.J. Müller, O. Pfannkuche, W. Schenke, G. Siedler, W. Zenk**
Kurzbericht über die METEOR-Expedition No. 6, Hamburg - Hamburg, 28.10.1987 - 19.5.1988.
29 pages, Bremen, 1988. (out of print)

No. 5 **Fischer, G.**
Stabile Kohlenstoff-Isotope in partikulärer organischer Substanz aus dem Südpolarmeer (Atlantischer Sektor). 161 pages, Bremen, 1989.

No. 6 **Berger, W.H. and G. Wefer**
Partikelfluß und Kohlenstoffkreislauf im Ozean.
Bericht und Kurzfassungen über den Workshop vom 3.-4. Juli 1989 in Bremen.
57 pages, Bremen, 1989.

No. 7 **Wefer, G. and cruise participants**
Bericht über die METEOR - Fahrt M 9/4, Dakar - Santa Cruz, 19.2. - 16.3.1989.
103 pages, Bremen, 1989.

No. 8 **Kölling, M.**
Modellierung geochemischer Prozesse im Sickerwasser und Grundwasser.
135 pages, Bremen, 1990.

No. 9 **Heinze, P.-M.**
Das Auftriebsgeschehen vor Peru im Spätquartär. 204 pages, Bremen, 1990. (out of print)

No. 10 **Willems, H., G. Wefer, M. Rinski, B. Donner, H.-J. Bellmann, L. Eißmann, A. Müller, B.W. Flemming, H.-C. Höfle, J. Merkt, H. Streif, G. Hertweck, H. Kuntze, J. Schwaar, W. Schäfer, M.-G. Schulz, F. Grube, B. Menke**
Beiträge zur Geologie und Paläontologie Norddeutschlands: Exkursionsführer.
202 pages, Bremen, 1990.

No. 11 **Wefer, G. and cruise participants**
Bericht über die METEOR-Fahrt M 12/1, Kapstadt - Funchal, 13.3.1990 - 14.4.1990.
66 pages, Bremen, 1990.

No. 12 **Dahmke, A., H.D. Schulz, A. Kölling, F. Kracht, A. Lücke**
Schwermetallspuren und geochemische Gleichgewichte zwischen Porenlösung und Sediment im Wesermündungsgebiet. BMFT-Projekt MFU 0562, Abschlußbericht. 121 pages, Bremen, 1991.

No. 13 **Rostek, F.**
Physikalische Strukturen von Tiefseesedimenten des Südatlantiks und ihre Erfassung in Echolotregistrierungen. 209 pages, Bremen, 1991.

No. 14 **Baumann, M.**
Die Ablagerung von Tschernobyl-Radiocäsium in der Norwegischen See und in der Nordsee.
133 pages, Bremen, 1991. (out of print)

No. 15 **Kölling, A.**
Frühdiagenetische Prozesse und Stoff-Flüsse in marinen und ästuarinen Sedimenten.
140 pages, Bremen, 1991.

No. 16 **SFB 261 (ed.)**
1. Kolloquium des Sonderforschungsbereichs 261 der Universität Bremen (14.Juni 1991):
Der Südatlantik im Spätquartär: Rekonstruktion von Stoffhaushalt und Stromsystemen.
Kurzfassungen der Vorträge und Poster. 66 pages, Bremen, 1991.

No. 17 **Pätzold, J. and cruise participants**
Bericht und erste Ergebnisse über die METEOR-Fahrt M 15/2, Rio de Janeiro - Vitoria,
18.1. - 7.2.1991. 46 pages, Bremen, 1993.

No. 18 **Wefer, G. and cruise participants**
Bericht und erste Ergebnisse über die METEOR-Fahrt M 16/1, Pointe Noire - Recife,
27.3. - 25.4.1991. 120 pages, Bremen, 1991.

No. 19 **Schulz, H.D. and cruise participants**
Bericht und erste Ergebnisse über die METEOR-Fahrt M 16/2, Recife - Belem, 28.4. - 20.5.1991.
149 pages, Bremen, 1991.